Springer ThesesRecognizing Outstanding Ph.D. Research

Fernanda Pinheiro

Multi-species Systems in Optical Lattices

From Orbital Physics in Excited Bands to Effects of Disorder



Springer Theses

Recognizing Outstanding Ph.D. Research

Aims and Scope

The series "Springer Theses" brings together a selection of the very best Ph.D. theses from around the world and across the physical sciences. Nominated and endorsed by two recognized specialists, each published volume has been selected for its scientific excellence and the high impact of its contents for the pertinent field of research. For greater accessibility to non-specialists, the published versions include an extended introduction, as well as a foreword by the student's supervisor explaining the special relevance of the work for the field. As a whole, the series will provide a valuable resource both for newcomers to the research fields described, and for other scientists seeking detailed background information on special questions. Finally, it provides an accredited documentation of the valuable contributions made by today's younger generation of scientists.

Theses are accepted into the series by invited nomination only and must fulfill all of the following criteria

- They must be written in good English.
- The topic should fall within the confines of Chemistry, Physics, Earth Sciences, Engineering and related interdisciplinary fields such as Materials, Nanoscience, Chemical Engineering, Complex Systems and Biophysics.
- The work reported in the thesis must represent a significant scientific advance.
- If the thesis includes previously published material, permission to reproduce this must be gained from the respective copyright holder.
- They must have been examined and passed during the 12 months prior to nomination.
- Each thesis should include a foreword by the supervisor outlining the significance of its content.
- The theses should have a clearly defined structure including an introduction accessible to scientists not expert in that particular field.

More information about this series at http://www.springer.com/series/8790

Fernanda Pinheiro

Multi-species Systems in Optical Lattices

From Orbital Physics in Excited Bands to Effects of Disorder

Doctoral Thesis accepted by Stockholm University, Sweden



Author
Dr. Fernanda Pinheiro
Institute for Theoretical Physics
University of Cologne
Cologne
Germany

Supervisor
Prof. Jonas Larson
Department of Physics, Albanova University
Centrum
Stockholm University
Stockholm
Sweden

Co-Supervisor
Prof. Jani-Petri Martikainen
Department of Applied Physics
Aalto University
Aalto
Finland

ISSN 2190-5053 Springer Theses ISBN 978-3-319-43463-6 DOI 10.1007/978-3-319-43464-3 ISSN 2190-5061 (electronic)

ISBN 978-3-319-43464-3 (eBook)

Library of Congress Control Number: 2016947030

© Springer International Publishing Switzerland 2016

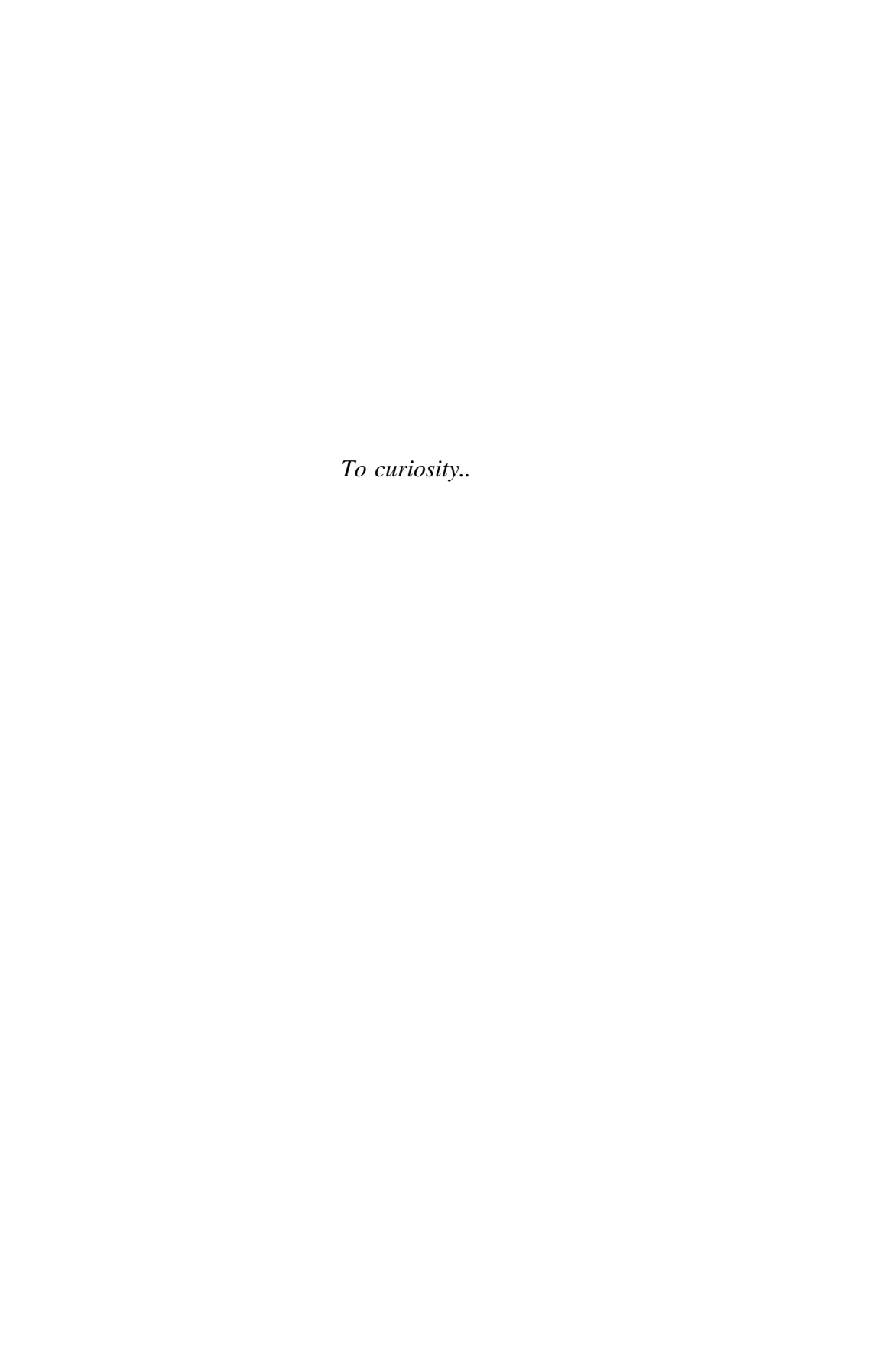
This work is subject to copyright. All rights are reserved by the Publisher, whether the whole or part of the material is concerned, specifically the rights of translation, reprinting, reuse of illustrations, recitation, broadcasting, reproduction on microfilms or in any other physical way, and transmission or information storage and retrieval, electronic adaptation, computer software, or by similar or dissimilar methodology now known or hereafter developed.

The use of general descriptive names, registered names, trademarks, service marks, etc. in this publication does not imply, even in the absence of a specific statement, that such names are exempt from the relevant protective laws and regulations and therefore free for general use.

The publisher, the authors and the editors are safe to assume that the advice and information in this book are believed to be true and accurate at the date of publication. Neither the publisher nor the authors or the editors give a warranty, express or implied, with respect to the material contained herein or for any errors or omissions that may have been made.

Printed on acid-free paper

This Springer imprint is published by Springer Nature
The registered company is Springer International Publishing AG Switzerland



Supervisors' Foreword

Thanks to a resolute activity, both theoretical and experimental, we have seen tremendous achievements in cooling, trapping, and controlling atoms in the past decades. As a result, AMO physics has branched out in diverse directions. The first demonstrations of condensation of dilute atomic gases paved the way to stretch the many-body physics aspect further. It was realized early on that tight confinement into lattice sites can map the physics of ultracold bosonic atoms into a Bose–Hubbard model supporting a superfluid-Mott insulator quantum phase transition. Few years after, the transition was experimentally studied in detail using rubidium atoms cooled down to temperatures close to zero degrees and held trapped in an optical lattice. The experiments benchmarked the field of ultracold atomic physics. The high degree of isolation from their environments together with the great experimental control make these systems ideal for systematic studies of strongly correlated many-body systems.

This spurred the interest in *quantum simulators*, tailor-made systems simulating quantum many-body problems that are intractable on classical computers. Today, almost one and a half decade after the first superfluid-Mott transition was demonstrated, we are just about to witness the first experiments that could be classified as proper quantum simulators. Indeed, the field has within the last years advanced with an enormous momentum and a plethora of different systems are studied in the lab; both bosonic and fermionic atoms, various lattice geometries also including ones with topologically non-trivial states, and spinor condensates comprised of atoms where the internal structure of an atom plays an essential role. This last example is very relevant when it comes to simulating spin models, *i.e.* quantum magnetism. An additional achievement, related to the present thesis, is the preparation of orbital atomic states within the lattice. To prepare and manipulate such states is highly desirable since we know that they play an important role in exotic metals and especially superconductors.

The thesis of Fernanda Pinheiro explores the timely topic of orbital physics in optical lattices. It is written such that it provides an accessible introduction to the field for the non-experts. A rather comprehensive introduction to the topic of orbital

states in optical lattices is followed by an in-depth study of topics that should be of interest also for experts. She derives the relevant models for both p- and d-band condensates and solves for the phase diagrams at a mean-field level. In particular, novel effects that the trapping potential causes in the condensation of p-band bosons are analyzed. The strongly correlated regime is discussed by a systematic mapping of the bosonic models onto spin models. For lower dimensions, this description of the atomic states as effective spins is different from those of spinor condensates; here the spin degree-of-freedom is encoded in the atomic orbital states and not internal electronic Zeeman levels. As is shown, this has several advantages in terms of realizing quantum simulators. In higher dimensions, when all three p-orbital states contribute, the specific shape of the atom-atom interactions implies an emerging SU(3) structure which suggests that magnetic models beyond the paradigm Heisenberg ones can be simulated.

In the last part, Fernanda considers a disordered 2D lattice model of coupled non-interacting atomic states. The freedom in choosing the coupling allows for realization of models that belong to different symmetry classes of the characterization table of disordered systems. This is of special relevance in two dimensions where the system properties change qualitatively depending on the symmetries, for example the zero energy states may either be metallic or localized/insulating. The versatility of the cold atom systems thereby offers an interesting platform for exploring the Anderson problem in different classes.

Stockholm Aalto July 2016 Prof. Jonas Larson Prof. Jani-Petri Martikainen

Abstract

In this thesis we explore different aspects of the physics of multi-species atomic systems in optical lattices. In the first part, we will study cold gases in the first and second excited bands of optical lattices—the p and d bands. The multi-species character of the physics in excited bands lies in the existence of an additional orbital degree of freedom, which gives rise to qualitative properties that are different from what is known for the systems in the ground band. We will introduce the orbital degree of freedom in the context of optical lattices and we will study the many-body systems both in the weakly interacting and in the strongly correlated regimes.

We start with the properties of single particles in excited bands, from where we investigate the weakly interacting regime of the many-body p- and d-orbital systems in Chaps. 2 and 3. This presents part of the theoretical framework to be used throughout this thesis. In Chap. 4, we study Bose–Einstein condensates in the p band, confined by a harmonic trap. This includes the finite temperature study of the ideal gas and the characterization of the superfluid phase of the interacting system at zero temperature for both symmetric and asymmetric lattices.

We continue with the strongly correlated regime in Chap. 5, where we investigate the Mott insulator phase of various systems in the p and d bands in terms of effective spin models. Here we show that the Mott phase with a unit filling of bosons in the p and d bands can be mapped, in two dimensions, to different types of XYZ Heisenberg models. In addition, we show that the effective Hamiltonian of the Mott phase with a unit filling in the p band of 3D lattices has degrees of freedom that are the generators of the SU(3) group. We discuss both the bosonic and fermionic cases.

In the second part, consisting of Chap. 6, we will change gears and study effects of disorder in generic systems of two atomic species. We consider different systems of non-interacting but randomly coupled Bose–Einstein condensates in 2D, regardless of an orbital degree of freedom. We characterize spectral properties and discuss the occurrence of Anderson localization in different cases, belonging to the different chiral orthogonal, chiral unitary, Wigner–Dyson orthogonal and Wigner–Dyson unitary symmetry classes. We show that the different properties of localization in the low-lying excited states of the models in the chiral and the

x Abstract

Wigner–Dyson classes can be understood in terms of an effective model, and we characterize the excitations in these systems. Furthermore, we discuss the experimental relevance of the Hamiltonians presented here in connection to the Anderson and the random-flux models.

Publications Related to This Thesis

Confined *p*-band Bose-Einstein condensates Fernanda Pinheiro, Jani-Petri Martikainen and Jonas Larson *Phys. Rev. A* **85** 033638, (2012).

XYZ quantum Heisenberg models with p-orbital bosons Fernanda Pinheiro, Georg M. Bruun, Jani-Petri Martikainen and Jonas Larson

Phys. Rev. Lett. 111 205302, (2013).

p orbitals in 3D lattices: Fermions, bosons and (exotic) models for magnetism Fernanda Pinheiro arXiv:1410.7828

Phases of *d*-orbital bosons in optical lattices Fernanda Pinheiro, Jani-Petri Martikainen and Jonas Larson *New J. Phys.* **17** 053004 (2015).

Disordered cold atoms in different symmetry classes Fernanda Pinheiro and Jonas Larson *Phys. Rev. A* **92**, 023612 (2015).

Acknowledgements

I thank my supervisors Jonas Larson and Jani-Petri Martikainen for all the learning and attention, for their support and for their comments on this thesis. I was extremely lucky for having such great supervisors, both from the scientific as well as from the personal sides of the story. I thank A.F.R. de Toledo Piza, Georg Bruun and Maciej Lewenstein for collaboration on different projects during these years. I thank the members of my Licentiate thesis committee, Magnus Johansson, Stephen Powell and Per-Erik Tegnér; and the members of my Ph.D. thesis pre-defense committee, Astrid de Wijn, Hans Hansson and Sten Hellman for carefully reading each of the theses and for their comments/suggestions.

In addition to my supervisors and collaborators, I had the opportunity to interact and learn from great scientists along the way. I use this opportunity to directly thank the ones that in one way or another influenced the work reported here. This is for you: Alessandro de Martino, Stephen Powell, Yasser Roudi, Andreas Hemmerich, Tomasz Sowiński, Julia Stasińska, Ravindra Chhajlany, Tobias Grass, André Eckardt, Jens Bardarson, Edgar Z. Alvarenga, Arsen Melikyan, Daniele Marmiroli, Dmitri Bagrets and Alexander Altland. I would also like to thank Alexander Balatsky for two unrequested pieces of advice that turned out to be very useful; Hans Hansson for making me learn an extremely beautiful part of physics until then unknown to me; and Michael Lässig for his support in this period of transition to the postdoctoral research. Last but not least, I thank the Swedish Research Council Vetenskapensrådet for financial support.

Contents

1		ambleerences.	1	
2			3	
2	Introduction to Optical Lattices and Excited Bands			
		l All That)	5	
	2.1	Optical Lattices	5	
	2.2	Single Particles in Periodic Potentials	8	
	2.3	Meet the Orbital States!	11	
		2.3.1 Orbital States in the Harmonic Approximation	12	
	2.4	From One to Many: Many-Body Systems in Excited Bands	16	
		2.4.1 The Many-Body System in the <i>p</i> Band	19	
		2.4.2 The Many-Body System in the <i>d</i> Band	23	
	2.5	How to Get There?	26	
	2.6	Loading Atoms to the <i>p</i> Band—The Experiment		
		of Müller et al	26	
	Appendix: p-Band Hamiltonian Parameters in the Harmonic			
		proximation	28	
		erences.	30	
	rcic	orenees.	50	
3		General Properties of the Bosonic System in the <i>p</i>		
	and	in the <i>d</i> Bands	33	
	3.1	p-Orbital Bosons from a Mean-Field Viewpoint	33	
		3.1.1 The Two-Dimensional Lattice	37	
		3.1.2 The Three-Dimensional Lattice	39	
	3.2	Mean-Field Properties of the Bosonic System in the d Band	41	
		3.2.1 Onsite Superfluid States	44	
	Refe	erences	48	
4	Con	fined p-Orbital Bosons	49	
-	4.1	The Ideal Gas	50	
		4.1.1 The Ideal Gas at Finite Temperatures	53	

xvi Contents

	4.2 4.3 Refe	Mean-Field Equations of the Interacting System in 2D	56 63 65
5	Han	ond the Mean-Field Approximation: Effective Pseudospin niltonians via Exchange Interaction	67
	5.1	Effective Hamiltonian for Describing the Mott Phase with Unit Filling	68
	5.2	p-Orbital Bosonic System in the 2D Lattice	71
	5.2	5.2.1 Properties of the Ground-State: The Phase	/ 1
		Diagram of the XYZ Model	75
		5.2.2 Experimental Probes, Measurements	, 0
		and Manipulations	80
		5.2.3 Experimental Realization	86
		5.2.4 Effective Model Including Imperfections	
		Due to s-Orbital Atoms	86
	5.3	3D System and Simulation of Heisenberg Models	
		Beyond Spin-1/2	89
		5.3.1 The Bosonic Case	89
		5.3.2 The Fermionic Case	95
	5.4	The <i>d</i> -Band System in 2D Lattices.	99
		endix: Coupling Constants of the $SU(3)$ Pseudospin	100
		niltonians	102
	кете	erences	104
6	Effe	cts of Disorder in Multi-species Systems	107
	6.1	Meet the Hamiltonians	108
	6.2	Symmetries of the Real-Valued Random-Field Case	109
	6.3	Symmetries of the Complex-Valued Random Field Case	111
	6.4	Spectral Properties	112
		6.4.1 Properties of the Ground State and Low Lying	
	- -	Excitations	113
	6.5	Effective Model for the Non-chiral Systems	119
	6.6	Experimental Realizations of Disordered Systems	121
		erences	122
7	Con	clusions	125
	Refe	erences	126

Chapter 1 Preamble

After the experimental realization of the optical lattices, and the subsequent observation in 2002 [1] of the *Mott-insulator to superfluid transition* predicted 15 years earlier [2], systems of cold atoms became a powerful tool for exploring manybody quantum phenomena [3]. The degree of control and manipulation in these systems is so great, that nowadays it is possible to engineer lattices with all sorts of different configurations, that allow for the study of many-body quantum physics both in the weakly interacting and in the strongly correlated regimes [4]. In other words, cold atoms in optical lattices provide highly controllable laboratories for testing models of solid state and condensed matter physics.

This is because, similar to the behavior of electrons that is described by the celebrated *Hubbard model*, the many-body dynamics in the optical lattice is dominated by the two basic ingredients consisting of hopping and repulsive interactions [5]. When the constituent particles are bosons, this is well described by the so called *Bose–Hubbard Hamiltonian*,

$$\hat{H}_{s} = -\sum_{\langle i,j \rangle} t(\hat{a}_{i}^{\dagger} \hat{a}_{j} + \hat{a}_{j}^{\dagger} \hat{a}_{i}) + \sum_{i} U \,\hat{n}_{i} \, (\hat{n}_{i} - 1), \tag{1.1}$$

1

where \hat{a}_i (\hat{a}_i^{\dagger}) destroys (creates) an atom in the ith site, in a site-localized state of the ground—the s band [5]. The first term describes nearest neighbors hopping, which occurs with amplitude t, and the second term describes the two-body interactions, which occur with matrix elements proportional to U.

Despite its apparent simple form, the list of experimental achievements with basis in this model is very long. It includes, among others, the simulation of phase transitions and magnetic systems [6, 7], the development of *single-site addressing* [8, 9], the realization of *topological states* [10] as well as studies of equilibration and of *Lieb–Robinson bounds* [11, 12]. What it doesn't include, however, is a whole class of interesting phenomena with origin on the degeneracy of the onsite, or orbital,

2 1 Preamble

wave-functions. *Orbital selective phenomena* has been widely studied in the condensed matter community and are important, for example, for explaining the transitions from metal to insulator in transition-metal oxides [13, 14], as well as magnetoresistance [15] and superconductivity in these and other materials [15], and in He³ systems [16]. But experimentally controllable systems to address related questions were not available until very recently, when the first steps were taken towards the study of orbital physics with cold atoms in optical lattices [17].

Excited bands of optical lattices provide a natural framework for the study of orbital physics [18]. Indeed, the site-localized states in isotropic square and cubic lattices feature an intrinsic degeneracy, that can be readily seen from analogy with the harmonic oscillator in two and three dimensions: Respectively, the first excited state is two- and three-fold degenerate, the second excited state is three- and six-fold degenerate, and so on. In addition, the wave-functions of the different states have different spatial profiles in the different directions, which directly determine the properties of the dynamics. At the single-particle level, for example, this anisotropy of the orbitals implies a tunneling rate that is direction dependent. At the many-body level, the non-vanishing matrix elements characterizing the interacting processes in the system are also strongly dependent on the spatial profile of the orbital states. These give rise to very rich phenomena beyond the Bose–Hubbard model of Eq. (1.1) [18, 19]. To cite just a few, it includes a superfluid phase with a complex-valued order parameter and that spontaneously breaks time-reversal symmetry [20, 21]; and insulating phases with different types of ordering [22] with possibility of frustration in 3D and that allow for the study of exotic models of magnetism [23]. Fermionic systems in the p band have also been characterized and feature very rich physics beyond the s-wave isotropy of the ground band [24, 25]. Moreover, these are also alternative systems that can realize multi-species Hamiltonians with cold atoms [18], and in particular, that can be used to overcome some of the experimental difficulties of the usual (multi-species) setups in low dimensions [18].

The purpose of this thesis is to provide an introduction to orbital physics in the excited bands of optical lattices, and to report a number of studies that have been performed on this and in another multi-species system in the past years. We will start by discussing the properties of a single particle in a periodic potential in Chap. 2, from where we introduce the orbital states and the dynamics of the many-body systems. The focus of Chap. 3 is the weakly interacting regime. Here we present an overview on mean-field techniques and study mean-field properties of the bosonic systems in the p band of two- and three-dimensional optical lattices, and in the d band of the two-dimensional case. We also compute the phase diagram of the Mott-insulator to superfluid transition for the d-band system. We present some results of previous studies on the topic, and part of the work of Ref. [26]. In Chap. 4, we study the superfluid phase of the p band system in two dimensions that is confined by a harmonic trap. We characterize how the inhomogeneous density of the confined system affects the physics of the homogeneous case, and we also study finite temperature properties of the non-interacting case. This is the topic of Ref. [27].

1 Preamble 3

Moving away from the mean-field territory, we study the strongly correlated regime in the p and d bands in Chap. 5. More specifically, we characterize the properties of the Mott phase with a unit filling of various systems in terms of effective spin models, that are obtained using perturbation theory with the tunneling as the small parameter. These systems are explored in the context of *quantum simulation*, where they are shown to be useful for the study of paradigm models of quantum magnetism. We take a step forward in this direction and present an experimental scheme for implementation and manipulation of the systems discussed. This is the most extensive chapter of this thesis, and is based on the material of Refs. [22, 23, 26].

Motivated by the studies of Chap. 5, we then investigate, in Chap. 6, a system of non-interacting Bose–Einstein condensates that are randomly coupled in a two-dimensional optical lattice. This is the content of Ref. [28]. Here we characterize spectral properties and discuss the occurrence of Anderson localization in different cases, that belong to different symmetry classes of the classification scheme of disordered systems [29]. These consist of the chiral orthogonal, chiral unitary, Wigner–Dyson orthogonal and Wigner–Dyson unitary symmetry classes. We will show that when compared to the chiral classes, the onset of localization in terms of the disorder strength is delayed in the Wigner–Dyson classes, and we explain this result in terms of an effective model obtained after integrating out the fastest modes in the system. We also characterize the excitations, which feature vortices in the unitary classes and domain walls in the orthogonal ones. Furthermore, we discuss the experimental relevance of these systems for studying both the Anderson and the random-flux models. Finally, we present the concluding remarks in Chap. 7.

References

- 1. Greiner M, Mandel O, Esslinger T, Hänsch TW, Bloch I (2002) Quantum phase transition from a superfluid to a Mott insulator in a gas of ultracold atoms. Nature 415(6867):39–44
- Fisher MPA, Weichman PB, Grinstein G, Fisher DS (1989) Boson localization and the superfluid-insulator transition. Phys Rev B 40(1):546
- Lewenstein M, Sanpera A, Ahufinger V, Damski B, Sen A, Sen U (2007) Ultracold atomic gases in optical lattices: mimicking condensed matter physics and beyond. Adv Phys 56(2):243–379
- 4. Bloch I, Dalibard J, Nascimbène S (2012) Quantum simulations with ultracold quantum gases. Nat Phys 8(4):267–276
- 5. Jaksch D, Bruder Ch, Cirac JI, Gardiner CW, Zoller P (1998) Cold bosonic atoms in optical lattices. Phys Rev Lett 81(15):3108–3111
- Struck J, Ölschläger C, Targat RL, Soltan-Panahi P, Eckardt A, Lewenstein M, Windpassinger P, Sengstock K (2011) Quantum simulation of frustrated classical magnetism in triangular optical lattices. Science 333(6045):996–999
- Simon J, Bakr WS, Ma R, Tai ME, Preiss PM, Greiner M (2011) Quantum simulation of antiferromagnetic spin chains in an optical lattice. Nature 472(7343):307–312
- 8. Sherson JF, Weitenberg C, Endres M, Cheneau M, Bloch I, Kuhr S (2010) Single-atom-resolved fluorescence imaging of an atomic Mott insulator. Nature 467(7311):68–72
- 9. Bakr WS, Gillen JI, Peng A, Fölling S, Greiner M (2009) A quantum gas microscope for detecting single atoms in a Hubbard-regime optical lattice. Nature 462(7269):74–77

4 1 Preamble

 Jotzu G, Messer M, Desbuquois R, Lebrat M, Uehlinger T, Greif D, Esslinger T (2014) Experimental realization of the topological Haldane model with ultracold fermions. Nature 515(7526):237–240

- Trotzky S, Chen Y-A, Flesch A, McCulloch IP, Schollwöck U, Eisert J, Bloch I (2012) Probing the relaxation towards equilibrium in an isolated strongly correlated one-dimensional Bose gas. Nat Phys 8(4):325–330
- Baillie D, Bisset RN, Ticknor C, Blakie PB (2014) Anisotropic number fluctuations of a dipolar Bose-Einstein condensate. arXiv:1406.3453
- 13. Imada M, Fujimori A, Tokura Y (1998) Metal-insulator transitions. Rev Mod Phys 70(4):1039
- Tokura Y, Nagaosa N (2000) Orbital physics in transition-metal oxides. Science 288(5465):462–468
- 15. Lewenstein M, Liu WV (2011) Optical lattices: orbital dance. Nat Phys 7(2):101–103
- Leggett AJ (1975) A theoretical description of the new phases of liquid He 3. Rev Mod Phys 47(2):331
- 17. Müller T, Fölling S, Widera A, Bloch I (2007) State preparation and dynamics of ultracold atoms in higher lattice orbitals. Phys Rev Lett 99(20):200405
- Isacsson A, Girvin SM (2005) Multiflavor bosonic Hubbard models in the first excited Bloch band of an optical lattice. Phys Rev A 72(5):053604
- Wu C, Liu WV, Moore J, Sarma SD (2006) Quantum stripe ordering in optical lattices. Phys Rev Lett 97(19):190406
- Liu WV, Wu C (2006) Atomic matter of nonzero-momentum Bose-Einstein condensation and orbital current order. Phys Rev A 74(1):013607
- Collin A, Larson J, Martikainen J-P (2010) Quantum states of p-band bosons in optical lattices. Phys Rev A 81(2):023605
- 22. Pinheiro F, Bruun GM, Martikainen J-P, Larson J (2013) XYZ quantum Heisenberg models with p-orbital bosons. arXiv:1304.3178
- 23. Pinheiro F (2014) p orbitals in 3D lattices; fermions, bosons and (exotic) models of magnetism. arXiv:1410.7828
- 24. Wu C (2008) Orbital ordering and frustration of p-band Mott insulators. Phys Rev Lett 100(20):200406
- Zhao E, Liu WV (2008) Orbital order in Mott insulators of spinless p-band fermions. Phys Rev Lett 100(16):160403
- 26. Pinheiro F, Martikainen J-P, Larson J (2015) Phases of d-orbital bosons in optical lattices. arXiv:1501.03514
- Pinheiro F, Martikainen J-P, Larson J (2012) Confined p-band Bose-Einstein condensates. Phys Rev A 85(3):033638
- Pinheiro F, Larson J (2015) Disordered cold atoms in different symmetry classes. Phys Rev A 92(2):023612
- Ryu S, Schnyder AP, Furusaki A, Ludwig AWW (2010) Topological insulators and superconductors: tenfold way and dimensional hierarchy. New J Phys 12(6):065010

Chapter 2 Introduction to Optical Lattices and Excited Bands (and All That)

"And God said, "Let there be light," and there was light. And God saw that light was good. Some time later, there were optical lattices; and then it was even better."

-Adapted from a famous book.

This chapter provides an introduction to the physics in excited bands of optical lattices. We will start by briefly discussing general features of the physics in optical lattices in Sect. 2.1. In Sect. 2.2 we review properties of single particles in periodic potentials and introduce the p and d orbitals in excited bands. The Hamiltonians of the many-body systems are discussed in Sect. 2.3, together with symmetry properties of each case. In Sect. 2.5 we present an overview about experiments with cold atoms in excited bands of optical lattices.

2.1 Optical Lattices

Optical lattices are spatially periodic potentials, created from the superposition of linearly polarized lasers, that can be used to trap neutral atoms via AC Stark shift [5].

The basic idea behind the implementation of optical lattices relies on the use of electric field with a spatial dependence for inducing a position-dependent shift on the energy levels of an atom [5, 6]. We will illustrate how this works by considering the interaction of a two-level atom with monochromatic laser light [7, 8]. For that, we

¹The presentation of the p-band case follows Refs. [1–3]. The discussion about the d-band case follows Ref. [4].

[©] Springer International Publishing Switzerland 2016 F. Pinheiro, *Multi-species Systems in Optical Lattices*, Springer Theses, DOI 10.1007/978-3-319-43464-3_2

start with the Hamiltonian describing two electronic atomic levels, i.e., the ground $|g\rangle$ and excited $|e\rangle$,

$$H_a = E_a |g\rangle\langle g| + E_e |e\rangle\langle e|, \tag{2.1}$$

where E_g and E_e are the corresponding ground and excited states energies and we define $\omega_0 = E_e - E_g$.

Let us assume that the wavelength of the laser λ_L is much greater than the atomic size² and write the Hamiltonian describing the dipole coupling of the atom with the oscillating electric field

$$H_I = -e \mathbf{r} \cdot \mathbf{E}_0 \cos(\omega_L t), \tag{2.2}$$

where $-e\mathbf{r}$ is the electric dipole moment operator, \mathbf{E}_0 is the electric field amplitude and ω_0 the laser frequency [7]. The Hamiltonian of the atom-laser interaction then follows

$$H = H_a + H_i = \hbar \begin{pmatrix} -\omega_0/2 & \Omega \cos(\omega_L t) \\ \Omega^* \cos(\omega_L t) & \omega_0/2 \end{pmatrix}, \tag{2.3}$$

where $\Omega = \frac{E_0}{\hbar} \langle g | e \mathbf{r} | e \rangle$ is the Rabi frequency, and due to parity selection rules $\langle g | \mathbf{r} | g \rangle = \langle e | \mathbf{r} | e \rangle = 0$.

Two situations are of particular interest here [9]: (i) close to resonance, when $\omega_0 \approx \omega_L$, $|\omega_0 - \omega_L| \ll \omega_0$, ω_L ; and (ii) far off resonance, when $|\omega_0 - \omega_L| \gg \omega_0$, ω_L . We consider them separately:

(i) Close to resonance, the probability of transition between the $|g\rangle$ and $|e\rangle$ states is time dependent and given by

$$P(t) = \frac{\Omega^2}{|\Omega|^2 + (\omega_L - \omega_0)^2} \sin^2\left(\frac{t}{2}\sqrt{|\Omega|^2 + (\omega_L - \omega_0)^2}\right).$$
 (2.4)

In particular, if an initial state is given such that all the atoms are in the $|g\rangle$ state, a pulse of π duration—the so called π pulse, is capable of exciting the entire population to the $|e\rangle$ state. This is not the regime for implementation of optical lattices, but as will be discussed later, it is of relevance for manipulations in experiments with cold atoms.

(ii) The regime of interest for creating optical lattices is far-off resonance, where one obtains the Stark shifts. In fact, in the rotating frame with respect to the light field, the effective Hamiltonian of the total system is static, and given by³

$$H = \frac{\hbar}{2} \begin{pmatrix} \Delta & 2\Omega \\ 2\Omega^* - \Delta \end{pmatrix},\tag{2.5}$$

²At the atomic scale, i.e., the Bohr radius, spatial variations of the electric field can be neglected. This is called the *dipole approximation* [7].

³To derive Eq. (2.5), one applies the *rotating wave approximation*, where rapidly oscillating terms are neglected.

where $\Delta = \omega_L - \omega_0$ is the detuning of the laser with respect to the atomic transition. Far from resonance, when $|\Delta| \gg |\Omega|$, the energies of the eigenstates of this effective system⁴ are then given by

$$\epsilon_g = -\frac{\hbar\omega_0}{2} + \frac{\hbar}{4} \frac{|\Omega|^2}{(\omega_L - \omega_0)}$$

$$\epsilon_e = \frac{\hbar\omega_0}{2} - \frac{\hbar}{4} \frac{|\Omega|^2}{(\omega_L - \omega_0)},$$
(2.6)

showing that as the result of atom-light interactions, we can create a conservative potential⁵ with the shifts of the atomic energy levels. Accordingly, if the electric field has a spatial dependence,⁶ then the induced shift on the atomic levels will also depend on the position. As stated in the beginning, this is the basic principle underlying the implementation of optical lattices⁷! The potential produced is in turn proportional to the intensity of the light field,

$$V = -\frac{1}{2}\alpha(\omega_L)|E|^2 = \frac{\hbar|\Omega|^2}{4\Delta},\tag{2.7}$$

with $\alpha(\omega_L)$ the polarizability of the atom [10].

In its simplest implementation, an optical lattice can be constructed from the interference of counter-propagating laser beams [10]. This gives rise to a standing wave

$$V(\mathbf{r}) = \sum_{\sigma} \frac{V_0}{4} \sin^2(k_{\sigma}\sigma), \qquad (2.8)$$

where $\sigma = \{x, y, z\}$ labels the different direction, $k_{\sigma} = 2\pi/\lambda_{\sigma}$ is the wave number of the laser in the direction σ and $V_0 = \hbar\Omega_0^2/4\Delta$. From here on, unless stated otherwise, all the periodic potentials are sinusoidal potentials, as in Eq. (2.8). In this context, any of the inverse wave vectors $l_{\sigma} = k_{\sigma}^{-1} = \lambda_{\sigma}/2\pi$ provide a natural choice for parametrizing the length scale, and any of the recoil energies $E_r^{\sigma} = \hbar^2 k_{\sigma}^2/2m$ (for an atom of mass m) provides a natural choice for fixing the energy scale.

A final disclaimer is in order: Whenever the words "dimensionless" and "position" appear together, we mean that position is scaled in terms of one of the l_{σ} . Whenever

⁴That is, the bare energies plus the Stark shifts.

⁵Dissipative processes involve spontaneous emission, that can be neglected in the large detuning case since excited states have vanishingly probability of being populated.

⁶That is, if $\Omega = \Omega(\mathbf{r})$.

⁷As a sidenote, we notice that this relies on the assumption of adiabatic motion of the atoms and therefore, outside the very low temperature regime, this derivation should include corrections.

⁸Notice that the size of each site in a 1*D* lattice taken in the direction σ , for example, is $\lambda_{\sigma}/2$, which is typically of the order of 400 nm. For comparison, the typical size of the cells in solid state is of the order of Ångströms.

"dimensionless" comes together with "energy", the energies are scaled in terms of one of the E_r^{σ} , for the direction σ to be specified. 1D, 2D and 3D are used to denote one, two and three dimensions, respectively.

2.2 Single Particles in Periodic Potentials

Two main properties characterize the problem of a quantum particle interacting with a periodic potential [11, 12]: (i) that the energy spectrum displays a band structure, where regions with allowed energies are separated by forbidden gaps, and (ii) that the solutions of the eigenvalue equation are given by *Bloch functions*. This is formulated in one dimension⁹ (1D) as

$$\hat{H}\Psi(x) = E\Psi(x)$$
, where $\hat{H} = -\frac{\hbar^2}{2m}\partial_x^2 + V(x)$ (2.9)

with m the mass of the particle and V(x) = V(x + d) the periodic potential with periodicity d. The expression for the Bloch functions can be obtained from the Bloch theorem [12] and is given by

$$\Psi_{\nu,q}(x) = e^{iqx} u_{\nu,q}(x), \tag{2.10}$$

where $u_{\nu,q}$ is a periodic function satisfying $u_{\nu,q}(x) = u_{\nu,q}(x+d)$. q and ν are good quantum numbers labeling, respectively, quasi-momentum and band index, and the use of ν implicitly assumes the reduced scheme where quasi-momentum $q \in [-\pi/d, \pi/d)$ varies in the first *Brillouin zone* [12]. To each of the values of ν and q there is an associated energy, and in general the relation between the free particle momentum and the quasi-momentum q appears in the form of a complicated (transcendental) equation. ¹⁰ Nevertheless, the eigenstates of Eq. (2.9) are plane waves (delocalized in the lattice) that experience a modulation due to the lattice periodicity.

As an alternative to Bloch functions, a basis that is commonly used for describing particles interacting with periodic potentials is given by the *Wannier functions* [11]. They are constructed in terms of the Bloch functions according to the prescription

$$w_{\nu,j}(x) = \sum_{q} e^{-iqR_j} \Psi_{\nu,q}(x),$$
 (2.11)

⁹Extensions to other dimensions are straightforward. We use the 1*D* case here just as an illustration. ¹⁰This is already the case in the simplest example, of the Kronig–Penney problem with a repulsive potential constructed from equally spaced δ -functions (see, e.g. [12, 13] for an application in the context of many-body physics in optical lattices).

where R_j labels the coordinates of the jth site and the sum runs over the quasimomenta in the first Brillouin zone. The Wannier basis differs from the Bloch basis in two main aspects [11]: First, the prescription given by Eq. (2.11) implies that each of the lattice sites accommodates only one Wannier function with band index ν . Second, this is a site localized basis labeled by the band index and the position in the lattice. Since Wannier functions are not the eigenstates of Eq. (2.9), quasimomentum is not a good quantum number to be used as a label here. Nevertheless, Wannier functions at different sites satisfy the following orthonormality condition in its quantum numbers

$$\int dx \, w_{\nu,j}(x) w_{\nu',i}(x) = \delta_{\nu\nu'} \delta_{ij}. \tag{2.12}$$

We will illustrate further properties of these systems by considering results obtained from numerical diagonalization of the *Mathieu equation* for a particle in a sinusoidal potential, Eq. (2.9), where

$$V(x) = V_0 \sin^2(k_x x), \tag{2.13}$$

and V_0 is the lattice amplitude.

The band structure in Fig. 2.1 immediately reveals that increasing values of V_0 are associated with larger energy gaps and band energies of smaller widths. This should be the case, because the size of the energy gap is proportional to the absolute value of the reflection coefficient in the barrier [12], which is larger for larger V_0 . In the same way, the width of the band is proportional to the absolute value of the transmission

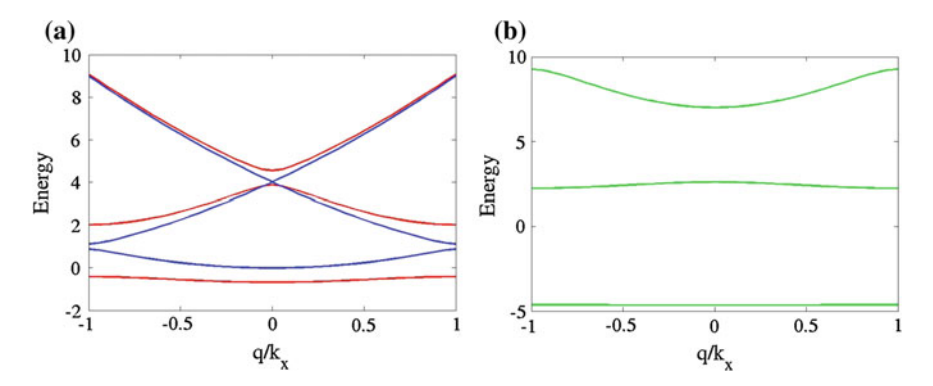


Fig. 2.1 Band structure of a system with $V_0 = 0.5E_r$ (blue), $V_0 = 5E_r$ (red) and $V_0 = 17E_r$ (green). As discussed in the text, the widths of the bands are larger for smaller values of the lattice amplitude. In addition, the energy gaps between the different bands increase for increasing values of V_0 (Color figure online)

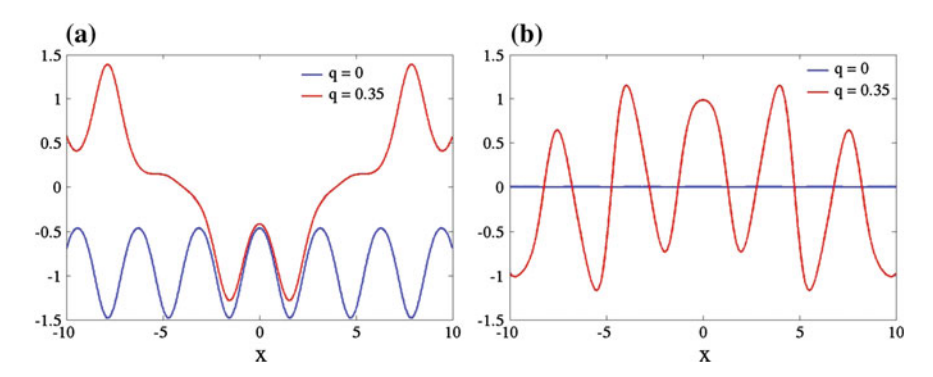


Fig. 2.2 a Real part of the Bloch functions of the first and **b** second bands for different values of quasi-momentum q and for $V_0 = 5E_r$. Notice here that the Bloch function of the 2nd band is strictly imaginary if q = 0

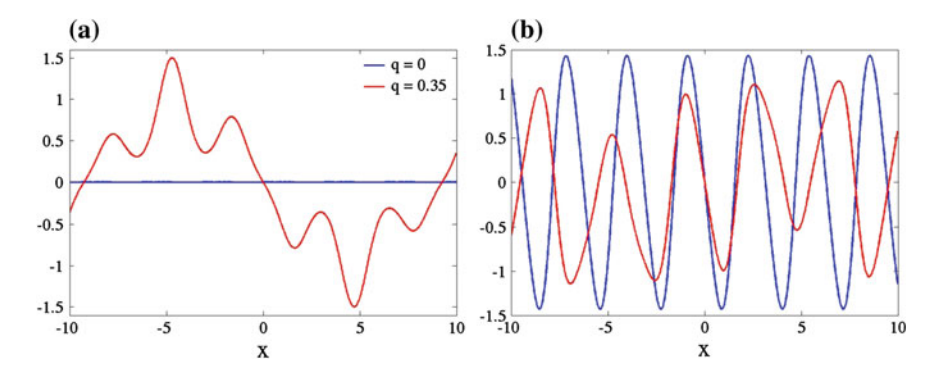


Fig. 2.3 Imaginary part of the Bloch functions of the first (in **a**) and second (in **b**) bands for different values of quasi-momentum q and for $V_0 = 5E_r$. The parameters of the color scheme in (**b**) are identical to the ones used in (**a**). In contrast to the result of Fig. 2.2, here we notice that the 1st band Bloch function with q = 0 is strictly real. We point out that there is an arbitrary phase to be fixed in the definition of the Bloch functions. Once this phase is fixed, however, and say, the Bloch function of the first band with q = 0 is purely real, then the Bloch function in the second band with q = 0 will be purely imaginary

coefficient [12], which is smaller for larger values of V_0 . ¹¹ Furthermore, the narrowing down of the band widths can be alternatively understood from the viewpoint of an *effective mass*, that is defined from the inverse of the band curvature. Namely, flatter bands are related to heavier effective masses and therefore reduced mobility in the lattice, whereas the contrary is valid for steeper bands [12].

We compare samples of the Bloch and Wannier functions of the first and second bands in Figs. 2.2, 2.3 and 2.4, for different values of V_0 , where the delocalized versus localized character of the Bloch versus Wannier functions can be immediately

¹¹For a more detailed discussion about how the transmission and reflection coefficients of the barrier are related to the size of the energy gaps and energy widths, see Exercise 1 (f) and (g) of Chap. 8 of Ashcroft and Mermin, Ref. [12].

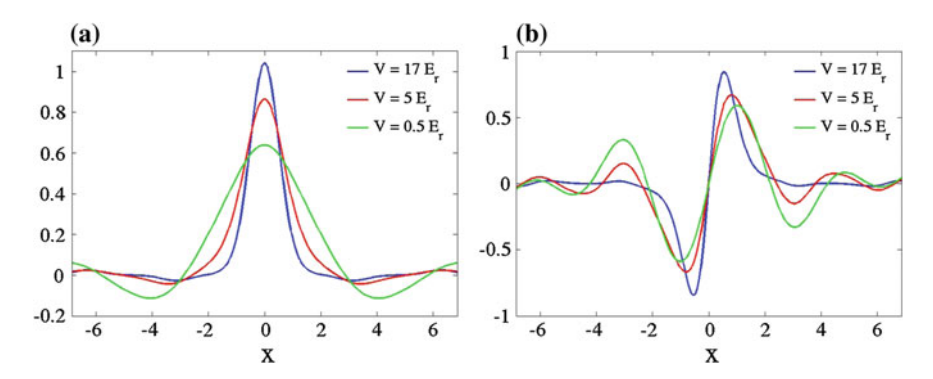


Fig. 2.4 Wannier functions of the first (a) and second (b) bands for systems with $V_0 = 0.5E_r$ (green), $V_0 = 5E_r$ (red) and $V_0 = 17E_r$ (blue). Notice that the Wannier functions are not positive definite. This is necessary in order to satisfy the orthonormality relation of Eq. (2.12) (Color figure online)

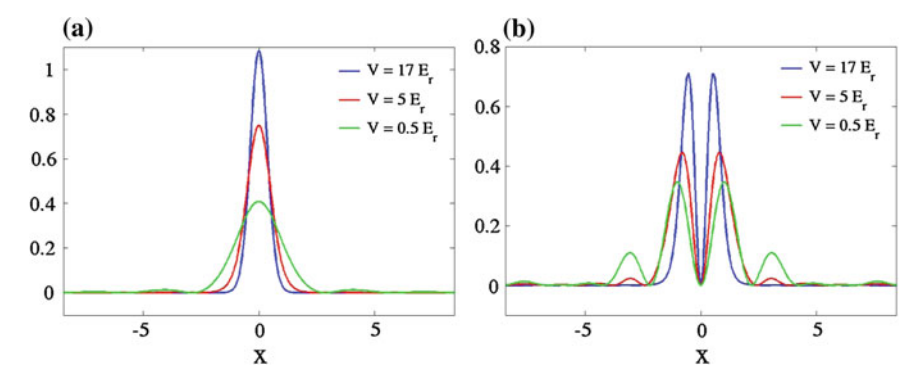


Fig. 2.5 Probability density of the first and second bands Wannier functions for systems with $V_0 = 0.5E_r$ (green), $V_0 = 5E_r$ (red) and $V_0 = 17E_r$ (blue) (Color figure online)

noticed. As for the Wannier functions, increasing values of the potential amplitude V_0 promote a faster decay from the position at the minimum of the potential, yielding Wannier functions that are more localized at each site. For completeness the probability density associated to each of these Wannier functions is given in Fig. 2.5a, b.

2.3 Meet the Orbital States!

In the context of optical lattices, *orbital states* are site-localized states in excited energy bands [1]. The first excited bands form the p, whereas the second excited bands form the d band. Accordingly, they have the associated p and d orbitals [1].

In isotropic square and cubic lattices in 2D and 3D, respectively, excited bands have an intrinsic degeneracy that gives rise to a degeneracy between the orbitals [1]. In particular, orbital states are anisotropic in magnitude and in some cases also in parity [14]. In this section, we characterize the properties of the systems in the p and d bands.

2.3.1 Orbital States in the Harmonic Approximation

In order to become more familiar with the physics in excited bands, we consider the system in the *harmonic approximation*. This consists in approximating each well of the sinusoidal potential with a harmonic potential, i.e., $V(x) = \sin^2(k_x x) \approx k_x^2 x^2$, and therefore exact solutions are easily obtained and simple enough to expose properties of the physics in analytical terms. We notice, however, that the harmonic approximation is justified only in very particular cases [15, 16] and that its quantitative predictions are otherwise very limited [2, 15]. Nevertheless, we use it here to construct an intuitive picture of the orbital states.

Let us then consider the eigenvalue problem in a 2D separable lattice, ¹⁴

$$\hat{H}\Psi = \left(-\frac{\hbar^2}{2m}\partial_x^2 + V_x \sin^2(k_x x) - \frac{\hbar^2}{2m}\partial_y^2 + V_y \sin^2(k_y y)\right)\Psi = E\Psi, \quad (2.14)$$

where V_{σ} and k_{σ} , $\sigma = \{x, y\}$ are the potential amplitude and wave vector in the direction σ . We also rescale the variables with k_y^{-1} to obtain the dimensionless positions $k_y y \to y'$ and $k_y x \to x'$, and with $E_r^y = \hbar^2 k_y^2 / 2m$ to obtain dimensionless energies $\tilde{V}_{\sigma} = V_{\sigma}/E_r^y$, and expand the potential around its minimum keeping only first order contributions. This yields,

$$\frac{\hat{H}}{E_r^y}\Psi = \left(-\partial_{x'}^2 + \tilde{V}_x \frac{k_x^2}{k_y^2} x'^2 - \partial_{y'^2}^2 + \tilde{V}_y y'^2\right)\Psi. \tag{2.15}$$

Since we are dealing with the case of a separable lattice, it is possible to find the solutions in the x- and y-directions by solving each of the equations independently. We start by solving the equation for y',

$$\left(-\partial_{y'}^2 + \tilde{V}_y y^2\right) \Psi(y') = \epsilon_{y'} \Psi(y'), \tag{2.16}$$

¹²The limit of very deep potential wells is required, for example.

¹³In fact, as we discuss later in greater details, the harmonic approximation can lead to misleading conclusions in the many-body system.

¹⁴By separable lattice we mean that the dynamics of different directions is decoupled.

from where we identify the characteristic length of the oscillator $y_0^{-4} = \tilde{V}_y$. The ground, first and second excited states, with corresponding energies ϵ_y^0 , ϵ_y^1 and $\epsilon_{y'}^2$, are given by

$$\phi_0(y') = \mathcal{N}_0(y_0)e^{-y^2/2y_0^2} = \mathcal{N}_0(\tilde{V}_y^{-1/4})e^{-\sqrt{\tilde{V}_y}y^2/2}, \tag{2.17}$$

$$\phi_1(y') = \mathcal{N}_1(y_0)y' \ e^{-y^2/2y_0^2} = \mathcal{N}_1(\tilde{V}_y^{-1/4})y' \ e^{-\sqrt{\tilde{V}_y}y'^2/2}, \tag{2.18}$$

and

$$\phi_2(y') = \mathcal{N}_2(y_0)(y'^2 - 1) \ e^{-y'^2/2y_0^2} = \mathcal{N}_2(\tilde{V}_y^{-1/4})(y'^2 - 1) \ e^{-\sqrt{\tilde{V}_y}y'^2/2}, \tag{2.19}$$

with the normalization factors

$$\mathcal{N}_0(z) = \left(\frac{1}{\pi^{1/4} z^{1/2}}\right),\tag{2.20}$$

$$\mathcal{N}_1(z) = \left(\frac{\sqrt{2}}{\pi^{1/4} z^{3/2}}\right),\tag{2.21}$$

and

$$\mathcal{N}_2(z) = \left(\frac{1}{\pi^{1/2} \left(\frac{3}{4} z^5 - z^3 + z\right)^{1/2}}\right). \tag{2.22}$$

The equations for x' are solved in the same way, but since the scaling has been taken with respect to the dynamics in the y direction, the characteristic length of the oscillator is given here by $x_0^{-4} = \tilde{V}_x k_x^2 / k_y^2$. The expression of the wave-functions of the ground and excited states, with energies $\epsilon_{x'}^0$, $\epsilon_{x'}^1$ and $\epsilon_{x'}^2$ follow as

$$\phi_0(x') = \mathcal{N}_0(x_0)e^{-x^2/2x_0^2} = \mathcal{N}_0(\tilde{V}_x^{-1/4}(k_x/k_y)^{-1/2})e^{-\frac{\sqrt{\tilde{V}_x}k_x}{k_y}x^2/2},$$
(2.23)

$$\phi_1(x') = \mathcal{N}_1(x_0)x' \ e^{-x^2/2x_0^2} = \mathcal{N}_1(\tilde{V}_x^{-1/4}(k_x/k_y)^{-1/2})x' \ e^{-\frac{\sqrt{\tilde{V}_x}k_x}{k_y}x^2/2},\tag{2.24}$$

and

$$\phi_2(x') = \mathcal{N}_2(x_0)(x^{'2} - 1) \ e^{-x^{'2}/2x_0^2} = \mathcal{N}_2(\tilde{V}_x^{-1/4}(k_x/k_y)^{-1/2})(x^{'2} - 1) \ e^{-\frac{\sqrt{\tilde{V}_x}k_x}{k_y}x^{'2}/2}.$$
(2.25)

With the expressions of the eigenfunctions at hand, we can now describe the energy levels and eigenstates of the 2 dimensional system in the harmonic approximation. For simplicity we consider from now on an isotropic lattice for which $\tilde{V}_x = \tilde{V}_y$ and $k_x = k_y$. The true ground state within this approximation has energy $E_0 = (\epsilon_{x'}^0 + \epsilon_{y'}^0)$ and its eigenfunction has a Gaussian profile in both the x and y directions:

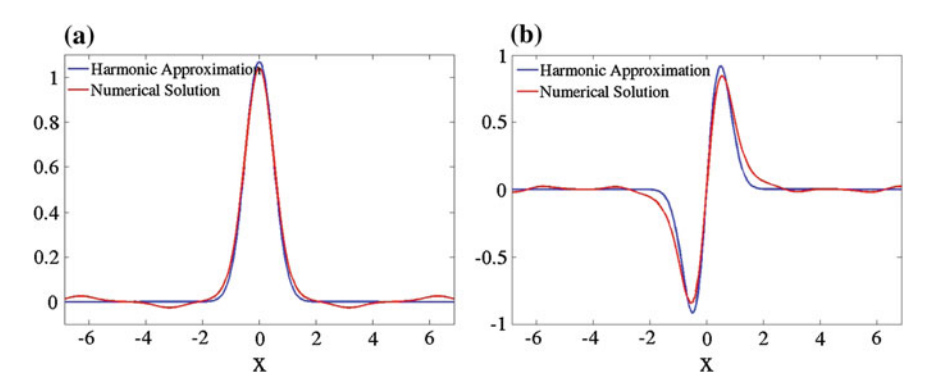


Fig. 2.6 Comparison between the numerically obtained Wannier functions and the Wannier functions in the harmonic approximation, Eqs. (2.17) and (2.19), for a 1D system with $V_0 = 17E_r$ (see discussion in the text)

$$\Psi_0(x', y') = \mathcal{N}_0(x_0) \mathcal{N}_0(y_0) e^{-x^2/2x_0^2 - y^2/2y_0^2}.$$
 (2.26)

p-Orbital States in the Harmonic Approximation

The first excited state is doubly degenerate. It has energy given by $E_1 = (\epsilon_{x'}^1 + \epsilon_{y'}^0) = (\epsilon_{y'}^0 + \epsilon_{y'}^1)$ and the corresponding eigenfunctions are

$$\Psi_{x}(x', y') = \mathcal{N}_{1}(x_{0})\mathcal{N}_{0}(y_{0})x' e^{-x'^{2}/2x_{0}^{2} - y'^{2}/2y_{0}^{2}}$$
(2.27)

and

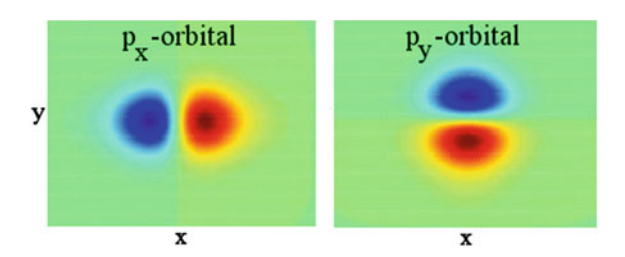
$$\Psi_{y}(x', y') = \mathcal{N}_{0}(x_{0})\mathcal{N}_{1}(y_{0})y' e^{-x^{2}/2x_{0}^{2} - y'^{2}/2y_{0}^{2}},$$
(2.28)

respectively. These are the p-orbital states¹⁵! As can be verified, the different directions are characterized by different parities, i.e., the spatial profile of the different orbitals are odd in the direction of the label α , in which the wave-function has a node, and even in the perpendicular direction. From here on, we denote the orbital states in the p band by p_{α} , with α referring to a spatial direction.

In Fig. 2.6 we compare the ground and first excited Wannier functions obtained from numerical diagonalization of the Mathieu equation with the ground and first excited states obtained in the harmonic approximation. It illustrates the situation where $V_0 = 17 E_r$, which represents a lattice with rather deep wells. This can be seen from the characteristic flatness of the bands in Fig. 2.1, and the harmonic approximation is expected to give a good qualitative picture of the system. In addition, in Fig. 2.7 we show the p_x and p_y orbitals obtained from diagonalization of the Math-

 $^{^{15}}$ These expressions are valid only in the harmonic approximation. The qualitative features, however, are still valid in the general case.

Fig. 2.7 *Left* and *right panels* show the p_x - and the p_y -orbital states, obtained from diagonalization of the Mathieu equation



ieu equation. Notice, however, the important difference that the energy bands are not equally spaced in sinusoidal lattices, as will always be the case in the harmonic approximation. This property has important consequences as we will discuss later in Sect. 2.6, since it helps improving the stability in experimental realizations of the many-body system in the p band [17].

d-orbital States in the Harmonic Approximation

We continue with the second excited state, which is triply degenerate in 2D. It has energy given by $E_2 = (\epsilon_{x'}^2 + \epsilon_{y'}^0) = (\epsilon_{x'}^0 + \epsilon_{y'}^2) = (\epsilon_{x'}^1 + \epsilon_{y'}^1)$ and the corresponding eigenfunctions are given, respectively, by

$$\Psi_{x^2}(x', y') = \mathcal{N}_2(x_0)\mathcal{N}_0(y_0)(x^{2} - 1) e^{-x^2/2x_0^2 - y^2/2y_0^2}, \tag{2.29}$$

$$\Psi_{v^2}(x', y') = \mathcal{N}_0(x_0)\mathcal{N}_2(y_0)(y'^2 - 1)e^{-x'^2/2x_0^2 - y'^2/2y_0^2}$$
(2.30)

and

$$\Psi_{xy}(x', y') = \mathcal{N}_1(x_0)\mathcal{N}_1(y_0)x'e^{-x^2/2x_0^2 - y^2/2y_0^2}.$$
 (2.31)

Now meet the d-orbitals ¹⁶! In analogy to the p-orbital system, from here on we use d_{x^2} , d_{y^2} and d_{xy} to denote the states in the d band. As illustrated in Fig. 2.8, these wave-functions are also labeled after the direction of the node, and the superscript refers to the existence of two nodes. In particular, the d_{xy} orbital has one node in both directions.

As a final remark, we notice that the use of the harmonic approximation might be very dangerous when describing the system in the d band [4]. As shown in Fig. 2.9, the anharmonicity of the sinusoidal lattice is capable of breaking the three-fold degeneracy suggested in analogy with the 2D harmonic oscillator, such that the d_{xy} orbital has slightly higher energy. The implications for the many-body system are studied in Sect. 3.2.

 $^{^{16}}$ In the same way as for the p orbitals, although these expressions are only valid in the harmonic approximation, the qualitative features of the states remain valid in the general case.

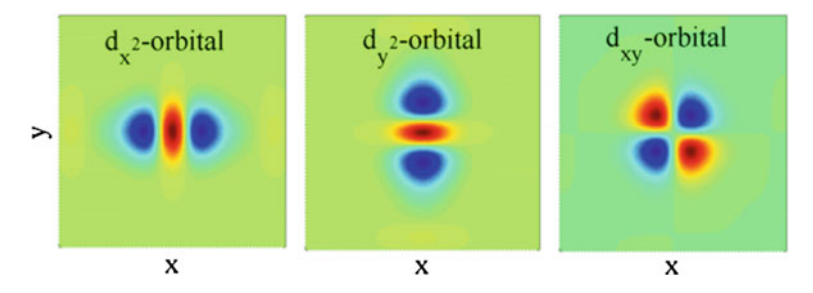
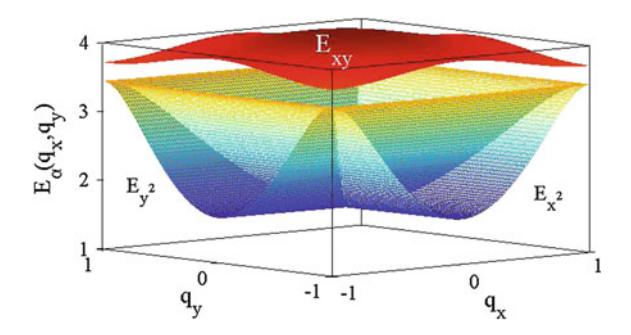


Fig. 2.8 *Left, center* and *right* panels show the d_{x^2} -, d_{y^2} - and the d_{xy} -orbital states, obtained from numerical diagonalization of the Mathieu equation

Fig. 2.9 The three d bands; $E_{x^2}(q_x, q_y), E_{y^2}(q_x, q_y)$ and $E_{xy}(q_x, q_y)$ obtained from numerical diagonalization of the Mathieu equation for the potential with amplitude $V_x = V_y = 20E_r$



2.4 From One to Many: Many-Body Systems in Excited Bands

In general terms, the dynamics of a gas of N atoms of mass m can be represented by a Hamiltonian of the type

$$H = \sum_{i=1}^{N} \left(\frac{p_i^2}{2m} - V_{\text{ext}}(\mathbf{r}_i) \right) + V_{\text{int}}(\{\mathbf{r}_i, \mathbf{r}_j\}), \tag{2.32}$$

where the first term describes single-particle contributions including effects of an external potential $V_{\rm ext}$, and the second term describes interactions between the atoms—thereby accounting for the effects of collective nature.

In the ideal scenario, $V_{\rm int}$ should include all interactions in the system, i.e., that appear from the result of two-body collisions, three-body collisions and so on.¹⁷ In real life, however, exact solutions for problems involving interacting many-body quantum particles are known only in very few or particular cases.¹⁸ The way out, therefore, involves the use of approximations that are capable of accounting not

¹⁷ "Ambition is the last refugee of failure"—Oscar Wilde.

¹⁸When it happens, its almost like finding a unicorn.

for all, but for all the relevant interactions required for a good description of the experimental reality.

Recall that our interest is the physics of (many and also a few) interacting atoms in excited bands of optical lattices. We therefore aim at describing systems of very cold and dilute gases, where the atoms occupy the orbital states discussed in Sect. 2.4. By "very cold" we mean that the temperatures considered are close to the absolute zero. ¹⁹ By "very dilute" we mean that the distance between any two atoms fixed by n = N/V—where N is the total number of particles and V the volume of the system—is very large. ²⁰ In the lab, for example, these systems are produced with densities ²¹ of the order of 10^{15} atoms per cm³. Under these circumstances, it is reasonable to truncate the interaction term to the two-body part [18, 19].

Due to the characteristic low densities, the distances between the particles are always large enough to justify the use of the asymptotic expression of the wave function of the relative motion [19]. In addition, as a consequence of the low temperatures T, the relative momentum corresponding to kinetic energies k_BT , where k_B is the Boltzmann constant, justifies that the collisions are effectively described by s-wave scattering processes, that are completely characterized by the corresponding phase shift [20]. At very low temperatures, however, the phase shift is not the best parameter for characterizing the cross section of the scattering processes.

The reason why this is the case can be illustrated²² by considering the (differential) cross section σ of two particles in a state with relative momentum k and energy $\hbar^2 k^2 / 2\mu$, where μ is the reduced mass:

$$\frac{d\sigma}{d\Omega} = \frac{\sin^2(\delta_0(k))}{k^2} \xrightarrow{k \to 0} a^2, \tag{2.33}$$

with $\delta_0(k)$ the phase shift and a a quantity with dimensions of length. Since at very low temperatures $\lim k \to 0$, the presence of k^2 in the denominator of Eq. (2.33) would require that $\sin(\delta_0(k))$ vanishes linearly for any value of the cross section [20].

The trick here is to use instead the scattering length a defined as

$$\lim_{k \to 0} \frac{k}{\sin(\delta_0(k))} \equiv -\frac{1}{a},\tag{2.34}$$

that is, up to the choice of a sign, exactly the same length parameter in Eq. (2.33). Now this is a good quantity for parametrizing the low energy scattering cross section, for it can also be further interpreted as the first term of the expansion in powers of k of the effective range expansion [20],

$$k \cot(\delta_0(k)) \equiv -\frac{1}{a} + \frac{r_0}{2}k^2 + \dots,$$
 (2.35)

 $^{^{19}}$ Or much less than the bandwidth. The temperature is typically of the order of \sim 1 nK.

²⁰Compared to the scattering length, as we discuss next.

²¹For comparison, the density of air at room temperature is $\sim 1.25 \times 10^{-3}$ g/cm³, the density of water is 1 g/cm^3 and the density of a white dwarf can be estimated as 1.3×10^6 g/cm³ [18].

²²This argument is based on the discussion presented in Ref. [20].

where r_0 is the so called *effective range* of the potential. In these terms, low energy scattering processes can be characterized by only two parameters, ²³ a and r_0 .

The values of a are determined with the standard scattering theory. Now assuming that a is a known quantity, the Hamiltonian (2.32) is implemented in terms of an effective interaction that we assume can capture the physics seen in the lab. We consider here that $V_{int}(\mathbf{r}_i, \mathbf{r}_j)$ describes short-range (contact) interactions, $V_{int} = g\delta(\mathbf{r}_i - \mathbf{r}_j)$, with coupling constant given by $g = 2\pi\hbar^2 a/\mu$, where μ is the reduced mass of the two particles [10]. Accordingly, the effective potential for two identical particles of mass m follows as

$$V_{int}(\mathbf{r}_i, \mathbf{r}_j) = \frac{4\pi\hbar^2 a}{m} \delta(\mathbf{r}_i - \mathbf{r}_j). \tag{2.36}$$

In the language of second quantization, this can be further re-written with the field operators $\hat{\Psi}(r)$ and $\hat{\Psi}^{\dagger}(r)$, that annihilate and create a particle of mass m at position r as

$$\hat{V}_{int} = \frac{4\pi\hbar^2 a}{m} \int d\mathbf{r}' d\mathbf{r} \hat{\Psi}^{\dagger}(\mathbf{r}') \hat{\Psi}^{\dagger}(\mathbf{r}) \delta(\mathbf{r} - \mathbf{r}') \hat{\Psi}(\mathbf{r}) \hat{\Psi}(\mathbf{r}') = \frac{4\pi\hbar^2 a}{m} \int d\mathbf{r}' \hat{\Psi}^{\dagger}(\mathbf{r}') \hat{\Psi}^{\dagger}(\mathbf{r}') \hat{\Psi}(\mathbf{r}') \hat{\Psi}(\mathbf{r}').$$
(2.37)

If the system is composed of bosonic atoms, the operators satisfy the commutation relations $[\hat{\Psi}(r), \hat{\Psi}^{\dagger}(r')] = \delta(r-r')$. If the atoms are fermions, then $\{\hat{\Psi}(r), \hat{\Psi}^{\dagger}(r')\} = \delta(r-r')$. Therefore, the full expression of the Hamiltonian describing the weakly-interacting many-body system is given by

$$\hat{H} = \int d\mathbf{r}' \Big\{ \hat{\Psi}^{\dagger}(\mathbf{r}') \left[-\frac{\hbar^2 \nabla^2}{2m} + V(\mathbf{r}') \right] \hat{\Psi}(\mathbf{r}') + \frac{\tilde{U}_0}{2} \hat{\Psi}^{\dagger}(\mathbf{r}') \hat{\Psi}^{\dagger}(\mathbf{r}') \hat{\Psi}(\mathbf{r}') \hat{\Psi}(\mathbf{r}') \hat{\Psi}(\mathbf{r}') \Big\},$$
(2.38)

where $V(\mathbf{r}')$ accounts for the effects of external potentials superimposed to the system, and the coupling constant $\tilde{U}_0 = 4\pi\hbar^2 a/m$.

We will now expand the field operators in terms of the orbital states of the p and d bands of the sinusoidal optical lattice²⁴

$$V_{\text{latt}}(\mathbf{r}) = \sum_{\sigma} \tilde{V}_{\sigma} \sin^2(\sigma')$$
 (2.39)

in 3D and 2D, respectively, and with σ the corresponding directions. We assume for the moment that no other external potential is present in the system and therefore we take $V(\mathbf{r}') = V_{\text{latt}}(\mathbf{r}')$ in Eq. (2.32).

 $^{^{23}}$ In fact, regardless of formal expressions, any two potentials that are characterized by the same s-wave scattering length a and effective range interaction r_0 will give rise to the same effective interaction.

²⁴Since we will restrict the atoms to live in the corresponding band, we are also assuming the *single-band approximation*.

In these terms, the expression of the field operators follows as

$$\hat{\Psi}^{\dagger}(\mathbf{r}) = \sum_{\alpha,j} w_{\alpha,j}^{*}(\mathbf{r}) \hat{a}_{\alpha,j}^{\dagger}(\mathbf{r})
\hat{\Psi}(\mathbf{r}) = \sum_{\alpha,j} w_{\alpha,j}(\mathbf{r}) \hat{a}_{\alpha,j}(\mathbf{r}),$$
(2.40)

where $\hat{a}_{\alpha j}^{\dagger}$ and $\hat{a}_{\alpha j}$ create and annihilate an atom in an orbital state $w_{\alpha j}(r)$, taken here as the lattice Wannier function in the jth site of the lattice $(j=(j_x,j_y,j_z),\,j_x,j_y,j_z\in\mathcal{N})$. We will use $\alpha=\{x,y,z\}$ whenever studying the p-band system with the p_{α} -orbital states in the 3D lattice; and $\alpha=\{x^2,y^2,xy\}$ whenever studying the d-band system in 2D.

As an additional point, let us stress here that the orbital states are not eigenstates of the single-particle Hamiltonian. We illustrate this by considering the explicit expression of the *p*-orbital wave-functions of a separable lattice, constructed with the site-localized Wannier functions, 25 $w_{\nu,j}(\alpha)$, with $\nu=1,2$ and α a spatial direction, 26 that are given by

$$w_{x,j}(\mathbf{r}) = w_{2,j_x}(x)w_{1,j_y}(y)w_{1,j_z}(z) w_{y,j}(\mathbf{r}) = w_{1,j_x}(x)w_{2,j_y}(y)w_{1,j_z}(z) w_{z,j}(\mathbf{r}) = w_{1,j_x}(x)w_{1,j_y}(y)w_{2,j_z}(z).$$
(2.41)

Now recall that the eigenstates of the single-particle Hamiltonian are Bloch functions (see Eq. (2.10)), and that the relation between Bloch and Wannier functions is given by

$$w_{\nu,\mathbf{R}_{j}(\mathbf{r})} = \sum_{\mathbf{q}} e^{-i\mathbf{q}\cdot\mathbf{R}_{j}} \phi_{\nu,\mathbf{q}}(\mathbf{r}),$$

where we use $\mathbf{R}_j = (x_j, y_j, z_j) = (\pi j_x, \pi j_y, \pi j_z)$ and $\mathbf{q} = (q_x, q_y, q_z)$ is the index which labels the quasi-momentum.

2.4.1 The Many-Body System in the p Band

The Bosonic Case

After inserting (2.40) in Eq. (2.38) and truncating the kinetic term to its leading contribution—the *tight-binding approximation*; and the interaction processes to happen only onsite, the Hamiltonian describing bosonic atoms in the p band of a 3D optical lattice is given by

$$\hat{H}_B = \hat{H}_0 + \hat{H}_{nn} + \hat{H}_{nn'} + \hat{H}_{OD}. \tag{2.42}$$

²⁵Which themselves are also not eigenstates of the single-particle Hamiltonian.

 $^{^{26} \}text{Our}$ notation here assumes that ν is the index which labels the energy band from which the Wannier function is computed.

The first term is the free Hamiltonian

$$\hat{H}_0 = -\sum_{\sigma,\alpha} \sum_{\langle i,j \rangle_{\sigma}} t_{\sigma}^{\alpha} (\hat{a}_{\alpha,i}^{\dagger} \hat{a}_{\alpha,j} + \hat{a}_{\alpha,j}^{\dagger} \hat{a}_{\alpha,i}), \qquad (2.43)$$

that describes the nearest neighbour tunneling of atoms in the p_{α} -orbital state, $\alpha = \{x, y, z\}$, in the direction $\sigma = \{x, y, z\}$. Notice the absence of tunneling events with change of orbital state: Such processes are excluded by parity selection rules.²⁷

The second and third terms of Eq. (2.42) describe different types of density–density interactions:

$$\hat{H}_{nn} = \sum_{\alpha} \sum_{i} \frac{U_{\alpha\alpha}}{2} \hat{n}_{\alpha,i} (\hat{n}_{\alpha,i} - 1), \qquad (2.44)$$

between atoms in the same orbital state, with $\hat{n}_{\alpha,i} = \hat{a}^{\dagger}_{\alpha,i}\hat{a}_{\alpha,i}$; and

$$\hat{H}_{nn'} = \sum_{\alpha,\beta,\alpha \neq \beta} \sum_{i} U_{\alpha\beta} \hat{n}_{\alpha,i} \hat{n}_{\beta,i}, \qquad (2.45)$$

 $\beta = \{x, y, z\}$, between atoms in different orbital states. Finally, the last term

$$\hat{H}_{OD} = \sum_{\alpha,\beta,\alpha \neq \beta} \sum_{i} \frac{U_{\alpha\beta}}{4} (\hat{a}_{\alpha,i}^{\dagger} \hat{a}_{\alpha,i}^{\dagger} \hat{a}_{\beta,i} \hat{a}_{\beta,i} + \hat{a}_{\beta,i}^{\dagger} \hat{a}_{\beta,i}^{\dagger} \hat{a}_{\alpha,i} \hat{a}_{\alpha,i})$$
(2.46)

describes interactions that transfer atoms within different types of orbital states.

The expression for the tunneling amplitude in the direction σ is given in terms of the orbital states by

$$t_{\sigma}^{\alpha} = -\int d\mathbf{r} \, w_{\alpha,j}^{*}(\mathbf{r}) \left[-\nabla^{2} + V(\mathbf{r}) \right] w_{\alpha,j+1_{\sigma}}(\mathbf{r}), \tag{2.47}$$

and due the different curvatures of the excited bands in the directions perpendicular (\bot) and parallel (\parallel) to the label of the orbital wave functions, $t_{\perp}t_{\parallel} < 0$, where t_{\perp} and t_{\parallel} refer to the tunnelings in the corresponding directions. In the same way, the expression of the interaction coefficients is given by

$$U_{\alpha\beta} = U_0 \int d\mathbf{r} |w_{\alpha \mathbf{j}}(\mathbf{r})|^2 |w_{\beta \mathbf{j}}(\mathbf{r})|^2.$$
 (2.48)

As a final remark we recall that in the bosonic case $[\hat{a}_{\alpha,i},\hat{a}^{\dagger}_{\beta,j}] = \delta_{\alpha\beta}\delta_{ij}$.

²⁷In the separable lattices considered here. This needs not to be the case in different setups.

Symmetries of the Many-Body Bosonic System in the p Band

Because each term in Eq. (2.42) has the same number of creation and annihilation operators, the Hamiltonian is clearly invariant under global U(1) transformations. This reflects the overall conservation of particle number in the system, and therefore

$$[\hat{H}, \sum_{i} (n_{j}^{x} + \hat{n}_{j}^{y} + \hat{n}_{j}^{z})] = 0.$$
 (2.49)

Here, however, the key ingredient that distinguishes the dynamics in the p band from the systems in the ground band, is the presence of processes that transfer atoms between different orbital states, Eq. (2.46). Although a similar term is present in the Hamiltonian describing spinor Bose-Einstein condensates, its relative strength compared to other processes is typically very small, such that these contributions can be safely neglected [3]. This is not the case for the p-band system, because the coupling constant of orbital changing processes is exactly the same as the one of mixed density-density interactions defined in Eq. (2.45). Furthermore, the presence of orbital changing processes implies that instead of a $U(1) \times U(1) \times U(1)$ global symmetry, the dynamics of bosonic atoms in the p band has a $U(1) \times Z_2 \times Z_2$ global symmetry, and therefore total population of each of the orbital states is conserved only modulo 2 [1]. This has also fundamental implications on the establishment of long-range phase coherence in the system, because the presence of Z_2 (discrete) symmetries violate the assumptions of the Hohenberg-Mermin-Wagner theorem [21, 22]. As a consequence, this system is not prohibited of (long-range) ordering even in low dimensions, and therefore the existence of a true condensate in the thermodynamic limit is not precluded for bosons in the p band.

We also notice that in isotropic lattices²⁸ transformations of the type

$$\hat{a}_{\alpha,j} \rightleftharpoons \pm \hat{a}_{\beta,j} \tag{2.50}$$

leave the Hamiltonian invariant for any permutation of α and β . Moreover, these lattices feature additional Z_2 symmetries, associated to the swapping of any two orbital states, followed by a change of indices in the lattice, i.e.,

$$\hat{a}_{\alpha,j} \to \hat{a}_{\beta,j'}
\hat{a}_{\beta,i} \to \hat{a}_{\alpha,i'},$$
(2.51)

where the $\mathbf{j} = (j_x, j_y, j_z)$ indices become $j_\alpha \to j_\beta$ and $j_\beta \to j_\alpha$ in \mathbf{j}' .

Let us now take a closer look at the symmetries of the 2D lattice by considering the isotropic case, where $U_{xx}=U_{yy},\,U_{xy}=U_{yx},\,t_{\parallel}^x=t_{\parallel}^y$ and $t_{\perp}^x=t_{\perp}^y$. Here the rotation

²⁸Where $t_{\parallel}^{\alpha} = t_{\parallel}^{\beta}$ and $t_{\perp}^{\alpha} = t_{\perp}^{\beta}$ for $\alpha \neq \beta$ and $U_{xx} = U_{yy} = U_{zz}$ with again all the $U_{\alpha\beta}$ equal for $\alpha \neq \beta$.

$$\begin{pmatrix} \hat{a}_{x,j}' \\ \hat{a}_{y,j}' \end{pmatrix} \to \begin{pmatrix} \cos \theta - \sin \theta \\ \sin \theta & \cos \theta \end{pmatrix} \begin{pmatrix} \hat{a}_{x,j} \\ \hat{a}_{y,j} \end{pmatrix}$$
(2.52)

leaves the Hamiltonian invariant for different values of $\theta = (0, \pi/2, \pi) \pm k\pi$, where $k \in Z$. This is not the case in asymmetric lattices, however, where even under the condition of orbital degeneracy the tunneling coefficients $t_{\parallel}^{\alpha} \neq t_{\parallel}^{\beta}$, $t_{\perp}^{\alpha} \neq t_{\perp}^{\beta}$. As a consequence, transformations of the type $\hat{a}_{x,j} \rightarrow \hat{a}_{y,j}$, $\hat{a}_{y,j} \rightarrow \hat{a}_{x,j}$ do not leave the Hamiltonian unaltered.

For asymmetric lattices there is a particular case for which the system contains an additional SO(2) symmetry [16]. This corresponds to the harmonic approximation in the limit of vanishing tunneling, ²⁹ where $U_{\alpha\alpha}=3U_{\alpha\beta}=U$. As pointed out in Ref. [16], this special case is better studied with the angular-momentum like annihilation operators $\hat{a}_{\pm j}=(\hat{a}_{xj}\pm i\hat{a}_{yj})/\sqrt{2}$, in terms of which the local part of the Hamiltonian can be written as [16]

$$\hat{H}_{j} = \frac{U}{2} \left[\hat{n}_{j} \left(\hat{n}_{j} - \frac{2}{3} \right) - \frac{1}{3} \right] + \delta \left[(\hat{n}_{j} - 1)(\hat{L}_{+j} + \hat{L}_{-j}) \right]$$

$$+ \lambda \left[\frac{1}{4} \hat{L}_{z,j}^{2} - 3(\hat{L}_{+j} - \hat{L}_{-j}^{2})^{2} - \hat{n}_{j} \right],$$
(2.53)

where $U = (U_{xx} + U_{yy})/2$, $\delta = (U_{xx} - U_{yy})/2$ and $\lambda = U_{xy} - U/3$. The density operator can be expressed as $\hat{n}_j = \hat{a}_{+j}^{\dagger} \hat{a}_{+,j} + \hat{a}_{-j}^{\dagger} \hat{a}_{-j}$, and the angular momentum operators are $\hat{L}_{z,j} = \hat{a}_{+,j}^{\dagger} \hat{a}_{+,j} - \hat{a}_{-,j}^{\dagger} \hat{a}_{-,j}$ and $\hat{L}_{\pm,j} = \hat{a}_{\pm,j}^{\dagger} \hat{a}_{\pm,j}/2$. It follows from the properties of the harmonic oscillator eigenstates that in the harmonic approximation $\lambda = \delta = 0$ for any lattice configuration, and therefore $[\hat{H}_j, \hat{L}_{z,j}] = 0$ [16]. This is not the case for sinusoidal optical lattices, for there λ , $\delta \neq 0$ destroys the axial symmetry, and consequently $[\hat{H}_j, \hat{L}_{z,j}] \neq 0$ [16]. Notice, however, that rather from being of geometric character, this dynamical enhancement [23] of the SO(2) symmetry appears entirely due to the specific form in which the eigenvalue problem can be rewritten in the harmonic approximation.³⁰

The Fermionic Case

Due to the *Pauli blockade* preventing the occupation of the same orbital state by more than one particle, fermionic atoms in the *p* band behave according to

$$\hat{H}_F = \hat{H}_0 + \hat{H}_{nn'},\tag{2.54}$$

with \hat{H}_0 and $\hat{H}_{nn'}$ defined in Eqs. (2.43) and (2.45), respectively. Here, however, $\{\hat{a}_{\alpha,i},\hat{a}_{\beta,j}\}=\delta_{\alpha\beta}\delta_{ij}$. The expressions for the tunneling elements and the various coupling constants are the same as in the bosonic case, defined in Eqs. (2.47) and (2.48).

Symmetries of the Many-Body Fermionic System in the p Band

Since Eq. (2.54) contains only number operators, the Hamiltonian of the fermionic system in the p band has the $U(1) \times U(1) \times U(1)$ symmetry. Accordingly, in addition

²⁹This is only valid in the case of separable lattices.

³⁰This is similar to the conservation of the *Laplace–Runge–Lenz vector* in Kepler problems (see e.g. Ref. [23]).

to a global U(1) transformation, associated to conservation of total number in the system, it also conserves the number of particles in each of the orbital states.

To P or not to P? (bands!)

-William Shakespeare. Adapted from the tragedy of Hamlet.

2.4.2 The Many-Body System in the d Band

We obtain the many-body Hamiltonian describing bosonic atoms in the d band by following the same procedure adopted for treating the p-band system: We expand the field operators, Eq. (2.40), in terms of the orbital states of the d band for $\alpha = \{x^2, y^2, xy\}$, ³¹ and assume the tight-binding and single-band approximations. The result is [4]

$$\hat{H} = \hat{H}^d + \hat{H}^{xy},\tag{2.55}$$

where the first term describes the processes involving only the d_{x^2} - and d_{y^2} - orbital states, while the second term contains all the processes that involve the d_{xy} orbital. The two parts of the Hamiltonian can be decomposed further, according to the different types of processes:

$$\hat{H}^d = \hat{H}_0^d + \hat{H}_t^d + \hat{H}_{nn}^d + \hat{H}_{da}^d + \hat{H}_{od}^d$$
 (2.56)

and

$$\hat{H}^{xy} = \hat{H}_0^{xy} + \hat{H}_t^{xy} + \hat{H}_{nn}^{xy} + \hat{H}_{da}^{xy} + \hat{H}_{od}^{xy}. \tag{2.57}$$

The first terms in each of these equations describe the onsite energies of the different orbitals E_{α} and E_{xy} , with $\alpha = \{x^2, y^2\}$,

$$\hat{H}_0^d = \sum_{\alpha} \sum_{i} E_{\alpha} \hat{n}_{\alpha,i}, \qquad (2.58)$$

and

$$\hat{H}_0^{xy} = \sum_{i} E_{xy} \hat{n}_{xy,i}.$$
 (2.59)

The second terms describe the tunneling processes,

$$\hat{H}_t^d = -\sum_{\sigma,\alpha} \sum_{\langle i,j \rangle_{\sigma}} \left(t_{\sigma}^{\alpha} \hat{d}_{\alpha,i}^{\dagger} \hat{d}_{\alpha,j} + H.c. \right)$$
 (2.60)

 $^{^{31}}$ We denote the creation and annihilation operators for the states in the d band by $\hat{d}_{\alpha}^{\dagger}$ and \hat{d}_{α} .

and

$$\hat{H}_{t}^{xy} = -\sum_{\sigma} \sum_{\langle i,j \rangle_{\sigma}} t^{p} \hat{d}_{xy,i}^{\dagger} \hat{d}_{xy,j}. \tag{2.61}$$

Notice here that while atoms in the d_{x^2} and d_{y^2} orbitals are characterized by anisotropic tunneling in the directions parallel (\parallel) and perpendicular (\perp) to the nodes of the orbital state, the d_{xy} -orbital atoms tunnel in both directions with the same magnitude, t^p . The expressions of the tunneling amplitudes are given below:

$$t_{\sigma}^{\alpha} = -\int d\mathbf{r} \, w_{\alpha,i}^{*}(\mathbf{r}) \left[-\nabla^{2} + V(\mathbf{r}) \right] w_{\alpha,i+\mathbf{1}_{\sigma}(\mathbf{r})}$$

$$t^{p} = -\int d\mathbf{r} \, w_{xy,i}^{*}(\mathbf{r}) \left[-\nabla^{2} + V(\mathbf{r}) \right] w_{xy,i+\mathbf{1}_{\sigma}}(\mathbf{r}).$$
(2.62)

In addition, as opposed to the situation in the p band, the parallel and perpendicular tunnelings in the d band satisfy $t_{\parallel}^{\alpha}t_{\perp}^{\alpha}>0$. Furthermore, $t^{p}<0$.

We turn now to the interacting part of the Eq. (2.55). It contains the density-density interactions, both between atoms in the same orbital, and in different orbital states,

$$\hat{H}_{nn}^{d} = \sum_{\alpha} \sum_{i} \frac{U_{\alpha\alpha}}{2} \hat{n}_{\alpha,i} \left(\hat{n}_{\alpha,i} - 1 \right) + \sum_{\alpha,\beta,\alpha \neq \beta} \sum_{i} U_{\alpha\beta} \hat{n}_{\alpha,i} \hat{n}_{\beta,i}$$
 (2.63)

and

$$\hat{H}_{nn}^{xy} = \sum_{i} \frac{U_{pp}}{2} \hat{n}_{xy,i} \left(\hat{n}_{xy,i} - 1 \right) + \sum_{\alpha} \sum_{i} 2U_{p\alpha} \hat{n}_{xy,i} \hat{n}_{\alpha,i}; \tag{2.64}$$

interactions that move population between the orbital states in pairs,³²

$$\hat{H}_{od}^{d} = \sum_{\alpha, \beta, \alpha \neq \beta} \sum_{i} \frac{U_{\alpha\beta}}{4} \left(\hat{d}_{\alpha,i}^{\dagger} \hat{d}_{\alpha,i}^{\dagger} \hat{d}_{\beta,i} \hat{d}_{\beta,i} + \hat{d}_{\beta,i}^{\dagger} \hat{d}_{\beta,i}^{\dagger} \hat{d}_{\alpha,i} \hat{d}_{\alpha,i} \right)$$
(2.65)

and

$$\hat{H}_{od}^{xy} = \sum_{\alpha} \sum_{i} \left[\frac{U_{p\alpha}}{2} \left(\hat{d}_{xy,i}^{\dagger} \hat{d}_{xy,i}^{\dagger} \hat{d}_{\alpha,i} \hat{d}_{\alpha,i} + \hat{d}_{\alpha,i}^{\dagger} \hat{d}_{\alpha,i}^{\dagger} \hat{d}_{xy,i} \hat{d}_{xy,i} \right) + \sum_{\beta \neq \alpha} U_{n_{\alpha}\alpha\beta} \hat{d}_{\alpha,i}^{\dagger} \hat{d}_{\beta,i}^{\dagger} \hat{d}_{xy,i} \hat{d}_{xy,i} \right]$$
(2.66)

 $^{^{32}}$ These are the same orbital-changing interactions of the *p*-band system.

and finally, the density-assisted processes that also transfer atoms, albeit without conserving any particle number apart from the total population, between the different orbital states:

$$\hat{H}_{da}^{d} = \sum_{\alpha,\beta,\alpha\neq\beta} \sum_{i} U_{n_{p}\alpha\beta} \left(\hat{d}_{\alpha,i}^{\dagger} \hat{n}_{\alpha,i} \hat{d}_{\beta,i} + \hat{d}_{\beta,i}^{\dagger} \hat{n}_{\alpha,i} \hat{d}_{\alpha,i} \right)$$
(2.67)

and

$$\hat{H}_{da}^{xy} = \sum_{\alpha,\beta,\alpha \neq \beta} \sum_{i} 2U_{n_{\rho}\alpha\beta} \hat{d}_{\alpha,i}^{\dagger} \hat{n}_{xy,i} \hat{d}_{\beta,i}. \tag{2.68}$$

The various coupling constants are given by

$$U_{\alpha\beta} = \frac{U_0}{2} \int d\mathbf{r} |w_{\alpha,i}(\mathbf{r})|^2 |w_{\beta,i}(\mathbf{r})|^2, \quad \alpha = (x, y, p), \text{ for } (x^2, y^2, xy),$$

$$U_{n_{\alpha}\alpha\beta} = \frac{U_0}{2} \int d\mathbf{r} |w_{\alpha,i}(\mathbf{r})|^3 |w_{\beta,i}(\mathbf{r})|, \quad \alpha = (x, y), \text{ for } (x^2, y^2),$$

$$U_{n_{p}\alpha\beta} = \frac{U_0}{2} \int d\mathbf{r} |w_{xy,i}(\mathbf{r})|^2 |w_{\alpha,i}(\mathbf{r})| |w_{\beta,i}(\mathbf{r})|, \quad \alpha = (x, y), \text{ for } (x^2, y^2).$$
(2.69)

Symmetries of the Many-Body Bosonic System in the d Band

Since each term in Eq. (2.55) contains the same number of operators and complex conjugates, the system is invariant under a global U(1) phase transformation that is associated to the overall conservation of number in the system. As opposed to the bosonic system in the p band, however, the presence of density-assisted processes in the d band breaks the conservation of number modulo 2 in each of the orbital states. Therefore, the only symmetry left is the Z_2 symmetry associated to the swapping of the d_{x^2} and d_{y^2} orbital states, followed by the interchange of spatial indices. More explicitly, the many-body Hamiltonian (2.55) is invariant under the transformation

$$\hat{d}_{x^2 j} \to \hat{d}_{y^2 j'}
\hat{d}_{y^2 j} \to \hat{d}_{x^2 j'},$$
(2.70)

where $\mathbf{j} = (j_x, j_y)$ and $\mathbf{j}' = (j_y, j_x)$. In particular, since the t^p tunneling amplitude is isotropic in the different directions, $\hat{d}_{xy,j} = \hat{d}_{xy,j'}$.

2.5 How to Get There?

The novel features of the dynamics in excited bands, and in particular, the possibility of probing orbital selective phenomena in optical lattices [17], stimulated considerable experimental effort in recent years for exploring the physics beyond the ground band. Although nowadays we are provided with different techniques [24, 25] for loading atoms to higher bands, in this section we restrict the discussion to experiments with bosons, and to the ones of greatest relevance to the lattice configurations that are covered in this thesis.

2.6 Loading Atoms to the *p* Band—The Experiment of Müller et al.

As reported in the experiment of Müller et al. [17], bosonic atoms³³ can be loaded from the Mott insulator phase in the s band to the p band of optical lattices with stimulated *Raman transitions*.

The idea here is to use the interaction of a two-level atom with the laser light to couple different vibrational levels of a sinusoidal and separable 3D lattice potential. Deep in the Mott insulator phase, single sites can be approximated by harmonic potentials, and different vibrational levels in this potential correspond to the different bands of the optical lattice.

To illustrate how this happens, consider a Raman coupling between electronic atomic states of ⁸⁷Rb. These are two-photon processes where the two levels are coupled with an intermediate virtual state, far detuned from all the other states of the system [17]. Because of this intermediate coupling, implementation of Raman transitions requires the use of two different lasers, whose corresponding wave vectors we denote here by k_{L_1} and k_{L_2} . In addition, since the photons carry momentum, this will also couple the vibrational levels that we call $|1\rangle$ and $|2\rangle$, with a matrix element given by

$$\frac{\Omega_1 \Omega_2^*}{\delta} \langle 2|e^{i(k_{L_1} - k_{L_2}) \cdot x}|1\rangle. \tag{2.71}$$

 Ω_i are the Rabi frequencies between the $|i\rangle$ states, i=1,2 with another far detuned auxiliary state of this system, say $|aux\rangle$, and δ is the detuning between $|aux\rangle$ and the virtual intermediate state.

Now recall the discussion on Sect. 2.1, where in the regime far off resonance the probability of transitions between the states of the two-level system are time dependent and given by Eq. (2.4). By selecting a pulse with the appropriate time,

 $^{^{33}}$ Fermionic atoms can be promoted to the p band by a different process, which is based on full occupation of the states in the s band in such a way that the next atoms are restricted to occupy the excited band.

and the laser wave vector with the appropriate configuration, ³⁴ it is then possible to transfer population from the ground to the excited vibrational level in a particular direction [8]. In other words, the coupling here is between the different orbital states!

With use of these techniques, Müller et al. experimented with atoms in the p band of 1D, 2D and 3D (separable) optical lattices. The main results are summarized here:

- (i) *Long lifetimes*: Atomic population was reported to survive in a metastable state in the excited band with considerable long lifetimes, of the order of 10–100 times larger than the characteristic scale for tunneling in the lattice. The lifetimes depend mainly on two factors, namely the atomic density, and the depth of the lattice sites.
- (ii) *Decay channels*: The reason why the lifetimes in the *p* band are affected both by the atomic density and the depth of the lattice sites is because the main decay channel stems from atom-atom collisions. Therefore the larger the densities, the larger the probability of atomic collisions. In the same way, the increased rate of tunneling in the limit of shallower potential wells increases the probability of encounters between two atoms, and consequently, the probability of atomic collisions. In addition, we notice that the anharmonicity of the sinusoidal lattices prevents the occurrence of first order processes in which the energy of a state of two atoms in the *p* band is resonant with the energy of a state with one atom in the *s* and the other in the *d* band. Although this increases the stability of the system in the *p* band, we remark that higher order processes can still contribute to the decay of population from the excited band.
- (iii) Establishment of coherence: the authors found that by changing the parameters of the system, i.e., by lowering the lattice such as to reach the regime of the superfluid phase, the system exhibited a state with long-range coherence at nonzero quasi-momentum. This observation was based on time of flight experiments, where the momentum distribution in the lattice was recorded. In particular, for specific conditions of hold times it was possible to notice a π phase difference in between neighbouring sites in the directions parallel to the label of the orbital wave functions.

We will address experimental considerations about many-body systems in the p band in Sect. 5.2.2, where the techniques used in this experiment are extended for further manipulation of the orbital states.

Going Even Higher—A Brief Comment Regarding Experiments in the d Band

The possibility of preparing atoms in the *d* band with 99 % fidelity has been recently reported in Ref. [25]. This realization is based on the use of a *standing-wave pulse*, for instantaneously switching an optical lattice on and off. This induces transitions between states of definite quasi-momentum in different bands that are allowed by selection rules. Starting from the ground-state of the system with the lattice switched off, for example, it is possible to prepare superpositions of states at even bands

³⁴That is, a pulse that couples the two states in different directions of the optical lattice.

 $s, d, g \dots$ Transitions between the states of odd bands are also possible, with use of a moving lattice.

Although this experimental scheme is not suitable for promoting atoms to the p band from the ground-state of a system without the lattice, the lifetime on the d band is quite long, of the order of μ s. As we discuss further in Sect. 5.4, this opens great opportunities in the context of quantum simulations.

Appendix: *p*-Band Hamiltonian Parameters in the Harmonic Approximation

For further reference, we compute here the various coupling constants in the harmonic approximation. As discussed before, under this assumption the Wannier functions are taken as Hermite polynomials, and therefore (2.48) and (2.47) can be obtained from computation of simple Gaussian integrals. Here

$$U_{xx} = U_0 \int dx \left(\frac{\sqrt{2}}{\pi^{1/4} x_0^{3/2}} \right)^4 x^4 e^{-2x^2/x_0^2} \int dy \left(\frac{1}{\pi^{1/4} y_0^{1/2}} \right)^4 e^{-2y^2/y_0^2}$$

$$= U_0 \left(\frac{\sqrt{2}}{\pi^{1/4} x_0^{3/2}} \right)^4 \frac{3}{4} \frac{\sqrt{\pi}}{2^{5/2}} x_0^5 \left(\frac{1}{\pi^{1/4} y_0^{1/2}} \right)^4 \sqrt{\frac{\pi}{2}} y_0 = U_0 \left(\frac{3}{8\pi} \frac{1}{x_0 y_0} \right).$$
(2.72)

Analogous calculation yields $U_{yy} = U_0 \left(\frac{3}{8\pi} \frac{1}{x_0 y_0} \right)$. We now compute U_{yy} :

$$U_{xy} = U_{0} \int dx \left(\frac{\sqrt{2}}{\pi^{1/4} x_{0}^{3/2}}\right)^{2} x^{2} e^{-x^{2}/x_{0}^{2}} \left(\frac{1}{\pi^{1/4} x_{0}^{1/2}}\right)^{2} e^{-x^{2}/x_{0}^{2}} \times \int dy \left(\frac{\sqrt{2}}{\pi^{1/4} y_{0}^{3/2}}\right)^{2} y^{2} e^{-y^{2}/y_{0}^{2}} \left(\frac{1}{\pi^{1/4} y_{0}^{1/2}}\right)^{2} e^{-y^{2}/y_{0}^{2}} = U_{0} \int dx \left(\frac{\sqrt{2}}{\pi^{1/2} x_{0}^{2}}\right)^{2} x^{2} e^{-2x^{2}/x_{0}^{2}} \int dy \left(\frac{\sqrt{2}}{\pi^{1/2} y_{0}^{2}}\right)^{2} y^{2} e^{-2y^{2}/y_{0}^{2}} = U_{0} \left(\frac{1}{8\pi} \frac{1}{r_{0} y_{0}}\right),$$

$$(2.73)$$

from where it follows that $U_{xx} = U_{yy} = 3U_{xy}$. Notice, however, that the relation $U_{\alpha\alpha}/U_{\alpha\beta} = 3$ is only true in the harmonic approximation, and that this is the case regardless of the wave vectors of the lattice k_x and k_y . In fact, it is very surprising that the coupling constants in the harmonic approximation do not even depend on the values of the lattice vector, but only on the lattice amplitudes V_x and V_y^{35} [16].

³⁵In the harmonic approximation this happens because the degeneracy condition fixes the ratio k_x/k_y .

This is not the case, however, when the Hamiltonian parameters are computed with use of the lattice Wannier functions.

Now according to Eq. (2.47), we use Eqs. (2.27) and (2.28) to compute the tunneling coefficients as

$$-t_{xx} = \left(\frac{\sqrt{2}}{\pi^{1/4}x_0^{3/2}}\right)^2 V_x \int dx \, x(x+d) \sin^2 x \, e^{-x^2/2x_0^2} e^{-(x+d)^2/2x_0^2}$$

$$+ \left(\frac{\sqrt{2}}{\pi^{1/4}x_0^{3/2}}\right)^2 \int dx \, \frac{d}{dx} (xe^{-x^2/2x_0^2}) \frac{d}{dx} \left((x+d)e^{(x+d)^2/2x_0^2}\right).$$
(2.74)

d is used here as the lattice constant, and we have already used that the integral in the y-direction yields 1. In the same way,

$$-t_{xy} = \left(\frac{1}{\pi^{1/4} y_0^{1/2}}\right)^2 V_y \int dy \sin^2 y \, e^{-y^2/2x_0^2} e^{-(y+d)^2/2y_0^2}$$

$$+ \left(\frac{1}{\pi^{1/4} y_0^{1/2}}\right)^2 \int dy \frac{d}{dy} e^{-y^2/2y_0^2} \frac{d}{dy} e^{-(y+d)^2/2y_0^2}.$$
(2.75)

The expressions for t_{yx} and t_{yy} are obtained by making $x \to y$ and $y \to x$ with $x_0 \to y_0$ and $y_0 \to x_0$ (Figs. 2.10 and 2.11).

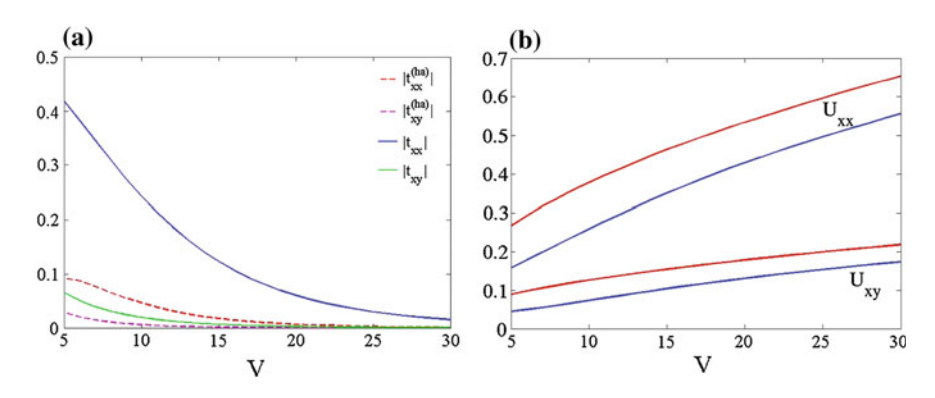
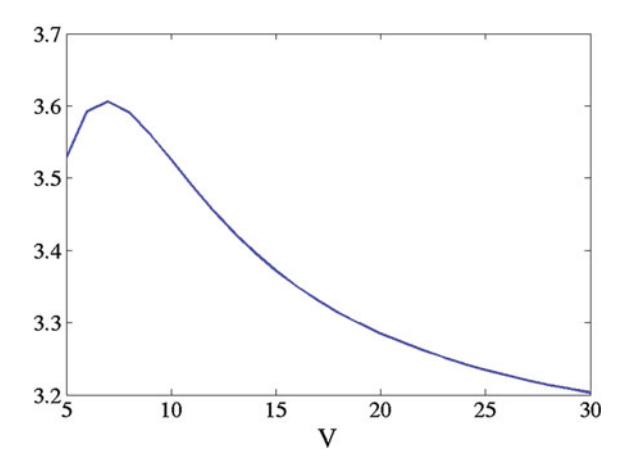


Fig. 2.10 Comparison between the values of the couplings obtained from analytical and numerical computations as a function of V. It is shown in $\bf a$ that the harmonic approximation fails to reproduce the results obtained numerically for the tunneling coefficients when tunneling occurs in the direction of the node. In $\bf b$ we show the results for the interaction coefficients. In particular the estimates obtained from the harmonic approximation are always larger than the values of the couplings computed numerically

Fig. 2.11 Ratio U_{xx}/U_{xy} for different values of the amplitude of the optical potential. Notice here that U_{xx}/U_{xy} is always larger than 3 for numerical computations with the lattice Wannier functions



References

- Isacsson A, Girvin SM (2005) Multiflavor bosonic Hubbard models in the first excited Bloch band of an optical lattice. Phys Rev A 72(5):053604
- Pinheiro F, Martikainen J-P, Larson J (2012) Confined p-band Bose-Einstein condensates. Phys Rev A 85(3):033638
- Larson J, Collin A, Martikainen J-P (2009) Multiband bosons in optical lattices. Phys Rev A 79(3):033603
- Pinheiro F, Martikainen J-P, Larson J (2015) Phases of d-orbital bosons in optical lattices. arXiv:1501.03514
- 5. Greiner M, Mandel O, Esslinger T, Hänsch TW, Bloch I (2002) Quantum phase transition from a superfluid to a Mott insulator in a gas of ultracold atoms. Nature 415(6867):39–44
- Jaksch D, Bruder C, Cirac JI, Gardiner CW, Zoller P (1998) Cold bosonic atoms in optical lattices. Phys Rev Lett 81(15):3108–3111
- 7. Foot CJ (2004) Atomic physics. Oxford University Press, Oxford
- 8. Haroche S, Raimond J-M (2013) Exploring the quantum: atoms, cavities, and photons (Oxford Graduate Texts). Oxford University Press, USA
- 9. Kollath C, Boulder Summer School Lecture Notes
- Leggett AJ (2006) Quantum liquids: Bose condensation and Cooper pairing in condensedmatter systems, vol 34. Oxford University Press, Oxford
- 11. Wannier GH et al (1959) Elements of solid state theory. University Press, Cambridge
- 12. Ashcroft NW, David Mermin N (1976) Solid state physics. Cengage Learning, 1st edn. 2 Jan 1976
- 13. Pinheiro F, de Toledo Piza AFR (2013) Delocalization and superfluidity of ultracold bosonic atoms in a ring lattice. J Phys B: At Mol Opt Phys 46(20):205303
- 14. Lewenstein M, Vincent Liu W (2011) Optical lattices: orbital dance. Nat Phys 7(2):101-103
- Collin A, Larson J, Martikainen J-P (2010) Quantum states of p-band bosons in optical lattices. Phys Rev A 81(2):023605
- Sowiński T, Łacki M, Dutta O, Pietraszewicz J, Sierant P, Gajda M, Zakrzewski J, Lewenstein M (2013) Dynamical restoration of symmetry breaking in realistic optical lattices. arXiv:1304.6299
- 17. Müller T, Fölling S, Widera A, Bloch I (2007) State preparation and dynamics of ultracold atoms in higher lattice orbitals. Phys Rev Lett 99(20):200405
- Pethick CJ, Smith H (2002) Bose-Einstein condensation in dilute gases. Cambridge University Press, Cambridge

References 31

19. Pitaevskii LP, Stringari S (2003) Bose-Einstein condensation, vol 116. Clarendon Press, Oxford

- Piza AFR (2004) Bose-Einstein condensation in dilute atomic gases. Braz J Phys 34(3B):1102– 1157
- 21. Mermin DN, Wagner H (1966) Absence of ferromagnetism or antiferromagnetism in one- or two-dimensional isotropic Heisenberg models. Phys Rev Lett 17(22):1133
- 22. Hohenberg PC (1967) Existence of long-range order in one and two dimensions. Phys Rev 158(2):383
- 23. Greiner W, Müller B (1994) Quantum mechanics. Symmetries, vol 2. Springer, Berlin
- 24. Wirth G, Ölschläger M, Hemmerich A (2010) Evidence for orbital superfluidity in the p-band of a bipartite optical square lattice. Nat Phys 7(2):147–153
- 25. Zhai Y, Yue X, Wu Y, Chen X, Zhang P, Zhou X (2013) Effective preparation and collisional decay of atomic condensate in excited bands of an optical lattice. arXiv:1306.3313

Chapter 3 General Properties of the Bosonic System in the *p* and in the *d* Bands

Since the majority of topics covered in this thesis are focused on the properties of many-body systems with bosons, we use this chapter to discuss general features of the bosonic case in more details. General properties of the fermionic system will be discussed whenever required.

The discussion will start with the system in the p band, with special emphasis on the mean-field formalism that is used to characterize the properties of the superfluid phase of the confined system in Chap. 4. This is the content of Sect. 3.1, where we also include an overview of the results of Ref. [1], which studied p-orbital bosons with homogeneous density in the lattice. Next, in Sect. 3.2, we characterize the superfluid phase of the bosonic system in the d band.

3.1 *p*-Orbital Bosons from a Mean-Field Viewpoint

Mean-field techniques provide an efficient first tool for investigating effects of collective nature in systems of interacting particles [3]. At this level of description, the system's symmetries become key ingredients, and the collective properties are characterized by the order parameters that encode the relevant degrees of freedom in the phases with broken symmetry [3]. This approach has been proven very successful in the study of the weakly interacting Bose gas [4], and will be adopted here to characterize the properties of the superfluid phase of bosonic atoms in the p band. The method used proceeds with the following program²:

 $^{^{1}}$ This is based on Ref. [2], which contains the first theoretical discussion of d-orbital bosons.

²As will become clear along the text, this approach is equivalent to analysis of the saddle-point solution of the path integral of Eq. (2.42).

[©] Springer International Publishing Switzerland 2016 F. Pinheiro, *Multi-species Systems in Optical Lattices*, Springer Theses, DOI 10.1007/978-3-319-43464-3_3

- (i) We will first obtain a mean-field version of the many-body Hamiltonian with use of the *coherent-state ansatz*;
- (ii) With the mean-field Hamiltonian at hand, we construct the corresponding Lagrangian, and consider independent variations with respect to the relevant degrees of freedom. This yields the equations of motion for the order parameter:
- (iii) In the last step we will propagate the Euler-Lagrange equations in imaginary time to obtain the configuration of the order parameters which minimizes the energy.

We will implement this routine by first considering the normal ordered version of Eq. (2.42), where we replace the operators $\hat{a}_{\alpha,j}$ with the complex numbers $\psi_{\alpha,j}$. This attributes a coherent state at each site,

$$|\Psi\rangle = \prod_{j} |\psi\rangle_{j} = \prod_{j} |\psi_{x,j}, \psi_{y,j}, \psi_{z,j}\rangle_{j}$$
(3.1)

such that $\hat{a}_{\alpha,j}|\Psi\rangle = \psi_{\alpha,j}|\Psi\rangle$. However, since the product form of Eq. (3.1) cannot capture effects of correlations between neighboring sites, this is used with self-consistent equations for obtaining the solutions of the problem in a self-consistent fashion.

We then continue with the expression of the the single site many-body wave function in the Fock basis

$$|\psi\rangle_{j} = \exp\left(-\frac{|\psi_{x,j}|^{2} + |\psi_{y,j}|^{2} + |\psi_{z,j}|^{2}}{2}\right) \sum_{n_{x},n_{y},n_{z}} \frac{\psi_{x,j}^{n_{x}} \psi_{y,j}^{n_{y}} \psi_{z,j}^{n_{z}}}{\sqrt{n_{x}! n_{y}! n_{z}!}} |\mathbf{n}\rangle_{j}, \quad (3.2)$$

where $|\mathbf{n}\rangle_j = |n_x, n_y, n_z\rangle_j$ represents the state with n_x atoms in the p_x orbital, n_y atoms in the p_y orbital and n_z atoms in the p_z orbital at the site \mathbf{j} . Since the onsite order parameter in this language is the coherent state $\psi_{\alpha,j} = \langle \Psi | \hat{a}_{\alpha,j} | \Psi \rangle$, which clearly does not preserve the number of particles,³ this is used to describe the phase with broken U(1) symmetry. Furthermore, we use it to express the *full onsite order parameter*, containing the onsite spatial dependence, by using the expansion of the annihilation operator (2.40) in terms of the Wannier functions introduced in Sect. 2.1:

$$\psi_{j}(\mathbf{r}) \equiv \langle \hat{\Psi}_{j}(\mathbf{r}) \rangle = \sum_{\alpha} w_{\alpha,j} \langle \hat{a}_{\alpha,j} \rangle. \tag{3.3}$$

The behavior of the order parameter ψ_{α} will be described from the equations of motion derived from independent variation of the Lagrangian

$$L = \sum_{\alpha} \sum_{j} \frac{i}{2} \left[\psi_{\alpha,j}^* \frac{d}{dt} \psi_{\alpha,j} - \psi_{\alpha,j} \frac{d}{dt} \psi_{\alpha,j}^* \right] - H_{MF}, \tag{3.4}$$

³In fact, number fluctuations computed on coherent states follow a Poissonian distribution [5].

with respect to $\psi_{\alpha,j}$ and $\psi_{\alpha,j}^*$. The mean-field Hamiltonian is given by

$$H_{MF} = -\sum_{\alpha,\sigma} \sum_{\langle i,j \rangle_{\sigma}} t_{\sigma}^{\alpha} \psi_{\alpha,i}^{*} \psi_{\alpha,j} + \sum_{\alpha} \sum_{j} \frac{U_{\alpha\alpha}}{2} n_{\alpha,j} n_{\alpha,j} + \sum_{\alpha,\beta,\alpha \neq \beta} \sum_{j} U_{\alpha\beta} n_{\alpha,j} n_{\beta,j}$$

$$+ \sum_{\alpha,\beta,\alpha \neq \beta} \sum_{j} \frac{U_{\alpha\beta}}{4} \left(\psi_{\alpha,j}^{*} \psi_{\alpha,j}^{*} \psi_{\beta,j} \psi_{\beta,j} + \psi_{\beta,j}^{*} \psi_{\beta,j}^{*} \psi_{\alpha,j} \psi_{\alpha,j} \right),$$
(3.5)

where the density of the p_{α} -orbital state is given by $n_{\alpha,j}=|\psi_{\alpha,j}|^2$ and normalization was imposed in the whole lattice as

$$N = N_x + N_y + N_z = \sum_{j} (|\psi_{x,j}|^2 + |\psi_{y,j}|^2 + |\psi_{z,j}|^2), \qquad (3.6)$$

with N the total number of atoms.

We are now ready to write the Euler-Lagrange equations for the order parameters,

$$-i\frac{\partial\psi_{x,j}}{\partial t} = -\sum_{\sigma\in\{x,y,z\}} t_{\sigma}^{x}(\psi_{x,j+1_{\sigma}} - 2\psi_{x,j} + \psi_{x,j-1_{\sigma}})$$

$$+ (U_{xx}|\psi_{x,j}|^{2} + (U_{xy} + U_{yx})|\psi_{y,j}|^{2} + (U_{xz} + U_{zx})|\psi_{z,j}|^{2})\psi_{x,j}$$

$$+ \left(\frac{U_{xy} + U_{yx}}{2}\right)\psi_{y,j}^{2}\psi_{x,j}^{*} + \left(\frac{U_{xz} + U_{zx}}{2}\right)\psi_{z,j}^{2}\psi_{x,j}^{*}$$

$$-i\frac{\partial\psi_{y,j}}{\partial t} = -\sum_{\sigma\in\{x,y,z\}} t_{\sigma}^{y}(\psi_{y,j+1_{\sigma}} - 2\psi_{y,j} + \psi_{y,j-1_{\sigma}})$$

$$+ (U_{yy}|\psi_{y,j}|^{2} + (U_{xy} + U_{yx})|\psi_{x,j}|^{2} + (U_{yz} + U_{zy})|\psi_{z,j}|^{2})\psi_{y,j}$$

$$+ \left(\frac{U_{xy} + U_{yx}}{2}\right)\psi_{x,j}^{2}\psi_{y,j}^{*} + \left(\frac{U_{zy} + U_{yz}}{2}\right)\psi_{z,j}^{2}\psi_{y,j}^{*}$$

$$-i\frac{\partial\psi_{z,j}}{\partial t} = -\sum_{\sigma\in\{x,y,z\}} t_{\sigma}^{z}(\psi_{z,j+1_{\sigma}} - 2\psi_{z,j} + \psi_{z,j-1_{\sigma}})$$

$$+ (U_{zz}|\psi_{x,j}|^{2} + (U_{xz} + U_{zx})|\psi_{x,j}|^{2} + (U_{yz} + U_{zy})|\psi_{y,j}|^{2})\psi_{z,j}$$

$$+ \left(\frac{U_{xz} + U_{zx}}{2}\right)\psi_{x,j}^{2}\psi_{z,j}^{*} + \left(\frac{U_{yz} + U_{zy}}{2}\right)\psi_{y,j}^{2}\psi_{z,j}^{*},$$

$$(3.7)$$

⁴Recall that the coherent-state expectation value is carried out with the normal-ordered version of Hamiltonian (2.42).

that correspond to a set of coupled (discrete) Gross–Pitaevskii equations, one for each of the p_{α} orbitals.

In the next step, Eqs. (3.7) are propagated (numerically) in imaginary time with a trial initial function. This is the last part of the program and the one which leads to the configuration of the order parameter at the global energy minimum.

To illustrate how this procedure works [6], let us consider the Schrödinger equation $\hat{H}\psi = E\psi$ such that the wave function ψ evolves in time according to $\psi(t) = e^{-i\hat{H}t}\psi(0)$, where we used $\hbar = 1$. Writing ψ in the basis of its energy eigenstates, $\psi = \sum_n c_n \phi_n$, with $c_n = \langle \psi | \phi_n \rangle$,

$$\psi(t) = \sum_{n} c_n e^{-iE_n t} \phi_n,$$

where E_n corresponds to the nth energy level of the system. Now using $t \to i\tau$, with

$$\psi(\tau) = \sum_{n} c_n e^{-E_n \tau} \phi_n,$$

the overlap between the ground state with the $\psi(\tau)$ propagated in imaginary time, and after a long propagation time, is given by

$$\langle \psi(\tau) | c_0 \phi(\tau) \rangle \to \lim_{\tau \to \infty} \frac{c_0^2 e^{-2E_0 \tau}}{c_0^2 e^{-2E_0 \tau} + \sum_{n=1} c_n^2 e^{-2E_n \tau}} = 1$$

Therefore, in the limit of $\tau\to\infty$, $\psi(\tau)$ will converge to the true ground state of the system, as long as the overlap between these states is non-vanishing. For finite τ , the corrections appear as

$$\psi(\tau) = c_0 e^{-E_0 \tau} \phi(0) + \mathcal{O}(e^{-\tau(E_1 - E_0)}).$$

This method can also be applied to the non-linear system described by Eq. (3.7), but in this case propagation has to be carried out self-consistently.

In the simpler cases, as e.g., when atomic population is homogeneously distributed in the lattice,⁵ much of the behavior of the system can be alternatively understood from direct study of Eq. (3.5). Since the order parameters are complex numbers, say

$$\psi_{\alpha,i} = e^{i\theta_{\alpha,j}} |\psi_{\alpha,i}|, \tag{3.8}$$

full characterization of the configuration with minimum energy involves knowledge on both the phases and densities.⁶ In the situation of equal density, however, we are only left with analysis of the phases.

From the non-interacting part of the mean-field Hamiltonian

$$H_{MF}^{0} = -\sum_{\alpha,\sigma} \sum_{\langle i,j \rangle_{\sigma}} t_{\sigma}^{\alpha} \psi_{\alpha,i}^{*} \psi_{\alpha,j} = -2 \sum_{\alpha,\sigma} \sum_{\langle i,j \rangle_{\sigma}} t_{\sigma}^{\alpha} |\psi_{\alpha,i}| |\psi_{\alpha,j}| \cos(\theta_{\alpha,j} - \theta_{\alpha,i}),$$
(3.9)

⁵That is, when $|\Psi_{\alpha,i}| = |\Psi_{\beta,i}|$.

⁶This discussion follows Ref. [1, 7].

we immediately identify that tunneling processes couple the phases of the onsite order parameters, within the same orbital state, at neighbouring sites. As discussed in Sect. 2.4, since $t_{\parallel}^{\alpha} < 0$ and $t_{\perp}^{\alpha} > 0$, these processes minimize energy by imposing a stripped configuration to the phases along the lattice. In fact, the phase of the p_{α} -orbital state has values in the lattice that satisfy $\theta_{\alpha,j} = \theta_{\alpha}(j_x, j_y, j_z) \pm \pi$ modulo $(j_{\alpha}, 2)$. Therefore, from tunneling contributions, the order parameters at neighbouring sites are set to exhibit the same phase in the directions perpendicular to the label of the orbitals, while in the parallel directions they exhibit a π phase difference.

Let us now consider the interacting part of the mean-field Hamiltonian. Substitution of (3.8) in the terms describing density-density interactions lead to

$$H_{nn}^{(j)} = \frac{U_{xx}}{2} |\psi_{x,j}|^4 + \frac{U_{yy}}{2} |\psi_{y,j}|^4 + \frac{U_{zz}}{2} |\psi_{z,j}|^4 + 2U_{xy} |\psi_{x,j}|^2 |\psi_{y,j}|^2 + 2U_{xz} |\psi_{x,j}|^2 |\psi_{z,j}|^2 + 2U_{yz} |\psi_{y,j}|^2 |\psi_{z,j}|^2.$$
(3.10)

Since (2.44) and (2.45) contain only number operators, this term is phase independent. This is not the case, however, for the processes describing the transfer of population between different orbitals.

$$H_{OD}^{(j)} = U_{xy} |\psi_{x,j}|^2 |\psi_{y,j}|^2 \cos(2(\theta_{x,j} - \theta_{y,j})) + U_{xz} |\psi_{x,j}|^2 |\psi_{z,j}|^2 \cos(2(\theta_{x,j} - \theta_{z,j})) + U_{yz} |\psi_{y,j}|^2 |\psi_{z,j}|^2 \cos(2(\theta_{y,j} - \theta_{z,j})),$$
(3.11)

where the order parameters are required to satisfy a specific onsite phase-locking. In what follows, we discuss the cases of the two- and three-dimensional lattices separately.

3.1.1 The Two-Dimensional Lattice

In the two-dimensional case, the phases between the p_x and p_y orbitals are locked with a $\pi/2$ phase difference. This can be easily noticed from the relation

$$H_{FD_{2D}}^{(j)} = U_{xy} |\psi_{x,j}|^2 |\psi_{y,j}|^2 \cos(2(\theta_{x,j} - \theta_{y,j})), \tag{3.12}$$

which is minimized for $\theta_{x,j} - \theta_{y,j} = \pm \pi/2$ ($U_{xy} > 0$). When this is combined with the stripped pattern imposed by the tunneling contributions, the phases of the order parameters become constrained as illustrated in Fig. 3.1.

Further properties of this system can be characterized from the expression of the full onsite order parameter defined in (3.3). Writing its explicit dependence on the orbital states wave-functions [7],

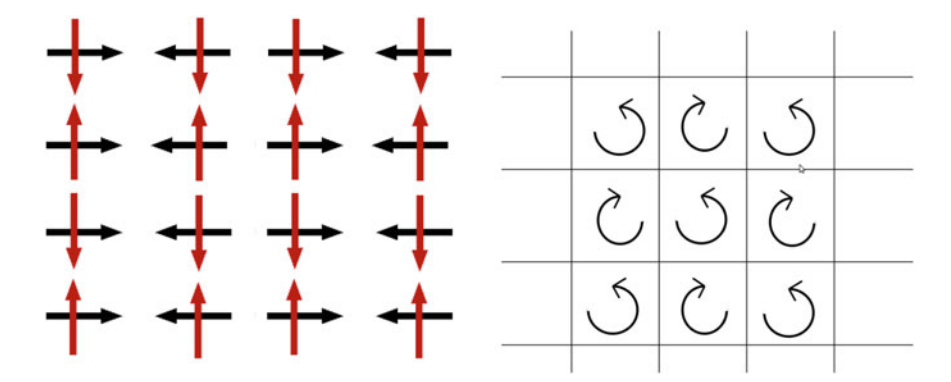


Fig. 3.1 Schematic representation of phase ordering of the different orbital states order parameters. *Left panel* The direction of the arrows are used here to define an angle. *Black* and *red arrows* describe $\theta_{x,j}$ and $\theta_{y,j}$, respectively. Notice the $\pi/2$ phase difference between $\theta_{x,j}$ and $\theta_{y,j}$, that is required for minimizing the onsite energy of the mean-field Hamiltonian Eq. (3.12). In the *right panel* we illustrate the vortex/anti-vortex structure at different lattice sites

$$\psi_j(\mathbf{r}) = \psi_{x,j} w_{x,j}(\mathbf{r}) + \psi_{y,j} w_{y,j}(\mathbf{r})$$
(3.13)

and using the condition of $\pi/2$ phase difference between the two orbitals, we obtain

$$\psi_{j}(\mathbf{r}) = |\psi_{x,j}| w_{xj}(\mathbf{r}) \pm i |\psi_{y,j}| w_{y,j}(\mathbf{r}). \tag{3.14}$$

Four lessons can be learnt from this expression: First, that the \pm sign alternates between neighbouring sites, defining a staggered configuration for the onsite current flowing between the condensates in the p_x and p_y orbitals. Second, that the phase locking of Eq. (3.14) enforces the density $|\psi_j(r)|^2$ to be maximally spread on the sites, which additionally minimizes the interaction energy. Third, that the complex character of the order parameter yields a lowest energy state with non-zero angular momentum. Finally, the fourth lesson we learn is that since the Wannier functions satisfy the orthonormality conditions (2.12), the onsite order parameter can be interpreted as a spinor with the form

$$\psi_{j} = \begin{bmatrix} |\psi_{x,j}| \\ \pm i |\psi_{y,j}| \end{bmatrix}, \tag{3.15}$$

where the basis states contain all the spatial dependence of the orbital wave-functions $w_{x,j}(\mathbf{r})$ and $w_{y,j}(\mathbf{r})$, and where the length of the spinor gives the onsite atom number, i.e., $N_j = \sqrt{|\psi_{x,j}|^2 + |\psi_{y,j}|^2}$. In this formulation the order parameter can be fully characterized by a *Bloch vector* $J_j = (J_{x,j}, J_{y,j}, J_{z,j})$, with components

$$J_{x,j} = \psi_{x,j}^* \psi_{y,j} + \psi_{y,j}^* \psi_{x,j},$$

$$J_{y,j} = i(\psi_{x,j}^* \psi_{y,j} - \psi_{y,j}^* \psi_{x,j}),$$

$$J_{z,j} = |\psi_{x,j}|^2 - |\psi_{y,j}|^2,$$
(3.16)

that corresponds to a mean-field version of the *Schwinger bosons* [8]. The length of the Bloch vector determines the total number of atoms at the site j, $|J_j| = N_j$, and $J_{z,j}$ computes the onsite population imbalance between atoms occupying p_x -and the p_y -orbital states. Due to the required onsite phase-locking relation, $J_{x,j}$ is always zero.

We now study the spatial dependence of the order parameter that is absent in the Bloch vector picture. In the simplest case of the harmonic approximation, where the Wannier functions can be taken as Hermite polynomials (see Sect. 2.3.1), the onsite order parameter is given by

$$\psi_{j}^{(ha)} = \left[|\psi_{x,j}| x \pm i |\psi_{y,j}| y \right] e^{-\frac{x^2 + y^2}{\sigma^2}}, \tag{3.17}$$

where the effective width of the oscillator σ^2 is determined from the lattice parameters. If $|\psi_{x,j}| = |\psi_{y,j}|$, then this is an angular momentum eigenstate, $L_{z,j} = -i\partial_{\theta_j}$, $L_{z,j}\psi_j^{(ha)}(\mathbf{r}) = \pm \psi_j^{(ha)}(\mathbf{r})$, and in the whole lattice, the order parameter is in a staggered-vortex configuration as shown in Fig. 3.1. In terms of the Bloch sphere, $J_{x,j} = 0$ for every j^7 and the Bloch vector points parallel to the direction defined by $J_{y,j}$.

Outside the harmonic approximation, when the Wannier functions are the proper solutions of the Mathieu equation, the onsite vortices/anti-vortices are not necessarily eigenstates of $L_{z,j}$ even when $J_{z,j} = 0$. However, the onsite order parameter has vanishing density at the center of the site with a vortex-like singularity. In the same way, a staggered-vortex-like solution permeates the entire lattice.

3.1.2 The Three-Dimensional Lattice

In three-dimensional lattices,⁸ the onsite order parameter has components L_{α} , $\alpha = \{x, y, z\}$ and

$$\Psi_{j} = \begin{bmatrix} \psi_{x,j} \\ \psi_{y,j} \\ \psi_{z,j} \end{bmatrix} = \begin{bmatrix} |\psi_{x,j}|e^{i\theta_{x,j}} \\ |\psi_{y,j}|e^{i\theta_{y,j}} \\ |\psi_{z,j}|e^{i\theta_{z,j}} \end{bmatrix}.$$
(3.18)

⁷This was already the case due to the $\pi/2$ phase difference between p_x and p_y orbitals.

⁸We follow here the analysis of Ref. [1].

The simplest case to characterize phase properties in the state with minimum energy is that of equal occupation of the three orbitals, i.e., when $|\psi_{x,j}| = |\psi_{y,j}| = |\psi_{z,j}|$. Here, Eq. (3.11) is minimized for $\theta_{x,j} - \theta_{y,j} = \theta_{y,j} - \theta_{z,j} = \theta_{z,j} - \theta_{x,j} = \pm 2\pi/3 \pm \pi$, such that

$$\Psi_{j} = \sqrt{\frac{N_{j}}{3}} e^{i\theta_{j}} \begin{bmatrix} 1\\ e^{2\pi i/3}\\ e^{4\pi i/3} \end{bmatrix}, \tag{3.19}$$

where N_j is the total atom number at the site j and θ_j is an arbitrary phase. Here each of the orbital states has a unit of angular momentum per atom which points along the axis $L \propto (\pm 1, \pm 1, \pm 1)$. Now since the phase relation to be satisfied is a (dependent) linear combination of the phases of the different orbital states and $U_{\alpha\beta} > 0$, the relative phases of the orbital order parameters are frustrated. This property was previously pointed out in Ref. [9], where it is argued that "the onsite frustrated phase configurations come in two different "chiralities" that cannot be converted into each other by shifting any one of the phases by the π shift allowed by the Z_2 symmetry". Namely, in a right-hand configuration defined by current flow from the $p_x \to p_y \to p_z \to p_x$ orbitals, the phases are given by $\theta_{x,j} = 0$, $\theta_{y,j} = 2\pi/3$ and $\theta_{z,j} = 4\pi/3$. Analogously, in the left-hand configuration current flows from the $p_x \leftarrow p_y \leftarrow p_z \leftarrow p_x$ orbitals and $\theta_{x,j} = 0$, $\theta_{y,j} = 4\pi/3$ and $\theta_{z,j} = 2\pi/3$. In particular, the direction of the current flow is not affected by addition of π to any of the phases.

In light of the frustrated character of the phase relation in the three orbital case, one can use known properties of the onsite phase lockings to investigate the system even further. For example, let us assume the specific phase locking of Eq. (3.19) and reverse the question by asking: Is this phase relation valid regardless of the values of $U_{\alpha\alpha}$ and $U_{\alpha\beta}$, or is there any condition imposed over the values of these couplings?

We follow here the approach of Ref. [1], and re-write the interacting part of the mean-field Hamiltonian as 10

$$H_{nn} = \frac{U_{xx}}{2} (n_x^2 + n_y^2 + n_z^2) + 2U_{xy} (n_x n_y + n_x n_z + n_y n_z),$$

$$H_{FD} = U_{xy} \left(\cos(\Delta_{xy}) n_x n_y + \cos(\Delta_{xz}) n_x n_z + \cos(\Delta_{xz} - \Delta_{xy}) n_y n_z \right),$$
(3.20)

where $n_{\alpha} = |\psi_{\alpha}|^2$, and $\Delta_{\alpha\beta} = 2(\theta_{\alpha} - \theta_{\beta})$. In these terms, defining $\mathbf{n} = (n_x, n_y, n_z)$, the interaction energy functional can be written in the quadratic form of the n_{α} variables,

$$E[\psi_x, \psi_y, \psi_z] = \mathbf{n}^T \mathbf{M} \mathbf{n}, \tag{3.21}$$

⁹We refer to the original reference [9] for more discussions on the properties of the broken symmetry phase of three orbital system.

¹⁰Due to typos in Ref. [1], there are different factors in the calculations presented here. We point out, however, that this does not change the conclusions drawn by the authors.

with

$$\mathbf{M} = \begin{bmatrix} U_{xx}/2 & U_{xy}(2 + \cos(\Delta_{xy})) & U_{xy}(2 + \cos(\Delta_{xz})) \\ U_{xy}(2 + \cos(\Delta_{xy})) & U_{xx}/2 & U_{xy}(2 + \cos(\Delta_{xz} - \Delta_{xy})) \\ U_{xy}(2 + \cos(\Delta_{xz})) & U_{xy}(2 + \cos(\Delta_{xz} - \Delta_{xy})) & U_{xx}/2 \end{bmatrix}.$$
(3.22)

Solving for the eigenvalues we find

$$\lambda_1 = U_{xx} - 3U_{xy}$$

$$\lambda_2 = U_{xx} - 3U_{xy}$$

$$\lambda_3 = U_{xx} + 6U_{xy},$$
(3.23)

which requires $U_{xx} > 3U_{xy}$ for having a positive definite matrix M. When this condition is violated, the onsite order parameters cannot lock the phases as in Eq. (3.21). In fact, since for this range of parameters M is not positive definite, fluctuations on the top of the state with definite phase become divergent and therefore any type of ordering is destroyed. Nevertheless, in sinusoidal optical lattices $U_{xx} > 3U_{xy}$, and therefore this analysis suggests the possibility of finding a degenerate ground-state with different configurations of phase locking. It also reveals an additional limitation of the harmonic approximation, in which case $U_{xx} = 3U_{xy}$.

As a final remark we stress that a complete characterization of the frustrated phases in the three-orbital state requires the study of the $|\psi_{x,j}| \neq |\psi_{y,j}| \neq |\psi_{z,j}|$ case, where qualitative properties are expected to be different. Here we refer the reader to Ref. [1].

3.2 Mean-Field Properties of the Bosonic System in the *d* Band

In this section we study the phase diagram of the superfluid to Mott-insulator transition of the system with bosonic atoms in the d band of 2D isotropic square lattices. While the properties of the Mott insulator phase are studied in details in Sect. 5.4, we focus here on the description of the superfluid phase from a mean-field perspective. Before proceeding, however, we discuss the techniques used in the computation of the phase diagram.

¹¹This section is based on the work of Ref. [10].

In the mean-field approach of Sect. 3.1, the superfluid phase of the p-band system was characterized by combining the onsite solutions minimizing the local part of the mean-field Hamiltonian, Eqs. (3.10) and (3.11), with the conditions required for minimizing the kinetic term. The result was the global (long-range) phase coherence implemented as a staggered-vortex configuration. While this approach usually provides an accurate description deep in the superfluid phase, it is not suitable for capturing the transition to the Mott insulator state.

A next step for improving this naïve mean-field description is provided by the Gutzwiller mean-field technique [11, 12]. It is based on the use of an ansatz for the system's wave-function, that although still factorized on the site indices, is constructed such as to include onsite number fluctuations in a self-consistent way. Next, this wave-function is used to compute an energy functional whose ground-state properties are used to characterize the many-body system. The improvement here is that the Gutzwiller method accounts for Gaussian fluctuations on the top of the saddle point solution, obtained from the partition function in the representation of coherent states. 12 More specifically, and already in the notation of the d orbitals,

$$|\Psi\rangle_{\text{Gutz}} = \prod_{i} c_i |\phi_i\rangle_i,$$
 (3.24)

with the wave-function at the site i given by

$$|\phi_{i}\rangle = \sum_{n_{\chi^{2},n_{\chi^{2}},n_{xy}}} c_{n_{\chi^{2},n_{\chi^{2}},n_{xy}}}^{(i)} |n_{\chi^{2}},n_{y^{2}},n_{xy}\rangle.$$
(3.25)

 $|n_{x^2},n_{y^2},n_{xy}\rangle$ is a Fock state with n_β atoms n the d_β orbital, for $\beta=\{x^2,y^2,xy\}$, which is normalized as $\sum_{n_{x^2},n_{y^2},n_{xy}}|c_{n_{x^2},n_{y^2},n_{xy}}^{(i)}|^2=1$. The energy functional is then written as $E_{\rm Gutz}\Big[c_{n_{x^2},n_{y^2},n_{xy}}^{(i)}\Big]={}_{\rm Gutz}\langle\Psi|\hat{H}|\Psi\rangle_{\rm Gutz}$, for the Hamiltonian of Eq. (2.55). This is further minimized with use of the Nelder–Mead algorithm, with the self-consistently obtained amplitudes $c_{n_{x^2},n_{y^2},n_{xy}}^{(i)}$. In particular, since the Mott state is characterized by vanishing number fluctuations, the Gutzwiller order parameter $\psi_{d_\beta}={}_{\rm Gutz}\langle\Psi|\hat{d}_\beta|\Psi\rangle_{\rm Gutz}$ also vanishes in this phase, in contrast with the superfluid, where it has nonzero values.

The Mott phases with different fillings are mapped out after inclusion of the chemical potential μ . This yields the Hamiltonian (see Eq. (2.55))

$$\hat{H}^d + \hat{H}^{xy} \to \hat{H}^d + \hat{H}^{xy} - \mu \sum_{i} \hat{n}_i,$$
 (3.26)

 $^{^{12}}$ In particular, even though mean-field methods are usually not very reliable in low dimensions, the Gutzwiller ansatz provides a good estimate of the boundaries of the superfluid to Mott insulator transition in the *s* band even in 2*D* [11, 12].

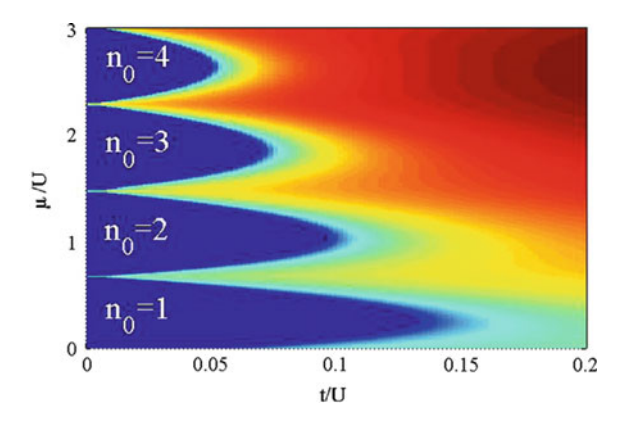


Fig. 3.2 Order parameter $\psi = |\langle \hat{d}_{x^2,i} \rangle| = |\langle \hat{d}_{y^2,i} \rangle|$ of the superfluid phase of bosonic atoms in the d band. The corresponding order parameter for the d_{xy} -orbital is approximately zero except for $t/U < 10^{-3}$ where it is, however, at least one order of magnitude smaller than ψ . As is seen, the chemical potential is varied such that the first four Mott lobes are illustrated (dark blue regions representing a vanishing superfluid order parameter). For this plot, the relative strengths between the interaction terms has been taken as $\{U_{xy}, U_{pp}, U_{px}, U_{n_pxy}, U_{n_xxy}\}/U = \{0.17, 0.9, 0.3, 0.04, -0.03\}$, with $U = U_{xx} = U_{yy}$ and corresponding to a lattice with amplitude V = 40. With this lattice depth, $E_{x^2} = E_{y^2} = 0$ and $E_{xy} = 1.6U$, and the relative tunnelings are $\{t_{\perp}^{\alpha}, |t^p|\}/t_{\parallel}^{\alpha} = \{0.002, 0.007\}$ (Reprinted from Ref. [2])

with $\hat{n}_i = \hat{n}_{x^2,i} + \hat{n}_{y^2,i} + \hat{n}_{xy,i}$. The numerical study is performed in a truncated Hilbert space of dimension 64, that accounts for up to three atoms in each of the three onsite orbital states. Also, since out of four nearest neighbours the tunneling amplitudes are t_{\parallel}^{α} and t_{\perp}^{α} for the two neighbouring sites in the directions parallel and perpendicular to the node of the wave-functions, the effective Gutzwiller tunneling is taken as $t = 2(t_{\parallel}^{\alpha} + t_{\perp}^{\alpha})$. The results, presented in Fig. 3.2, show the superfluid order parameter $\psi = \langle \hat{d}_{x^2,i} \rangle = \langle \hat{d}_{y^2,i} \rangle$ in the μt -plane for the energies scaled with $U_{\alpha\alpha}$ (see Eq. (2.69)). The order parameter signalling occupation of the d_{xy} orbital, ψ_{xy} is zero everywhere, except for $t/U_{\alpha\alpha} < 10^{-3}$. However, still in this case the occupation of the d_{xy} orbital is two orders of magnitude smaller than of the other two orbitals, and therefore, the dynamics of bosons on the d band can be described by the effective two-orbital model of Eq. (2.56). In addition, Fig. 3.2 also shows that the extent of the Mott lobes fall off with n_0^{-1} , for n_0 the lattice filling. This is in agreement with mean-field results obtained for the Bose-Hubbard model in the ground band.

At higher fillings when the typical interaction energy becomes considerably larger than the gap between the E_{xy} and E_{α} bands, we expect that the d_{xy} orbital will also become populated. Indeed, as we checked numerically, for the same parameters used in Fig. 3.2, and $\{\mu, t\}/U = \{5, 0.5\}$, for example, the occupations of the three orbitals are given by $(\langle \hat{n}_{x^2} \rangle, \langle \hat{n}_{y^2} \rangle, \langle \hat{n}_{xy} \rangle) \approx (3.3, 3.3, 1.7)$. Here, however, due to the higher truncation required in the number of particles, computations are considerably more costly than for the system at low densities, and are thus carried out for a fixed value of the chemical potential μ/U and for varying t/U. In addition, this suggests that

the spatial structure of the onsite order parameter should be studied separately for the system with both low and high densities, as we continue next.

3.2.1 Onsite Superfluid States

Low/Moderate Atomic Densities The same approach used in Sect. 3.1.1 to study the spatial shape of the onsite order parameter of the system in the p band can be adapted for the d-band case. Direct generalization of the onsite vortex structure suggest that the full onsite order parameter in the d band is characterized by doubly-quantized vortices, as described by a state of the form

$$\Psi(\mathbf{r}) = \frac{\sqrt{N_s}}{2} \left[w_{x^2}(\mathbf{r}) + w_{y^2}(\mathbf{r}) \pm \sqrt{2}i w_{xy}(\mathbf{r}) \right]$$

$$\Leftrightarrow$$

$$\Psi = \sqrt{N_s}/2 \begin{pmatrix} 1 \\ -1 \\ \pm \sqrt{2}i \end{pmatrix},$$
(3.27)

where N_s is the number of atoms at the site and is fixed a priori. At low densities the existence of such a state is precluded, however, since according to the Gutzwiller study the d_{xy} orbital has negligible occupation. In addition, it is not possible to construct a doubly-quantized vortex with only the d_{x^2} and d_{y^2} states.

To explore the possibilities and to characterize the spatial properties of the full onsite order parameter, we study the mean-field version of Hamiltonian (2.55), obtained with use of the coherent-state ansatz. In this picture

$$\hat{d}_{\alpha,i} \to \psi_{\alpha,i} = |\psi_{\alpha,i}| e^{i\theta_{\alpha,i}},\tag{3.28}$$

which yields

$$H_{MF}^{d} = -\sum_{\sigma,\alpha} \sum_{\langle i,j \rangle_{\sigma}} 2t_{\sigma}^{\alpha} |\psi_{\alpha,i}| |\psi_{\alpha,j}| \cos\left(\theta_{\alpha,i} - \theta_{\alpha,j}\right) + \sum_{\alpha} \sum_{i} E_{\alpha} n_{\alpha,i} + \sum_{\alpha} \sum_{i} \frac{U_{\alpha\alpha}}{2} n_{\alpha,i}^{2} + \sum_{\alpha} 2U_{\alpha\beta} n_{\alpha,i} n_{\beta,i} + \sum_{\alpha} \sum_{i} U_{\alpha\beta} |\psi_{\alpha,i}|^{2} |\psi_{\beta,i}|^{2} \cos\left(2(\theta_{\alpha,i} - \theta_{\beta,i})\right) + \sum_{\alpha} \sum_{i} 2U_{n_{\alpha}\alpha\beta} |\psi_{\alpha,i}|^{3} |\psi_{\beta,i}| \cos\left(\theta_{\alpha,i} - \theta_{\beta,i}\right),$$

$$(3.29)$$

for α , $\beta = \{x^2, y^2\}$, and with the sum over nearest neighbours running through each pair only once. Even though this approximation is valid for systems with up to ~ 10 particles per site, we believe this still gives a good picture of the superfluid state. Indeed, as we see next, the study of the three-orbital system predicts a similar state for describing the onsite superfluid.

In the same way as for the system in the p band, the order parameter of the superfluid phase in the d band is a complex number and requires the study of both the density and phase properties. But with the atoms occupying only the d_{x^2} and d_{y^2} states, and with equal population, we can resume the study to characterization of phase properties. We then start with the local part of (3.29) and notice the dependence on the relative phase $\delta_i = \theta_{x,i} - \theta_{y,i}$ of the individual order parameters for the superfluid in the d_{x^2} and d_{y^2} orbitals. Contrary to the system in the p band, where the relative phase of $\pi/2$ is determined by the orbital changing processes, the system in the p band features the additional density-assisted interactions that are minimized by a p relative phase at each site. We therefore minimize the full Eq. (3.29) with respect to δ_i to obtain

$$\bar{\delta}_i = \arccos\left(-\frac{U_{n_x x y}}{U_{x y}}\right),\tag{3.30}$$

where $\bar{\delta}_i$ is the relative phase, onsite, at the energy minimum.

This leads to the solution

$$\Psi_{\text{vor}}(\mathbf{r}) = \sqrt{\frac{N_s}{2}} \left(w_{x^2}(\mathbf{r}) e^{i\delta_i} + w_{y^2}(\mathbf{r}) \right), \qquad (3.31)$$

which is illustrated in Fig. 3.3 for the system with V=40. In Fig. 3.3a we show the atomic onsite density $|\Psi_{vor}(\mathbf{r})|^2$, and in b, the phase of the order parameter

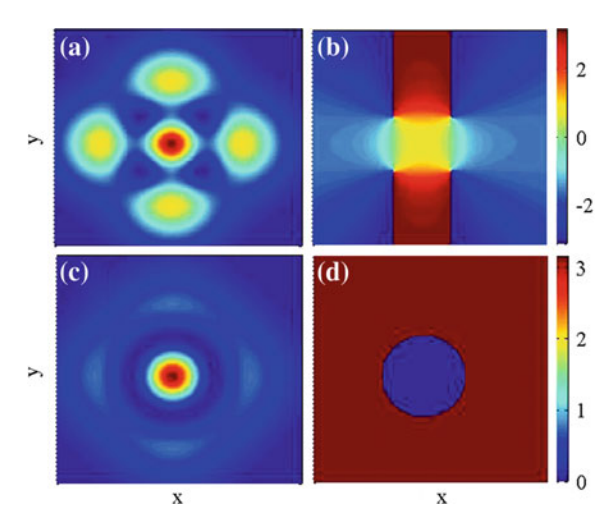


Fig. 3.3 The onsite density $|\Psi(\mathbf{r})|^2/N_s$ and the corresponding phases $\text{Arg}[\Psi(\mathbf{r})]$ in \mathbf{a} and \mathbf{c} , and \mathbf{b} and \mathbf{d} , respectively. Here we assumed that the atomic density is rather low such that we can neglect any population of the d_{xy} orbital. In the *upper* two plots we consider a lattice with an amplitude V=40. It is seen in (b) that the phase of the order parameter winds 2π at the four points where the density vanishes. This reflects the presence of four vortices - two vortex/anti-vortex pairs. In the *lower* two plots we use the same parameters but put $U_{n_x xy} = -2U_{xy}$ in order to reach the regime where the state qualitatively changes. Here a *dark* soliton is separating the central peak from the surrounding *circle* (Reprinted from Ref. [2])

Arg[$\Psi(r)$]. At each site, the condensate order parameter is characterized by two vortex/anti-vortex pairs, each of which has a $\pm 2\pi$ phase winding around the singularity point. Now since the tunneling in the d band has the same sign in both the parallel and the perpendicular directions, i.e., t_{\parallel}^{α} , $t_{\perp}^{\beta} > 0$, the orientation of the onsite vortices at neighbouring sites is the same. Due to the underlying Z_2 symmetry of the system, each of the two vortex-lattices with different orientations correspond to a state with spontaneously broken symmetry. In the solution of Fig. 3.3, and starting at the upper left corner, the phase winding is clockwise/anti-clockwise/clockwise/anti-clockwise/clockwise/anti-clockwise/clockwise winding instead.

Now how does the state with restored Z_2 symmetry looks like? We answer this question by noticing that the phase dependence on $R = U_{n_x xy}/U_{xy}$ is the factor determining the shape of the onsite vortex pairs. In fact, for R = 1, the vortices are annihilated by the anti-vortices. When R > 1, the onsite order parameter is given by

$$\Psi_{\text{sol}}(\mathbf{r}) = \sqrt{\frac{N_s}{2}} \left(w_{d_{x^2}} \pm w_{d_{y^2}} \right), \tag{3.32}$$

and as shown in Fig. 3.3c, d, it is characterized by an immobile *dark soliton* with vanishing density at the circle, together with a phase jump from 0 to π . In case where the ratio R could be externally controlled, this system would be driven through a phase transition from a "soliton"-superfluid to a "vortex"-superfluid with broken Z_2 symmetry. In addition, the discontinuity of $\partial_R H_{MF}^d|_{R=1}$ suggests the existence of a first order phase transition. We remark, however, that even though this external tuning of R might be experimentally non-trivial, this analysis is nevertheless useful for shedding additional light on the properties of the superfluid phase of bosonic atoms in the d band.

High Atomic Densities At large fillings, $n_0 \gg 1$, minimization of the energy functional must be handled with the additional d_{xy} orbital. Therefore we use Eq. (3.28) together with the equivalent expression for the d_{xy} orbital $\psi_{xy,i} = |\psi_{xy,i}|e^{i\theta_{xy,i}}$, and we write the full mean-field Hamiltonian for the system in the d band

$$H_{MF} = H_{MF}^d + H_{MF}^{xy}, (3.33)$$

where

$$H_{MF}^{xy} = -\sum_{\sigma} \sum_{\langle i,j \rangle_{\sigma}} 2t^{p} \cos\left(\theta_{\alpha,i} - \theta_{\alpha,j}\right) + \sum_{i} \frac{U_{pp}}{2} n_{xy,i} \left(n_{xy,i} - 1\right) + \sum_{\alpha} \sum_{i} 2U_{p\alpha} n_{xy,i} n_{\alpha,i}$$
$$+ \sum_{\alpha} \sum_{i} \left[U_{p\alpha} |\psi_{xy,i}|^{2} |\psi_{\alpha,i}|^{2} \cos\left(2(\theta_{\alpha,i} - \theta_{xy,i})\right) + \sum_{\beta} 4U_{n_{p}xy} \cos\left(\theta_{\alpha,i} - \theta_{\beta,i}\right) + \sum_{\beta} 2U_{n_{\alpha}xy} |\psi_{xy,i}|^{2} |\psi_{\alpha,i}| |\psi_{\beta,j}| \cos\left(2\theta_{xy,i} - (\theta_{\alpha,i} - \theta_{\beta,i})\right) \right].$$
(3.34)

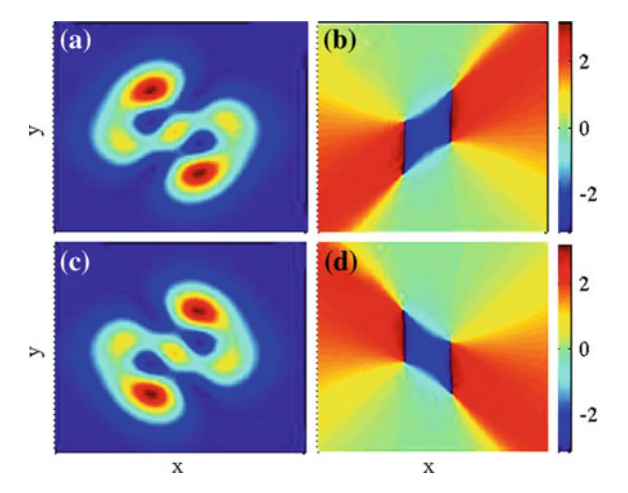


Fig. 3.4 The same as Fig. 3.3 but deep in the superfluid phase $(n_0 \gg 1)$ where all three orbitals are considerably populated. The difference between the *upper* and *lower* plots is the sign of the order parameter $\psi_{d_{xy}}$ (the two states have equal energy), which reflects the states in two neighbouring sites in the lattice. Despite the fact that the d_{xy} orbital is largely populated in this case, the general structure of the superfluid state shown in Fig. 3.3 a and b survives, i.e., the onsite order parameter hosts two vortex/anti-vortex pairs. However, the state gets distorted with two of the vortices at the very edge of the distribution. As for Fig. 3.3, the potential amplitude V=40 (Reprinted from Ref. [2])

Since the analytical expression of the fix point is not of much help in this case, we continue with a numerical study. Here again, we minimize the mean-field Hamiltonian with use of the Nelder-Mead algorithm. The result is shown in Fig. 3.4, where the onsite occupations of the orbitals are given by $(d_{x^2}, d_{y^2}, d_{xy}) =$ (0.36, 0.33, 0.31) such that no specific dominance is found. In comparison with the results of the previous case, the vortex/anti-vortex pairs are rotated in the presence of d_{xy} -orbital atoms, and the atomic distribution is squeezed. In addition, this example clearly shows the tendency of the vortices with positive winding to migrate to the center of the site, where the density is higher. This suggests that as interactions become stronger, and the density more squeezed, two of the vortices will be located in regions with vanishingly small density such that the onsite state would be closer to a state with doubly quantized vortices. However, this continuous deformation does not violate conservation of angular momentum, since in reality this corresponds to two singly excited vortices coming infinitely closed to each other. Furthermore, due to $t^p < 0$, the ψ_{xy} changes sign between neighbouring sites such that the orientation of the doubly excited vortices alternate in the full lattice, yielding a state with zero angular momentum. The two possible orientations are again related to the breaking of the Z₂ symmetry, and we have checked that also here, the state with restored symmetry is characterized by a dark soliton.

In summary, even in the presence of the third d_{xy} orbital, the onsite superfluid preserves the structure of the effective two-orbital system discussed in the

previous section. Therefore, rather than doubly quantized vortices, as one could in principle expect in analogy with the results obtained for the p-band system, the onsite superfluid state in the d band features pairs of vortices/anti-vortices.

References

- Collin A, Larson J, Martikainen J-P (2010) Quantum states of p-band bosons in optical lattices. Phys Rev A 81(2):023605
- Pinheiro F, Martikainen J-P, Larson J (2015) Phases of d-orbital bosons in optical lattices. arXiv:1501.03514
- Altland A, Simons B (2006) Condensed matter field theory. Cambridge University Press, Cambridge
- Pethick CJ, Smith H (2002) Bose-Einstein condensation in dilute gases. Cambridge University Press, Cambridge
- Scully MO, Zubairy SM, Walmsley LA (1999) Quantum optics. vol 67, 1st edn. Cambridge University Press, Cambridge
- 6. Behroozi P (2008) http://large.stanford.edu/courses/2008/ph372/behroozi2/
- 7. Pinheiro Fernanda, Martikainen Jani-Petri, Larson Jonas (2012) Confined p-band Bose-Einstein condensates. Phys Rev A 85(3):033638
- 8. John SJ (1985) Mechanics modern quantum, Tuan San Fu (eds) vol 1. Wesley Addison,
- Isacsson A, Girvin SM (2005) Multiflavor bosonic Hubbard models in the first excited Bloch band of an optical lattice. Phys Rev A 72(5):053604
- Pinheiro F (2014) p orbitals in 3D lattices; fermions, bosons and (exotic) models of magnetism. arXiv:1410.7828
- Amico Luigi, Penna Vittorio (1998) Dynamical mean field theory of the Bose-Hubbard model. Phys Rev Lett 80(10):2189
- 12. Jaksch D, Venturi V, Cirac JI, Williams CJ, Zoller P (2002) Creation of a molecular condensate by dynamically melting a Mott insulator. Phys Rev Lett 89(4):040402

Chapter 4 Confined *p*-Orbital Bosons

In the laboratory, experiments with optical lattices are most often performed in the presence of an additional external potential for confining the atoms. The confining potential is typically much weaker¹ than the optical lattice, and has a characteristic length scale much larger than the lattice period. However, the presence of an external trap gives the system an inhomogeneous density, which can have important consequences for the phase diagram. In fact, different regions with locally homogeneous densities are now allowed to coexist in the lattice for a given set of parameters, and therefore considerations of trapped systems are important for obtaining a more realistic picture of the systems under study.

The mean-field analysis carried in Chap. 3 revealed the structure of the order parameter characterizing the homogeneous system of bosonic atoms in the p band. In isotropic square lattices, for example, we have seen that the state with minimum energy exhibits alternating vortices/anti-vortices at neighbouring sites, that define a staggered configuration for the onsite current flowing between the condensates in the p_x and p_y orbitals. But how is this picture modified when the system is in the presence of an external confining potential?

In this chapter, we study the superfluid phase of p-orbital bosons confined by a harmonic trap. In light of the anisotropic tunneling in the p band, how is the inhomogeneous density modifying the physics of the homogeneous system? This is the question addressed in Ref. [1]. We will follow it here, starting with the analysis of the the ideal gas in the p band in Sect. 4.1, where we also study finite temperature properties. We consider the interacting case from a mean-field perspective in Sect. 4.2, and conclude with a study of the system in anisotropic lattices in Sect. 4.3.

¹In the sense that the leading physics stems from the optical potential.

4.1 The Ideal Gas

Let us start by considering the simplest case of the non-interacting system in an isotropic optical lattice and in the presence of the harmonic trap

$$V_{\text{trap}}(\mathbf{r}) = \frac{m\tilde{\omega}}{2}(x^{2} + y^{2}) = \frac{\omega}{2}(x^{2} + y^{2}). \tag{4.1}$$

Here $\tilde{\omega}$ is the trap frequency, $\omega = \sqrt{2}m\tilde{\omega}/\hbar k^2$ is the dimensionless trap frequency, with k the wave-vector of the laser, and $x = kx^{'}$ and $y = ky^{'}$ are dimensionless positions.

The Hamiltonian describing this system is given by

$$H^{(0)} = -\sum_{\sigma,\alpha} \sum_{\langle i,l \rangle_{\sigma}} t_{\sigma}^{\alpha} \psi_{\alpha,i}^{*} \psi_{\alpha,j} + \sum_{\alpha} \sum_{j} \frac{\omega^{2}}{2} (x_{j}^{2} + y_{j}^{2}) n_{\alpha,j}, \tag{4.2}$$

where $n_{\alpha,j} = |\psi_{\alpha,j}|^2$ is the onsite density of the p_{α} -orbital state, $\alpha = \{x, y\}$.

A remark is in order: For consistency with the notation used in the analysis to be carried out in the next section, we use here the mean-field notation for the analysis of the ideal gas. Notice, however, that since the non-interacting case has a quadratic Hamiltonian, we have actual access to the exact solutions of the problem, rather than that of an effective description.

We proceed with the Schrödinger equation for (4.2),

$$i\frac{\partial}{\partial t}\Psi = H^{(0)}\Psi. \tag{4.3}$$

As stated before, this equation is governed by a quadratic Hamiltonian that we notice, furthermore, has similar structure to the Mathieu equation expanded in momentum eigenstates [2]. This can be written in matrix form, for each of the orbital states and say, for the 2D system³ as

²Notice that the characteristic length of the trap $l_{\text{trap}} \gg \lambda/2$, where λ is the wavelength of the laser.

 $^{^3}$ Since it is straightforward to write the matrix form of the ideal gas Hamiltonian in the 3D lattice, we only write explicit expressions of the 2D case here.

4.1 The Ideal Gas 51

$$i\frac{\partial}{\partial t} \begin{pmatrix} \vdots \\ \psi_{\alpha,(i-1,\{j\})} \\ \psi_{\alpha,(i,\{j\})} \\ \psi_{\alpha,(i+1,\{j\})} \\ \vdots \end{pmatrix} = \begin{pmatrix} \ddots & \vdots \\ h_{i-2,\{j\}}^{(0)} & -t_{y}^{\alpha} & 0 & 0 & 0 \\ \dots & -t_{y}^{\alpha} & h_{i-1,\{j\}}^{(0)} & -t_{y}^{\alpha} & 0 & 0 & \dots \\ \dots & 0 & -t_{y}^{\alpha} & h_{i,\{j\}}^{(0)} & -t_{y}^{\alpha} & 0 & \dots \\ \vdots & & \ddots & \vdots \end{pmatrix} \begin{pmatrix} \vdots \\ \psi_{\alpha,(i-1,\{j\})} \\ \psi_{\alpha,(i,\{j\})} \\ \psi_{\alpha,(i+1,\{j\})} \\ \vdots \end{pmatrix}.$$

$$\vdots & \ddots & \vdots$$

$$\vdots & \ddots & \vdots \\ (4.4)$$

In this notation, $H^{(0)}$ is a $2N \times 2N$ matrix, where N counts the number of sites, $\psi_{\alpha,(i,\{j\})}$ is a $N \times 1$ vector whose label j runs over all the columns of the ith row, i.e., $\psi_{\alpha,(i,\{j\})}^* = (\psi_{\alpha,(i,1)}, \psi_{\alpha,(i,2)}, \ldots)$,

$$\boldsymbol{h}_{i,\{j\}}^{(0)} = \begin{pmatrix} \ddots & & \vdots & & & \\ & \frac{\omega^2}{2} R_{i,j-2}^2 & -t_x^{\alpha} & 0 & 0 & 0 \\ \dots & -t_x^{\alpha} & \frac{\omega^2}{2} R_{i,j-1}^2 & -t_x^{\alpha} & 0 & 0 & \dots \\ \dots & 0 & -t_x^{\alpha} & \frac{\omega^2}{2} R_{i,j}^2 & -t_x^{\alpha} & 0 & \dots \\ & 0 & 0 & -t_x^{\alpha} & \frac{\omega^2}{2} R_{i,j+1}^2 -t_x^{\alpha} & & & \\ & \vdots & & \ddots \end{pmatrix}$$

$$(4.5)$$

is a 1*D* tight-binding Hamiltonian, and $-t_y^{\alpha} = -t_y^{\alpha} \mathbb{1}_{N \times N}$, where $\mathbb{1}_{N \times N}$ is the identity matrix of size $N \times N$. Analytical solutions of Eq. (4.4) can be obtained for special cases, from Fourier expansions of the Mathieu functions. However, since the expressions can be cumbersome, not much is learnt by taking a step in this direction [2].

On the other hand, an analytical study of the trapped system can be performed in the continuum limit, where the solutions of the problem have simpler closed form. In this framework we make $\psi_{\alpha,j} \to \psi_{\alpha}(x,y)$, and the expression of the kinetic energy becomes

$$\psi_{\alpha,j+\mathbf{1}_{\sigma}} - 2\psi_{\alpha,j} + \psi_{\alpha,j-\mathbf{1}_{\sigma}} \to \frac{\partial^2}{\partial \sigma^2} \psi_{\alpha}(x,y).$$

The corresponding Schrödinger equations then reads,

$$i\frac{\partial}{\partial t}\psi_{x}(x,y) = \left[-|t_{x}^{x}|\partial_{x}^{2} - |t_{y}^{x}|\partial_{y}^{2} + \frac{\omega^{2}}{2}(x^{2} + y^{2})\right]\psi_{x}(x,y)$$

$$i\frac{\partial}{\partial t}\psi_{y}(x,y) = \left[-|t_{x}^{y}|\partial_{x}^{2} - |t_{y}^{y}|\partial_{y}^{2} + \frac{\omega^{2}}{2}(x^{2} + y^{2})\right]\psi_{y}(x,y),$$

$$(4.6)$$

where we have imposed a phase imprint in the wave-function ansatz. In fact, with the equations in this form, the phase factors associated to the stripped pattern in the lattice are absorbed in the redefinition of the tunneling coefficients, where we have transformed $t_{\alpha}^{\alpha} \rightarrow -t_{\alpha}^{\alpha}$.

By introducing the *effective mass* $m_{\alpha\beta} = |t_{\beta}^{\alpha}|^{-1}/2$, and parallel and transverse frequencies

$$\omega_{\parallel} = \omega \sqrt{2|t_{\beta}^{\alpha}|}, \quad \alpha = \beta$$

$$\omega_{\perp} = \omega \sqrt{2|t_{\beta}^{\alpha}|}, \quad \alpha \neq \beta,$$
(4.7)

Equation (4.6) can be further re-written as

$$i\frac{\partial}{\partial t}\psi_{x}(x,y) = \left[\frac{p_{x}^{2}}{2m_{xx}} + \frac{p_{y}^{2}}{2m_{xy}} + \frac{m_{xx}\omega_{\parallel}^{2}}{2}x^{2} + \frac{m_{xy}\omega_{\perp}^{2}}{2}y^{2}\right]\psi_{x}(x,y), \quad (4.8)$$

with a corresponding equation for the p_y orbital state. We notice, moreover, that by implementing the stripped pattern in the wave-function ansatz prior to taking the continuum limit, we avoid dealing with a Hamiltonian that is not bounded from below. This is nothing but a gauge transformation with the overall effect of inverting the p band and shifting its minimum energy to the center of the Brillouin zone, but the physics remains unaltered.

In any way, this shows that the continuum approximation enormously simplifies analytical considerations by re-writing Eq. (4.4) as the eigenvalue problem of a 2D anisotropic harmonic oscillator. In this picture, since both $m_{\alpha\sigma}$ and $\omega_{\alpha\sigma}$ (see Eq. (4.7)) depend intrinsically on the tunneling anisotropy, the ground-state $\psi_{\alpha}(x,y)$ of Eq. (4.8) will have a Gaussian profile, with different widths in the different directions. This fact can be used to characterize the system in more general terms, by defining the anisotropy parameter

$$S_x = \sqrt{\frac{(\Delta_x x)^2}{(\Delta_x y)^2}},\tag{4.9}$$

where $(\Delta_{\alpha}\beta)^2 = \langle \beta^2 \rangle_{\alpha} - \langle \beta \rangle_{\alpha}^2$, and $\langle ... \rangle_{\alpha}$ represents the expectation value taken with respect to $\psi_{\alpha}(x, y)$. Accordingly, the anisotropy in the density of p_y -orbital atoms is characterized by an equivalent expression, that in isotropic square lattices satisfies

4.1 The Ideal Gas 53

 $S_x S_y = 1$. For this reason we will now drop the subscript and use $S = S_x$ whenever discussing such anisotropies. In particular, in the continuum case discussed here

$$S_{cont} = \left(\frac{|t_x^x|}{|t_y^x|}\right)^{1/4} = \left(\frac{\omega_{\parallel}}{\omega_{\perp}}\right). \tag{4.10}$$

The limit where $\omega_{\parallel} = \omega_{\perp}$ corresponds to the case of isotropic tunneling, and yields S=1. As soon as this isotropy is broken, however, $S \neq 1$. Accordingly, this reveals that the density of atoms in each of the orbital states is narrowed down in the direction perpendicular to the label.

4.1.1 The Ideal Gas at Finite Temperatures

The possibility of re-writing the Schrödinger equation of the non-interacting system in a rather simple form allows for the study of thermodynamic properties of condensation in the p band. Let us proceed with this analysis by first considering the simplest case of the continuum limit, described in Eq. (4.6), where known properties of condensation in harmonically trapped systems can be directly used [3]. The *critical temperatures* for Bose–Einstein condensation in 2D and 3D are given by

$$T_c^{(2D)} = \omega_{eff}^{(2D)} \sqrt{6N/\pi^2} \tag{4.11}$$

and

$$T_c^{(3D)} = \omega_{eff}^{(3D)}(N/\zeta(3))^{1/3},$$
 (4.12)

where $\zeta(3) \approx 1.20206$. The effective trapping frequencies are defined [3] as

$$\omega_{eff}^{(2D)} = 3\omega \sqrt{|t_x^x||t_y^x|} \tag{4.13}$$

and

$$\omega_{eff}^{(3D)} = 4\omega(|t_x^x||t_y^x||t_z^x|)^{1/3} = 4\omega(|t_x^x||t_y^x|^2)^{1/3}.$$
 (4.14)

The critical temperatures for the discrete model can also be computed. This is done with use of numerically obtained eigenvalues of Eq. $(4.4)^4$ in

$$N_T = \sum_{n \neq 0} \frac{1}{e^{\beta(E_n - \mu)} - 1},\tag{4.15}$$

⁴Diagonalization is performed on the Hamiltonian of a truncated lattice.

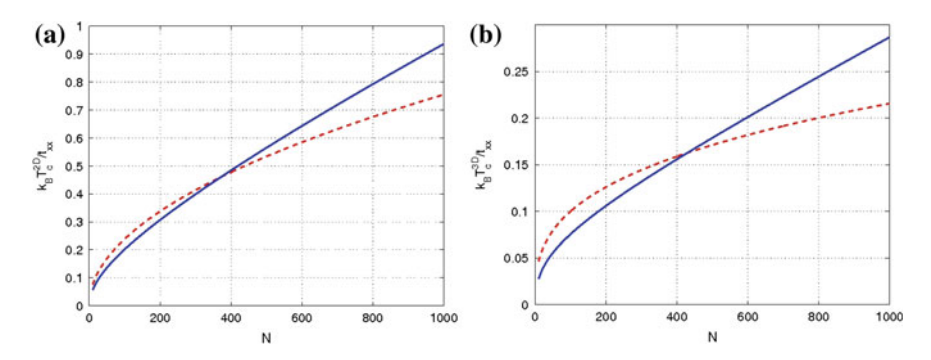


Fig. 4.1 Critical temperature for the establishment of Bose–Einstein condensation in the p band as a function of the atom number denoted by N. **a** shows the results of the 2D system while **b** shows the results for the 3D system. We also compare the results obtained for the continuum approximation (dashed line) with the results of the discrete model obtained numerically (solid line). The parameters here are $\omega^2/2 = 0.001$ for the dimensionless trap strength and $|t_x^x/t_y^x| = 20.1$, which corresponds to the ratio between the tunneling coefficients for $V_x = V_y = 17$ (Reprinted from Ref. [1]. In order to concile with the notation used here we notice that $t_{\alpha\beta} = t_{\alpha}^{\alpha}$)

where $\beta = E_r/k_BT$ is the inverse (dimensionless) temperature and μ is the chemical potential computed for a fixed number of atoms N_T .

The results are shown in Fig. 4.1, where we compare the critical temperatures of both the discrete and continuous cases. In particular, we notice the disagreements between the two predictions, which become more pronounced for increasing values of N. We understand this difference as a consequence of the different density of states in the two cases. In fact, since the general expression for the critical temperature of a confined ideal gas in d dimensions $k_B T_c \propto N^{1/d}$ depends on the density of states [4], any difference between the two cases should become more pronounced for large N.

We proceed by examining the 2D case with more details. In particular, we are interested in characterizing the behavior of the density as one crosses the transition to the condensed state: Is there any difference in the profile of the atomic density as the temperature is lowered below T_c ?

In the high temperature limit, we expect the system to show isotropic density. This is because in this regime, the system should be described by the Boltzmann distribution, which is itself isotropic. However, as the temperature is lowered, low temperature properties become relevant and the condensed state of p-orbital bosons is characterized by a bimodal structure with the atoms squeezed either in the x or the y direction of the lattice. This is illustrated in Fig. 4.2a and b, where we show the density

$$n_{total}(j) = N_0 |\psi_0(j)|^2 + \sum_{n \neq 0} \frac{|\psi_n(j)|^2}{e^{\beta(E_n - \mu)} - 1}$$
(4.16)

for two different temperatures, above T_c and for the ground state (where T=0). As expected, this behavior follows as a consequence of the tunneling anisotropy.

4.1 The Ideal Gas 55

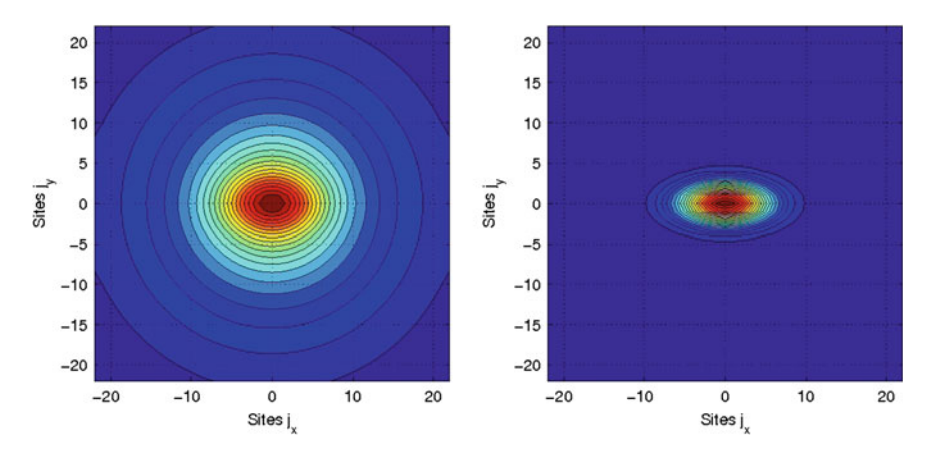
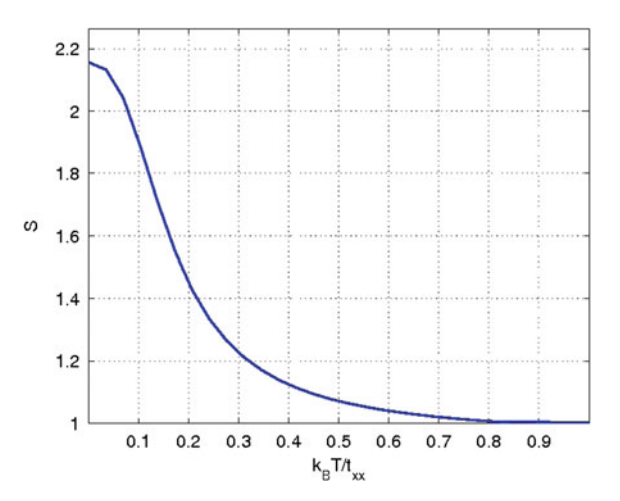


Fig. 4.2 Populations per site of the 2D Bose gas in the p band and for a single orbital state. **a** shows a situation where $T > T_c$, while in **b** T = 0. In both cases the total number of atoms in the system $N_{tot} = 1000$, the dimensionless trap strength $\omega^2/2 = 0.001$ and potential depths are $V_x = V_y = 17$ (Reprinted from Ref. [1])

Fig. 4.3 The anisotropy parameter S (see text) that is used to characterize the anisotropy in the density in the 2D system, and as a function of the temperatures scaled with t_x^x . The number of atoms considered is N=1000, the dimensionless trap strength is $\omega^2/2=0.001$ and $V_x=V_y=17$ (Reprinted from Ref. [1]. Again we notice that $t_{\alpha\beta}=t_{\beta}^{\alpha}$ in the notation of this thesis)



To conclude this analysis, we use the anisotropy parameter defined in Eq. (4.9) to characterize the density anisotropy as a function of the temperature for a system with 1000 atoms, in Fig. 4.3. As shown in Fig. 4.1a, above the (scaled) critical temperature $T_c \approx 0.9$, the atomic density becomes isotropic in the xy-plane.

4.2 Mean-Field Equations of the Interacting System in 2D

In this section we extend the approach used in Sect. 3.1 to study the interacting system of bosons in the p band confined by a harmonic potential. We first recall that the expression of the many-body Hamiltonian, Eq. (2.42), was obtained from expansion of the field operators of Eq. (2.38) in terms of the p-orbital states (2.40). For the confined system, however, the external potential contribution contains an additional term to describe the harmonic trap, i.e.,

$$V(\mathbf{r}) \rightarrow V_{\text{latt}}(\mathbf{r}) + V_{\text{trap}}(\mathbf{r}),$$
 (4.17)

where as usual

$$V_{\text{latt}}(\mathbf{r}) = V_x \sin^2(x) + V_y \sin^2(y),$$
 (4.18)

and the expression of the trap potential is given by Eq. (4.1).

As stated previously, we are considering the regime where the characteristic length of the trap $l_{\rm trap}\gg\lambda/2$, such that the system can be treated in the *local density approximation*. Under this assumption the lattice potential is approximately periodic, and the orbital states can be taken as the site-localized Wannier functions of the non-trapped case. The effects of the confinement are implemented locally, as a shift of the onsite energies, in what amounts to describing the system with a position-dependent chemical potential. The many-body Hamiltonian then follows as

$$\hat{H}_{2D} = -\sum_{\alpha} \sum_{\langle i,j \rangle_{\sigma}} t_{\sigma}^{\alpha} \hat{a}_{\alpha,i}^{\dagger} \hat{a}_{\alpha,j} + \sum_{\alpha} \sum_{j} \frac{\omega}{2} (x_{j}^{2} + y_{j}^{2}) \hat{n}_{\alpha,j}
+ \sum_{\alpha} \sum_{j} \frac{U_{\alpha\alpha}}{2} \hat{n}_{\alpha,j} (\hat{n}_{\alpha,j} - 1) + \sum_{\alpha\beta,\alpha\neq\beta} \sum_{j} U_{\alpha\beta} \hat{n}_{\alpha,j} \hat{n}_{\beta,j}
+ \sum_{\alpha\beta,\alpha\neq\beta} \sum_{j} \frac{U_{\alpha\beta}}{4} (\hat{a}_{\alpha,j}^{\dagger} \hat{a}_{\alpha,j}^{\dagger} \hat{a}_{\beta,j} \hat{a}_{\beta,j} + \hat{a}_{\beta,j}^{\dagger} \hat{a}_{\beta,j}^{\dagger} \hat{a}_{\alpha,j} \hat{a}_{\alpha,j}),$$
(4.19)

where again $\hat{n}_{\alpha,j} = \hat{a}^{\dagger}_{\alpha,j} \hat{a}_{\alpha,j}$ is the number operator of the p_{α} -orbital state.

To proceed with the study, we implement the program discussed in Sect. 3.1, and characterize mean-field properties of the system. This starts with use of the coherent-state ansatz in Eq. (4.19), which yields the corresponding mean-field Hamiltonian. This mean-field Hamiltonian is then used in the Euler–Lagrange equations, that are propagated in imaginary time with a trial wave-function. The result is the state with minimum energy, that corresponds to the order parameter describing the superfluid phase of the confined p-orbital bosonic system.

⁵Notice, however, that because of the tunneling anisotropy, the local chemical potential is not the only factor determining local properties of the density.

As in Sect. 3.6, we impose the normalization in the whole lattice as

$$N = N_x + N_y = \sum_{j} |\psi_{x,j}|^2 + \sum_{j} |\psi_{y,j}|^2,$$
 (4.20)

where N is the total number of atoms, and the order parameters are again governed by a set of coupled (discrete) Gross-Pitaevskii equations, one for each orbital-state p_{α} ,

$$-i\frac{\partial\psi_{x,j}}{\partial t} = -\sum_{\sigma\in\{x,y\}} t_{\sigma}^{x}(\psi_{x,j+1_{\sigma}} - 2\psi_{x,j} + \psi_{x,j-1_{\sigma}}) + \frac{\omega^{2}}{2}(x_{j}^{2} + y_{j}^{2})\psi_{x,j}$$

$$+ (U_{xx}|\psi_{x,j}|^{2} + (U_{xy} + U_{yx})|\psi_{y,j}|^{2})\psi_{x,j} + \left(\frac{U_{xy} + U_{yx}}{2}\right)\psi_{y,j}^{2}\psi_{x,j}^{*}$$

$$-i\frac{\partial\psi_{y,j}}{\partial t} = -\sum_{\sigma\in\{x,y\}} t_{\sigma}^{y}(\psi_{y,j+1_{\sigma}} - 2\psi_{y,j} + \psi_{y,j-1_{\sigma}}) + \frac{\omega^{2}}{2}(x_{j}^{2} + y_{j}^{2})\psi_{y,j}$$

$$+ (U_{yy}|\psi_{y,j}|^{2} + (U_{xy} + U_{yx})|\psi_{x,j}|^{2})\psi_{y,j} + \left(\frac{U_{xy} + U_{yx}}{2}\right)\psi_{x,j}^{2}\psi_{y,j}^{*},$$

$$(4.21)$$

where the expressions for the couplings are given by Eqs. (2.47) and (2.48).⁶

Propagation of a trial wave-function in imaginary time is carried on with Eq. (4.21) re-written in the form

$$i\frac{\partial \Psi_j}{\partial t} = \begin{bmatrix} H_{11} & H_{12} \\ H_{21} & H_{22} \end{bmatrix} \Psi_j,\tag{4.22}$$

where
$$\Psi_{j} = \begin{bmatrix} \psi_{x,j} \\ \psi_{y,j} \end{bmatrix}$$
 and
$$H_{11} = -t_{x}^{x} \partial_{x}^{2} - t_{y}^{x} \partial_{y}^{2} + U_{xx} |\psi_{x,j}|^{2} + (U_{xy} + U_{yx}) |\psi_{y,j}|^{2},$$

$$H_{22} = -t_{x}^{y} \partial_{x}^{2} - t_{y}^{y} \partial_{y}^{2} + U_{yy} |\psi_{y,j}|^{2} + (U_{xy} + U_{yx}) |\psi_{x,j}|^{2},$$

$$H_{12} = \left(\frac{U_{xy} + U_{yx}}{2}\right) \psi_{y,j} \psi_{x,j}^{*},$$

$$H_{21} = \left(\frac{U_{xy} + U_{yx}}{2}\right) \psi_{x,j} \psi_{y,j}^{*}.$$
(4.23)

Since time evolution is performed by a Hamiltonian containing both position- and momentum-dependent terms, this step is implemented numerically with the use of the *split-operator method* [5]. This method uses the *Trotter expansion* to factorize

⁶We remind that the coupling constants and tunneling coefficients are computed with lattice Wannier functions obtained from numerical solution of the Mathieu equation for the potential (4.18).

the evolution operator, and therefore becomes exact only in the limit of vanishingly small time steps. For better accuracy, we propagate the system with a tiny time step that was chosen after consistently checking the results against time steps of different sizes.

Details of the computation are given in the following:

• The time evolution operator is written as

$$U(\delta t) = e^{-iH\delta t} = \exp\left\{-i \begin{bmatrix} H_{11} & H_{12} \\ H_{21} & H_{22} \end{bmatrix} \delta t \right\}$$
$$= \exp\left\{-i \left(\begin{bmatrix} H_{11} & 0 \\ 0 & H_{22} \end{bmatrix} + \begin{bmatrix} 0 & H_{12} \\ H_{21} & 0 \end{bmatrix} \right) \delta t \right\}$$

and since we assume the $\lim \delta t \to 0$, this equation is further approximated as

$$U(\delta t) \approx \underbrace{e^{-i\delta t} \begin{bmatrix} H_{11} & 0 \\ 0 & H_{22} \end{bmatrix}}_{U_1(\delta t)} \underbrace{e^{-i\delta t} \begin{bmatrix} 0 & H_{12} \\ H_{21} & 0 \end{bmatrix}}_{U_2(\delta t)}. \tag{4.24}$$

• We expand $U_2(\delta t)$:

$$\begin{bmatrix} 0 & H_{12} \\ H_{21} & 0 \end{bmatrix}^{2} = \begin{bmatrix} \left(\frac{U_{xy} + U_{yx}}{2}\right)^{2} |\psi_{x,j}|^{2} |\psi_{y,j}|^{2} & 0 \\ 0 & \left(\frac{U_{xy} + U_{yx}}{2}\right)^{2} |\psi_{x,j}|^{2} |\psi_{y,j}|^{2} \end{bmatrix}$$
(4.25)

and

$$\begin{bmatrix} 0 & H_{12} \\ H_{21} & 0 \end{bmatrix}^{3} = \left(\frac{U_{xy} + U_{yx}}{2}\right)^{3} |\psi_{x,j}|^{2} |\psi_{y,j}|^{2} \begin{bmatrix} 0 & \psi_{y,j}\psi_{x,j}^{*} \\ \psi_{x,j}\psi_{y,j}^{*} & 0 \end{bmatrix}, \quad (4.26)$$

from where it follows

$$\frac{(-i\delta t)^n}{n!}A^n = \frac{(-i\delta t)^n}{n!}|\psi_{x,j}|^{n-1}|\psi_{y,j}|^{n-1}\begin{bmatrix} 0 & \psi_{y,j}\psi_{x,j}^* \\ \psi_{x,j}\psi_{y,j}^* & 0 \end{bmatrix}$$
(4.27)

for odd n, and

$$\frac{(-i\delta t)^n}{n!}A^n = \frac{(-i\delta t)^n}{n!}|\psi_{x,j}|^n|\psi_{y,j}|^n \begin{bmatrix} 1 & 0\\ 0 & 1 \end{bmatrix}$$
(4.28)

for even n.

Gathering all the terms of this expansion,

$$U_2(\delta t) = \begin{bmatrix} U_2^{(11)} & U_2^{(12)} \\ U_2^{(21)} & U_2^{(22)} \end{bmatrix}, \tag{4.29}$$

where

$$\begin{split} &U_{2}^{(11)} = U_{2}^{(22)} = \cos\left(\left(\frac{U_{xy} + U_{yx}}{2}\right) \delta t |\psi_{x,j}| |\psi_{y,j}|\right), \\ &U_{2}^{(12)} = -i \delta t \left(\frac{U_{xy} + U_{yx}}{2}\right) \operatorname{sinc}\left(\left(\frac{U_{xy} + U_{yx}}{2}\right) \delta t |\psi_{x,j}| |\psi_{y,j}|\right) \psi_{y,j} \psi_{x,j}^{*} \end{split}$$

and

$$U_2^{(21)} = -i\delta t \left(\frac{U_{xy} + U_{yx}}{2}\right) \operatorname{sinc}\left(\left(\frac{U_{xy} + U_{yx}}{2}\right) \delta t |\psi_{x,j}| |\psi_{y,j}|\right) \psi_{x,j} \psi_{y,j}^*.$$

The idea now is to make $\Psi(\delta t) = U_1(\delta t)U_2(\delta t)\Psi = U_1(\delta t)\Psi_1$, where $\Psi_1 = U_2(\delta t)\Psi$ with $U_1(\delta t)$ defined in (4.24). This involves evolution with a diagonal matrix which contains different types of contributions (see the expressions of H_{11} and H_{22} in Eq. (4.23)). Namely, it features a first part with dependence on the spatial derivatives; and a second part that depends on the densities of the orbital order parameters. We will first evolve Ψ_1 with the part of U_1 that depends on the densities. This yield $\Psi_1 \to \tilde{\Psi}_1$. After this step, the remaining part is handled in momentum space. By means of a Fourier transform we obtain the expression of $\tilde{\Psi}_1$ in the momentum representation, $\mathcal{F}[\tilde{\Psi}_1] = \tilde{\Psi}$, which can then be easily evolved with the lattice dispersion relations⁷

$$\begin{bmatrix} \tilde{\psi}_{x,j}(\delta t) \\ \tilde{\psi}_{y,j}(\delta t) \end{bmatrix} = \begin{bmatrix} e^{-i\delta t [2t_x^X(1-\cos k_{xx}) + 2t_y^X(1-\cos k_{xy})]} & 0 \\ 0 & e^{-i\delta t [2t_x^Y(1-\cos k_{yx}) + 2t_y^Y(1-\cos k_{yy})]} \end{bmatrix} \begin{bmatrix} \tilde{\psi}_{x,j} \\ \tilde{\psi}_{y,j} \end{bmatrix}.$$

$$(4.30)$$

By Fourier transforming it back to the position representation, the final result is $\Psi(\delta t)$ (cf. Eq. (4.22)). This is used again as a new trial wave-function, that is propagated in imaginary time. This procedure is repeated until convergence has been reached.

Figure 4.4 shows the density profile of the p_x - and p_y -orbital order parameters in the confined system in (a) and (b), respectively. Comparison with Fig. 4.2b, reveals the same trend observed for the ideal gas case, where the density is elongated in the direction of the orbital label. Figure 4.4c shows the population imbalance in the lattice that corresponds to the *z*-component of the Bloch vector defined in (3.16), $J_{z,j}$.

 $^{^7}$ In momentum space the term $-t_\sigma^\alpha\partial_\sigma^2$ corresponds to $t_\sigma^\alpha k_{\alpha\sigma}^2$. Here however we use $k_{\alpha\sigma}^2 \to 2t_\sigma^\alpha(1-\cos k_{\alpha\sigma})$ to account for the (inverted) shape of the p band and the discrete character of the system.

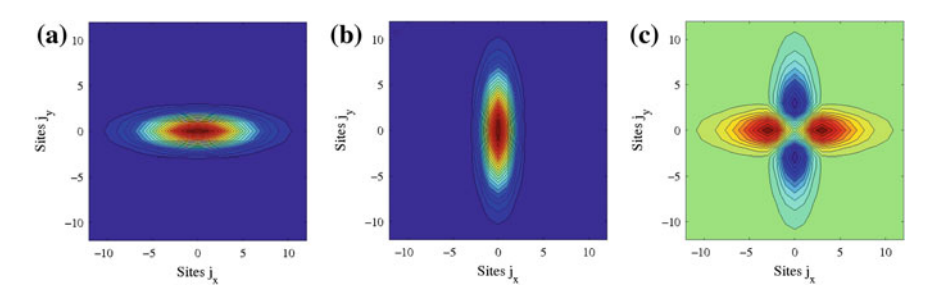


Fig. 4.4 a and b show populations in the p_x - and in the p_y -orbital states respectively. c illustrates the corresponding population imbalance $J_{z,j}$. The dimensionless system parameters are $V_x = V_y = 17$, $\omega = 0.005$, and $U_0N = 1$. Excess of atoms in the p_x -orbital state appears in the horizontal axis and is indicated by red color, while in the vertical axis the system displays excess of atoms in the p_y -orbital state (Reprinted from Ref. [1])

Since the density anisotropy is a consequence of the tunneling anisotropy, what happens in the regime where interactions start to dominate over the tunneling contributions? More importantly, how does the system react as we change the parameters to cross the different regimes? Tunneling contributions can be suppressed in this lattice in two ways. In the most immediate one, the intensity of the laser is tuned such as to yield very deep potential wells where the atoms have reduced mobility. The other way is via Feshbach resonances, that increase the coupling constant \tilde{U}_0 (see Eq. (2.38)) and therefore decrease the relative strength of the tunneling relative to interacting processes. This limit, where interactions are so strong that other effects of the dynamics can be neglected, is also known as the *Thomas–Fermi limit* [3].

In the interacting system, anisotropies in the density of the order parameters will be also characterized with the same quantity defined in Sect. 4.1 for the ideal gas:

$$S = \sqrt{\frac{(\Delta_x x)^2}{(\Delta_x y)^2}}.$$

We computed it here for different values of the system's parameters. As Fig. 4.5 shows, this anisotropy parameter approaches $S \to 1$ in the limit of vanishing tunneling regardless of the way chosen for suppressing such processes. However, we notice that suppression of tunneling via the deepening of the lattice potential leads to an initial increase of S in the V axis. After reaching a maximum value, S decays monotonically, until reaching 1. Although there is no particular reason for expecting such behavior, that in fact is not even hinted in the analysis of the continuum limit (S_{cont}^{8} cf. Eq. (4.10)), this can be a consequence of the poor description provided by the tight-binding approximation in the limit of shallow sites. Accordingly, the results

⁸It should be noticed, however, that the expression provided by S_{cont} is obtained in the limit of $U_0=0$ and it does not approach 1 as $V\to\infty$. On the other hand, since the kinetic term relative to interaction becomes negligible under these circumstances, any small $U_0>0$ is sufficient to make $S_{cont}\to 1$. For moderate values of the lattice depth V, S_{cont} increases monotonically with increasing

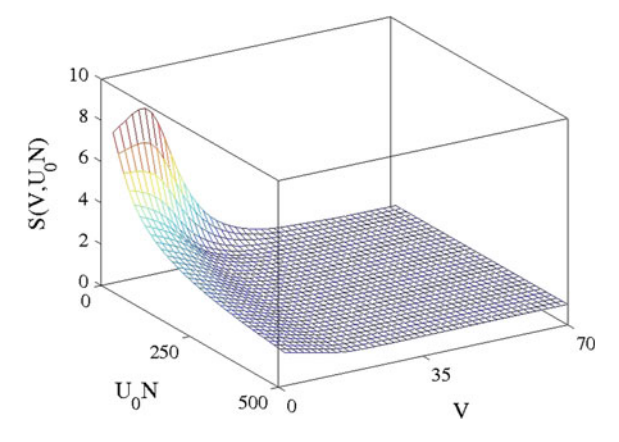


Fig. 4.5 The condensate anisotropy parameter S (see Eq. (4.9)) as a function of the interaction strength U_0N and of the lattice amplitude $V=V_x=V_y$ for the system with dimensionless trap frequency $\omega=0.005$. It illustrates that the system enters the Thomas–Fermi regime whenever the relative strength of the tunneling compared to interactions becomes small, i.e., $S \to 1$ (Reprinted from Ref. [1])

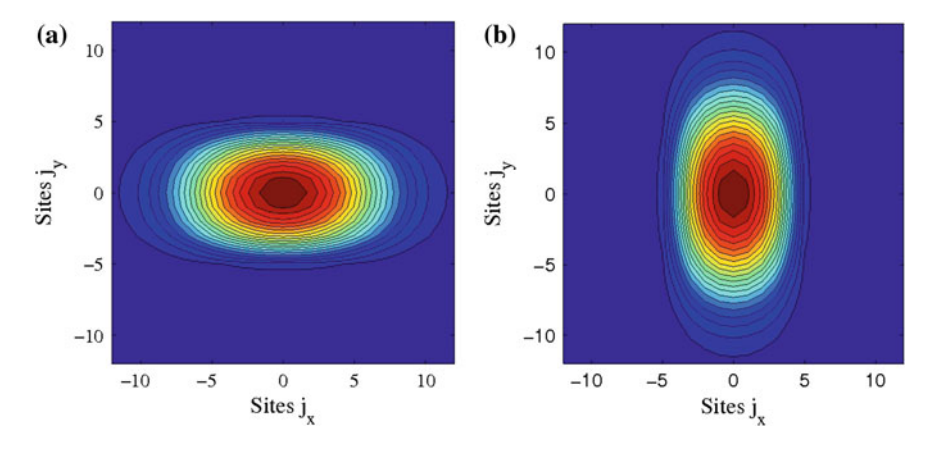


Fig. 4.6 These plots display populations in the p_x -(a) and p_y -(b) orbital states, for $V_x = V_y = 17$, $\omega = 0.005$ and $U_0N = 15$. Due to the strength of interactions, the anisotropy in the density is not so pronounced as compared to the results in Fig. 4.4a and b (Reprinted from Ref. [1])

should not be taken too literally in that region. We complement the analysis by showing the density profile of the p_x and p_y orbitals in Fig. 4.6a and b for a situation with moderate interaction, where $U_0N=15$, $\omega=0.005$ and $V=V_x=V_y=17$. As expected, it confirms the previous conclusions driven in this section.

values of V. This behavior is not predicted by the discrete model (Eq. (4.6)), and therefore we keep in mind that the two descriptions yield qualitatively different predictions in the limit of deep lattices.

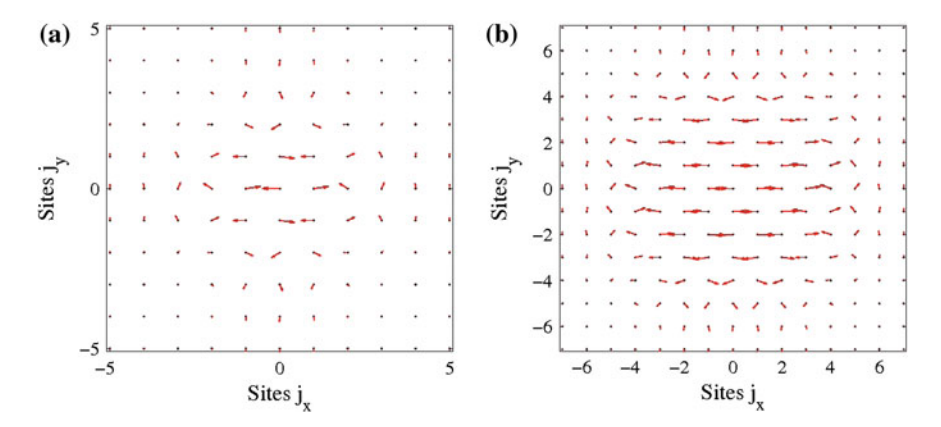


Fig. 4.7 Bloch vector at different sites of the optical lattice. We use the horizontal axis to represent the y-component of the spin and the vertical axis to represent the spin z-component. The x-component of the spin is strictly zero due to the specific onsite phase locking between the p_x -and the p_y -orbital states. Information about the density is encoded in the length of the Bloch vector (see Eq. (3.16)) and the offset from the horizontal axis encodes information about the breakdown of the antiferromagnetic order. The black dots are used to denote the lattice sites. In a $U_0N = 1$ and in b $U_0N = 15$. The other parameters are the same as in Fig. 4.6. This illustrates, in particular, that the staggered-vortex solution remains valid in a larger number of sites in the center of the trap in the limit of large interactions (Reprinted from Ref. [1])

Now in light of the inhomogeneous density profile in the confined system, what is the fate of the staggered vortex solution predicted for the homogeneous case? In order to characterize the stability of the staggered-vortex solution in the presence of population imbalance between the two orbital states, we invoke the mean-field version of Schwinger bosons, discussed previously in Sect. 3.1.1. As we argued there, the profile of the full onsite order parameter Eq. (3.3), features true vortices/antivortices, in the sense of eigenstates $\hat{L}_{z,j}$, only in the harmonic approximation. Outside this limit, the condition $\hat{J}_{z,j}=0$ is not enough to ensure a perfect staggered vortex solution.

In the confined system, we have seen that the tunneling anisotropy introduces a natural population imbalance in the lattice (see, e.g., Fig. 4.4), and therefore $J_{z,j}$ is typically nonzero everywhere. However since population imbalance is more pronounced at the edges of the condensed cloud, it is still possible to have regions of non-trapped like physics at the center of the trap, where $J_{z,j} \approx 0$. This is illustrated in Fig. 4.7a and b, which display the Bloch vector in the yz-plane, $^{10} J_j = (0, J_{y,j}, J_{z,j})$. Here, we use the horizontal axis to represent the y-spin direction, and the vertical axis to represent the z-spin direction. Therefore, a clear dominance of the $J_{y,j}$ component appears at the center of the trap. At the edges, the Bloch vector is no longer pointing to the horizontal direction, revealing the breakdown of the staggered vortex

⁹Cf. the analysis of Chap. 3.

¹⁰Recall here that $J_{x,i}$ is always zero.

solution in these regions. This study also shows, in addition, that in the limit of large interactions, the staggered vortex solution can survive in a larger number of sites in the center of the trap.

As a final remark, we notice that an interesting direction consists of the generalization of this study to the case of the 3D confined lattice. In the same way as for the 2D system, we expect that the center of the trap can be approximately described by the homogeneous density case, as discussed in Sect. 3.1.2. However, instead of the SU(2) structure of the two-orbital system, the structure of the three-orbital one is intrinsically SU(3). In addition, since this case can accomodate frustrated states, it would be relevant to investigate how effects of the confinement affect frustration. Furthermore, since the tunneling anisotropy creates population imbalance for only one of the orbital states (i.e., the one with the parallel label) in each direction, a systematic study of the properties on the edges of the cloud are also of interest.

4.3 Properties of the System in the Anisotropic Lattice

All the properties discussed so far addressed the case of a symmetric lattice, where the orbital states are automatically degenerate. In asymmetric or anisotropic lattices, however, the presence of small asymmetries/anisotropies can be enough to lift this degeneracy, thereby modifying the picture put forward in the previous section. It is therefore important to investigate how robust is the physics of the symmetric lattice with respect to such imperfections. What are the properties of the physics in the anisotropic lattice, and how stable are the properties of the symmetric lattice with respect to small imperfections?

Anisotropies in the lattice model discussed here can in principle be introduced in two ways: either with the use of lasers with different wave vectors, i.e., $k_x \neq k_y$, or either by manufacturing the lattice with different amplitudes. We investigate these issues by considering the second scenario, of a lattice with $V_x \neq V_y$. In order to control the ratio between the lattice depths in the different directions, we define the anisotropy parameter

$$R = \frac{V_{y}}{V_{r}},\tag{4.31}$$

where it is clear that the case of R = 1 recovers the symmetric lattice discussed previously.

We verified numerically that the main effect of asymmetries is to shift the energy levels and to lift the degeneracy between the orbital states. In the limit of very deep lattice sites, this splitting is site independent and does not considerably affect the

¹¹The SU(3) structure of the Mott phase with a unit filling of the three-orbital system in the p band is discussed in details in Sect. 5.3.

physics of the system. Indeed, the splitting energy can be estimated in the harmonic approximation as

$$\Delta = E_{y} - E_{x} = 2\sqrt{V_{x}}(\sqrt{R} - 1), \tag{4.32}$$

where $E_{\alpha} = \int d\mathbf{r} \ w_{\alpha,j}^*(\mathbf{j})[-\nabla^2 + V_{lat}(\mathbf{r})]w_{\alpha,j}(\mathbf{j})$ is the energy of the p_{α} orbital state at the jth site, and therefore, as long as the splitting energy Δ is much smaller than the energy scale set by the interaction terms, $E_U \sim U_0 N |\psi_x|^2$, it has only very small effects on the system.

However, this picture becomes more complex when the potentials become shallower and correlations between sites become relevant. In this case, the interaction can couple the order parameters of the different orbital states in a small region δ around R=1, such that small perturbation of the lattice parameters can lead to drastic changes in the properties of the ground state. This is an important point, because the possibility of accurately controlling the lattice in a neighbourhood around the degeneracy point opens up a great window of new possibilities for applications of this system. Of particular interest is the study of phenomena similar to adiabatic ramping through an avoided crossing (as discussed in Ref. [6]).

In this sense, the parameter

$$J_z = \frac{1}{N} \sum_{j} J_{z,j},$$
 (4.33)

which computes population imbalance between the different orbital states arises as a natural candidate for characterizing sensitivity of the system with respect to R. When $J_z=-1$, all the particles occupy only p_y orbital states, and in the same way, when $J_z=1$ all the particles occupy only p_x orbital states. The case of $J_z=0$ recovers the symmetric lattice, that is characterized by the equal sharing of population among the different orbitals. We remark, however, that since the trap defines an effective size for the system that is fixed by ω , the sensitivity under variations of R is expected to depend strongly on the values of the trap frequency. He has in illustrated in Fig. 4.8, where the behavior of J_z around R=1 is compared for different values of ω . In particular, since the range of δ becomes smaller for larger systems, this implies that qualitative properties of the ground state are expected to change more abruptly with increasing systems sizes. We also verified numerically that δ increases with increasing values of the interaction strength U_0N , which confirms the picture that the orbital order parameters are coupled by interactions.

Therefore, from the study of the asymmetric lattice, we learn that a better tuning of the (symmetric) lattice parameters is required when studying the *p*-orbital bosons

¹²In the proper sense of changing the symmetry of the ground state.

¹³It is important to point out, however, that since here the densities of different orbital states are spatially different, adiabatic driving could lead to macroscopic flow of particles within the trap.

¹⁴Since the trap frequency also determines the susceptibility of the system to finite size effects, it can transform energy level crossings into avoided crossings, for example.

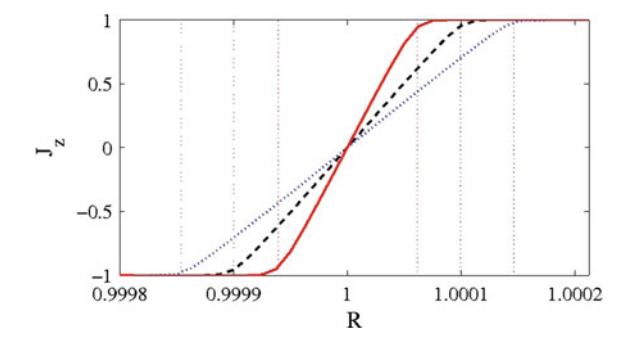


Fig. 4.8 The parameter for measuring population imbalance J_z as a function of the lattice asymmetry parameter, R, and for different values of the trapping frequency. Here $U_0N=1$ and $V_x=17$. The *vertical dashed lines* are used to denote the typical sizes δ of the transition region where atoms coexist in the two orbital states. In particular, smaller values of ω are associated with smaller values of δ . This means that the transition becomes sharper as the system's size increases (Reprinted from Ref. [1])

in the weakly interacting regime. As interactions become stronger, the properties discussed previously become more robust to the presence of imperfections. In fact, even a small temperature could already contribute to the establishment of phase coherence between the order parameters of the p_x and p_y orbital states in experimental realizations. This is a consequence of the reduced energy gap between the ground and first excited states around the R=1 point, that contributes to the occupation of the first excited state (this is particularly needed for balancing the population of the two orbitals). We furthermore notice that the transition from one to the other extreme of J_z is smooth for non-zero ω , and that by controlling the lattice amplitudes this system could realize a many-body Landau–Zener transition [7], which when R is tuned externally, could form a play-ground of the Kibble–Zurek [8] mechanism. A more detailed study in this direction is presented in Ref. [9].

References

- Pinheiro F, Martikainen J-P, Larson J (2012) Confined p-band Bose-Einstein condensates. Phys Rev A 85(3):033638
- Aunola M (2003) The discretized harmonic oscillator: Mathieu functions and a new class of generalized Hermite polynomials. J Math Phys 44(5):1913–1936
- Pethick CJ, Smith H (2002) Bose-Einstein Condensation in Dilute Gases. Cambridge University Press, Cambridge
- Schroeder DV, Pribram, JK (1999) An introduction to thermal physics. Am J Phys 67(12):1284– 1285
- Feit MD, Fleck JA Jr, Steiger A (1982) Solution of the Schrödinger equation by a spectral method. J Comput Phys 47(3):412–433
- Ölschläger Matthias, Wirth Georg, Kock Thorge, Hemmerich Andreas (2012) Topologically induced avoided band crossing in an optical checkerboard lattice. Phys Rev Lett 108(7):075302

- Altland A, Gurarie V, Kriecherbauer T, Polkovnikov, A (2009) Nonadiabaticity and large fluctuations in a many-particle Landau-Zener problem. Phys Rev A, 79(4):042703
- Damski B (2005) The simplest quantum model supporting the Kibble-Zurek mechanism of topological defect production: Landau-Zener transitions from a new perspective. Phys Rev Lett 95(3):035701
- 9. Larson J (2014) Interaction-induced Landau-Zener transitions. EPL (Europhysics Letters) 107(3):30007

Chapter 5 Beyond the Mean-Field Approximation: Effective Pseudospin Hamiltonians via Exchange Interaction

In the previous chapters we investigated the weakly interacting regime of the many-body bosonic system in the p and d bands. The properties of the order parameters describing the superfluid phases in both cases were characterized with use of mean-field techniques, which among other features revealed the onsite structure of vortices in the different cases. In this chapter we move away from the weakly interacting territory to explore the physics in the strongly correlated regime of the Mott insulator phase.

In the approach used here, the dynamics of the Mott insulator phase with a unit filling (Mott-1) is described by an effective model derived from perturbative treatment of the tunneling processes relative to the onsite interaction terms. We study p-orbital systems in 2D and 3D, and the d-orbital system in 2D.

As it was first shown in Ref. [1], which we explain in details in this text, the case of bosonic atoms in the p band of a 2D optical lattice can be mapped into the spin-1/2 XYZ quantum Heisenberg model in an external field. This model is of particular interest in the study of quantum magnetism [2, 3], and falls into the class of nonintegrable models [4], where analytical solutions are not known in closed form. We explore the correspondence between these two systems and use known properties of the XYZ model to understand the physics in the p band. At the same time, we study the p-orbital system in the context of quantum simulation [5, 6], where we propose manipulation and detection schemes for experimentally probing observables that are relevant in the study of quantum magnetism.

The techniques used in the study of the 2D system are further extended and applied to the 3D three-orbital case. In this case, the Mott phase with a unit filling in the p band is effectively described by a Hamiltonian with degrees of freedom that are the generators of the SU(3) group. This was first shown in Ref. [7], which is the basis of this part of the text. We will investigate both the bosonic and the fermionic cases, and we will show that the anisotropies in the couplings of the effective models intrinsically depend on the statistics of the atoms. Manipulation and detection schemes are also discussed for probing the physics of SU(3) Heisenberg models.

Finally, we use the same approach to characterize the Mott phase of the d-orbital system in 2D. As discussed in Sect. 3.2, this corresponds to the situation where occupation of the d_{xy} orbital vanishes for a large range of experimentally relevant system's parameters, such that the effective spin model is derived from the corresponding two-orbital description. In particular, we show that due to the presence of density-assisted processes, the effective spin model for bosonic atoms in the d band is of the spin-1/2 XYZ type¹ with an external field even in the 2D isotropic lattice. In addition, breaking the isotropy of the lattice while still keeping the two orbitals degenerate adds Dzyaloshinskii– $Moriya\ exchange\ processes\ (DM)$. We discuss qualitative properties of the ground-state phase diagram and the different phases expected for this system. These studies were reported in Ref. [8].

We will start this chapter by presenting the perturbative method for treating a general system of multi-species that can be used to encode a (pseudo) spin degree of freedom. We then apply this method to obtain the effective spin models in the p band in Sects. 5.2 and 5.3, respectively, for the 2- and 3-orbital systems in 2D and 3D. We use Sect. 5.2.3 to discuss the experimental probes for the p-orbital system and the effects due to imperfections in the loading process are investigated in Sect. 5.2.4. In Sect. 5.4 we characterize the effective spin Hamiltonians describing the Mott phase with a unit filling in the d band, and generalizations of this method are also discussed throughout the text.

5.1 Effective Hamiltonian for Describing the Mott Phase with Unit Filling

As a starting point for the derivations to be presented here, let us assume that $\hat{H} = \hat{H}_K + \hat{H}_U$ is the Hamiltonian describing a generic many-body system in an optical lattice. \hat{H}_K contains the kinetic part which describes tunneling processes with amplitude proportional to t, and \hat{H}_U contains interaction terms with strength proportional to U. We assume that the system is deep in the Mott insulator phase, where $t \ll U$, and study the dynamics in terms of an effective Hamiltonian where tunneling processes are treated perturbatively [3, 9].

Since the Mott phase is characterized by a fixed number of particles per site, derivation of the effective Hamiltonian can be naturally handled with use of projection operators that divide the Hilbert space of the eigenvalue problem in orthogonal subspaces according to site occupations. Our interest is the Mott phase with a unit filling, and therefore we define the \hat{P} and \hat{Q} operators, $\hat{P}^2 = \hat{P}$, $\hat{Q}^2 = \hat{Q}$ and $\hat{P} + \hat{Q} = 1$, that project, respectively, into the Hilbert space of singly occupied sites \mathcal{H}_P , and the states that have at least one site with double occupation \mathcal{H}_Q . The eigenvalue problem can be written as

$$\hat{H}(\hat{P} + \hat{Q})\Psi \rightarrow (\hat{H}_K + \hat{H}_U)(\hat{P} + \hat{Q})\Psi = E\Psi, \tag{5.1}$$

¹That is, with anisotropic couplings in the interactions of all the spin components.

which becomes

$$\left(\hat{Q}\hat{H}_K\hat{P} + \hat{Q}\hat{H}_K\hat{Q} + \hat{Q}\hat{H}_U\hat{P} + \hat{Q}\hat{H}_U\hat{Q}\right)\Psi = E\hat{Q}\Psi, \tag{5.2}$$

$$\left(\hat{P}\hat{H}_K\hat{P} + \hat{P}\hat{H}_K\hat{Q} + \hat{P}\hat{H}_U\hat{P} + \hat{P}\hat{H}_U\hat{Q}\right)\Psi = E\hat{P}\Psi$$
 (5.3)

after operating from the left with the \hat{P} and \hat{Q} projectors in Eq. (5.1).

From all contributions, $\hat{P}\hat{H}_K\hat{P}$, $\hat{P}\hat{H}_U\hat{Q}$ and $\hat{P}\hat{H}_U\hat{P}$ are identically zero. The first two, for computing overlaps between elements of the basis in disjoint subspaces of the Hilbert space. The last term, for computing two-body interactions in singly occupied sites. Thus, we are left with

$$\hat{Q}\Psi = -\frac{1}{\hat{Q}\hat{H}\hat{Q} - E}\hat{Q}\hat{H}_K\hat{P}\Psi,\tag{5.4}$$

which leads to

$$\hat{H}_{Mott_1} = -\hat{P}\hat{H}_K \hat{Q} \frac{1}{\hat{Q}\hat{H}\hat{Q} - E} \hat{Q}\hat{H}_K \hat{P}.$$
 (5.5)

So far this expression is exact, and it provides the basic framework for the derivation of the various effective spin Hamiltonians to be discussed here. Now under the assumptions of the Mott phase, the resolvent $\hat{K}=1/(\hat{Q}\hat{H}\hat{Q}-E)$ can be expanded such that the effective Hamiltonian contains contributions to second order in t/U [3, 9]. Thus, it readily follows that the intermediate and final states of the perturbative procedure in the \mathcal{H}_Q and \mathcal{H}_P subspaces, respectively, are connected via tunneling processes. In addition, since $E \sim t^2/U$, $\hat{K} \sim H_Q^{-1}$, and due to the tight-binding approximation, it is possible to restrict the study to the two-site problem. We describe it in terms of a basis denoted by $|\text{site } j, \text{site } j+1\rangle$. Now let us consider an initial situation with a unit filling of the lattice sites. Via action of the tunneling, the atom at the site j tunnels to the site j+1, which becomes doubly occupied. This is the intermediate state in \mathcal{H}_Q , with an energy cost due to the interaction, that is given by the processes defined in \hat{H}_U . After interaction has taken place, one of the atoms tunnels back to site j, and the final state is again characterized by unit filling—therefore, in the \mathcal{H}_P subspace.

Let us assume that this generic system described by \hat{H} is composed of at least two different atomic species, with corresponding tunneling amplitudes t_{σ}^{α} and t_{σ}^{β} in the direction σ , and write all the different possible states in the \mathcal{H}_P subspace as

$$\mathcal{H}_P \to \{ |\alpha, \alpha\rangle, |\alpha, \beta\rangle \},$$
 (5.6)

where $\alpha \neq \beta$ and α , β should account for all the possible combinations between the components, and $|\alpha,\beta\rangle=\hat{a}_{\alpha,i}^{\dagger}\hat{a}_{\beta,j}^{\dagger}|0\rangle$.

In the same way, the different states in the basis of the \mathcal{H}_O subspace follow

$$\mathcal{H}_O \to \{|0, 2\alpha\rangle, |0, \alpha\beta\rangle\},$$
 (5.7)

where $|0,2\alpha\rangle=2^{-1/2}\hat{a}_{\alpha,j}^{\dagger}\hat{a}_{\alpha,j}|0\rangle$ and $|0,\alpha\beta\rangle=\hat{a}_{\alpha,j}^{\dagger}\hat{a}_{\beta,j}^{\dagger}|0\rangle$, with again α and β accounting for all the possible combinations between the multiple components. Let us furthermore assume that this system does not include tunneling processes with change of state, i.e., only operators of the type $\hat{a}_{\alpha,j}^{\dagger}\hat{a}_{\alpha,i}$ generate non-vanishing contributions. In addition, let us call $K_{\alpha\beta}^{\alpha\beta}=\langle 0,\alpha\beta|\hat{K}|0,\alpha\beta\rangle$ the elements of $\hat{K}=\hat{H}^{-1}$ in the basis of the $\mathcal{H}_{\mathcal{Q}}$ subspace. A list of all the possible transitions between the different states in this two-species system follow:

The states of the type $|\alpha_i, \alpha_j\rangle$ are connected via tunneling to the three different intermediate states in the $\mathcal{H}_{\mathcal{Q}}$ subspace, i.e.,

$$\begin{split} \hat{K} \, \hat{a}_{\alpha,j}^{\dagger} \hat{a}_{\alpha,i} |\alpha_i, \alpha_j\rangle &= \sqrt{2} \hat{K} |0, 2\alpha_j\rangle \\ &= \sqrt{2} \left(K_{\alpha\alpha}^{\alpha\alpha} |0, 2\alpha_j\rangle + K_{\alpha\alpha}^{\alpha\beta} |0, \alpha_j\beta_j\rangle + K_{\alpha\alpha}^{\beta\beta} |0, 2\beta_j\rangle \right). \end{split}$$

The possible transitions are

(i) To $|\alpha_i, \alpha_j\rangle$ via action of $\hat{a}_{\alpha,j}^{\dagger} \hat{a}_{\alpha,i}$, which contribute to the effective Hamiltonian with terms of the type

$$-\sum_{\langle i,j\rangle_{\sigma}} \sum_{\alpha,\beta} 2 |t_{\sigma}^{\alpha}|^2 K_{\alpha\alpha}^{\alpha\alpha} \,\hat{n}_{\alpha,i} \hat{n}_{\alpha,j}. \tag{5.8}$$

(ii) To $|\alpha_i, \beta_j\rangle$ via action of $\hat{a}^{\dagger}_{\alpha,j}\hat{a}_{\alpha,i}$, contributing to the effective Hamiltonian with

$$-\sum_{\langle i,i\rangle_{\sigma}} \sum_{\alpha,\beta} \sqrt{2} |t_{\sigma}^{\alpha}|^2 K_{\alpha\alpha}^{\alpha\beta} \,\hat{n}_{\alpha,i} \hat{a}_{\beta,j}^{\dagger} \hat{a}_{\alpha,j}. \tag{5.9}$$

(iii) To $|\beta_i, \alpha_j\rangle$ via action of $\hat{a}^{\dagger}_{\beta,j}\hat{a}_{\beta,i}$, contributing to the effective Hamiltonian with

$$-\sum_{\langle i,i\rangle_{\sigma}} \sum_{\alpha,\beta} \sqrt{2} \, t_{\sigma}^{\alpha} t_{\sigma}^{\beta} K_{\alpha\alpha}^{\beta\alpha} \, \hat{a}_{\beta,i}^{\dagger} \hat{a}_{\alpha,i} \hat{n}_{\alpha,j}. \tag{5.10}$$

(iv) To $|\beta_i,\beta_j\rangle$ via action of $\hat{a}^\dagger_{\beta,j}\hat{a}_{\beta,i}$, which contribute to the effective Hamiltonian with terms of the type

²This assumption is used here only because in the systems to be discussed next, these processes yield vanishing contributions. We notice, however, that this method can be easily extended to account for other situations.

$$-\sum_{\langle i,j\rangle_{\sigma}}\sum_{\alpha\beta}2t_{\sigma}^{\alpha}t_{\sigma}^{\beta}K_{\alpha\alpha}^{\beta\beta}\hat{a}_{\beta,i}^{\dagger}\hat{a}_{\alpha,i}\hat{a}_{\beta,j}^{\dagger}\hat{a}_{\alpha,j}.$$
(5.11)

The states of the type $|\alpha_i, \beta_j\rangle$ are also connected via tunneling to the three intermediate states in the $\mathcal{H}_{\mathcal{Q}}$ subspace:

$$\hat{K}\hat{a}_{\alpha,i}^{\dagger}\hat{a}_{\alpha,j}|\alpha_{i},\beta_{j}\rangle = \hat{K}|0,\alpha_{j}\beta_{j}\rangle
= \left(K_{\alpha\beta}^{\alpha\alpha}|0,2\alpha_{j}\rangle + K_{\alpha\beta}^{\alpha\beta}|0,\alpha_{j}\beta_{j}\rangle + K_{\alpha\beta}^{\beta\beta}|0,2\beta_{j}\rangle\right).$$
(5.12)

Here, in addition to the conjugates of Eqs. (5.9) and (5.10), the other possible transitions are

(v) To $|\alpha_i,\beta_j\rangle$ via action of $\hat{a}_{\alpha,j}^\dagger\hat{a}_{\alpha,i}$, which contribute to the effective Hamiltonian with

$$-\sum_{\langle i,j\rangle_{\sigma}} \sum_{\alpha,\beta} |t_{\sigma}^{\alpha}|^2 K_{\alpha\beta}^{\alpha\beta} \,\hat{n}_{\alpha,i} \hat{n}_{\beta,j}. \tag{5.13}$$

(vi) To $|\beta_i, \alpha_j\rangle$ via action of $\hat{a}^{\dagger}_{\beta,i}\hat{a}_{\beta,i}$, contributing with

$$-\sum_{\langle i,i\rangle_{\sigma}} \sum_{\alpha,\beta} t_{\sigma}^{\alpha} t_{\sigma}^{\beta} K_{\alpha\beta}^{\beta\alpha} \hat{a}_{\beta,i}^{\dagger} \hat{a}_{\alpha,i} \hat{a}_{\alpha,j}^{\dagger} \hat{a}_{\beta,j}. \tag{5.14}$$

In the following sections we apply this method to different systems, with explicit computations for each case.

5.2 *p*-Orbital Bosonic System in the 2*D* Lattice

We recall the explicit expression of the local part of the Hamiltonian describing the bosonic system in the p band of a 2D optical lattice,

$$\hat{H}_{U} = \sum_{i} \frac{U_{xx}}{2} \hat{n}_{x,i} \left(\hat{n}_{x,i} - 1 \right) + \sum_{i} \frac{U_{yy}}{2} \hat{n}_{y,i} \left(\hat{n}_{y,i} - 1 \right) + \sum_{i} 2U_{xy} \hat{n}_{x,i} \hat{n}_{y,i} + \sum_{i} \frac{U_{xy}}{2} \left(\hat{a}_{x,i}^{\dagger} \hat{a}_{x,i}^{\dagger} \hat{a}_{y,i} \hat{a}_{y,i} + \hat{a}_{y,i}^{\dagger} \hat{a}_{y,i}^{\dagger} \hat{a}_{x,i} \hat{a}_{x,i} \right)$$
(5.15)

with the parameters given by Eq. (2.48).

For this system, with the p_x and p_y orbitals, the basis of states in the \mathcal{H}_P and \mathcal{H}_Q subspaces are given by

$$\mathcal{H}_P \to |x, x\rangle, |x, y\rangle, |y, x\rangle, |y, y\rangle$$
 (5.16)

and

$$\mathcal{H}_Q \to |0, 2x\rangle, |0, 2y\rangle, |0, xy\rangle.$$
 (5.17)

With the basis in this order,

$$\hat{H}_{Q} = \begin{pmatrix} U_{xx} & U_{xy} & 0 \\ U_{xy} & U_{yy} & 0 \\ 0 & 0 & 2U_{xy} \end{pmatrix}. \tag{5.18}$$

Due to the processes that transfer the atoms between the orbital states, however, \hat{H}_Q is not diagonal in the basis of intermediate states of the perturbative treatment, of doubly occupied sites. We thus adapt the usual procedure and compute the matrix elements characterizing the exchange interaction from the inverse $\hat{K} = \hat{H}_Q^{-1}$. Explicitly,

$$\hat{K} = \begin{pmatrix} U_{yy}/U^2 & -U_{xy}/U^2 & 0\\ -U_{xy}/U^2 & U_{xx}/U^2 & 0\\ 0 & 0 & 1/2U_{xy}, \end{pmatrix}$$
(5.19)

where $U^2 = U_{xx}U_{yy} - U_{xy}^2$.

We are now ready to gather all the processes contributing to the effective spin Hamiltonian from the list of transitions of Sect. 5.1. But first, let us notice the fact that since the Hamiltonian in the p band conserves the number of atoms in each of the orbital states modulo 2, the processes of number (ii) and (iii) are excluded. In fact, all the elements $K_{\alpha\beta}^{\alpha\alpha} = 0$ in Eq. (5.19). Using the explicit expressions of the matrix elements of \hat{K} obtained from (5.19) in the (i), (iv), (v) and (vi) processes of the above list, we obtain the effective Hamiltonian describing the Mott-1 phase of bosons in the p band

$$\hat{H}_{\text{Mott}_{1}} = -\sum_{\sigma,\alpha\neq\beta} \sum_{\langle i,j\rangle_{\sigma}} \left(2 \frac{|t_{\sigma}^{\alpha}|^{2} U_{\beta\beta}}{U^{2}} \hat{n}_{\alpha,i} \hat{n}_{\alpha,j} + \frac{|t_{\sigma}^{\alpha}|^{2}}{2 U_{xy}} \hat{n}_{\alpha,i} \hat{n}_{\beta,j} \right. \\ \left. - 2 \frac{t_{\sigma}^{\alpha} t_{\sigma}^{\beta} U_{\alpha\beta}}{U^{2}} \hat{a}_{\alpha,i}^{\dagger} \hat{a}_{\beta,i} \hat{a}_{\alpha,j}^{\dagger} \hat{a}_{\beta,j} + \frac{t_{\sigma}^{\alpha} t_{\sigma}^{\beta}}{2 U_{\alpha\beta}} \hat{a}_{\alpha,i}^{\dagger} \hat{a}_{\beta,i} \hat{a}_{\beta,j}^{\dagger} \hat{a}_{\alpha,j} \right).$$

$$(5.20)$$

We now use the orbital states to define the Schwinger spin operators [3, 10]

$$\hat{S}_{i}^{z} = \frac{1}{2} \left(\hat{a}_{x,i}^{\dagger} \hat{a}_{x,i} - \hat{a}_{y,i}^{\dagger} \hat{a}_{y,i} \right)$$

$$\hat{S}_{i}^{+} = \hat{S}_{i}^{x} + i \hat{S}_{i}^{y} = \hat{a}_{x,i}^{\dagger} \hat{a}_{y,i}$$

$$\hat{S}_{i}^{-} = \hat{S}_{i}^{x} - i \hat{S}_{i}^{y} = \hat{a}_{y,i}^{\dagger} \hat{a}_{x,i},$$
(5.21)

³See the last line in Eq. (5.15).

and together with the constraint of a unit filling of the lattice sites in the first Mott lobe, $\hat{n}_{x,i} + \hat{n}_{y,i} = 1$, we re-write Eq. (5.20) as

$$\hat{H}_{\text{Mott}_1} = -\sum_{\sigma} \sum_{\langle i,j \rangle_{\sigma}} \left(J^{zz} \hat{S}_{i}^{z} \hat{S}_{j}^{z} + J^{xx} \hat{S}_{i}^{x} \hat{S}_{j}^{x} + J^{yy} \hat{S}_{i}^{y} \hat{S}_{j}^{y} \right) + \sum_{i} J^{z} \hat{S}_{i}^{z}, \quad (5.22)$$

where the various couplings depend intrinsically on the lattice configuration and are given by

$$J^{xx} = 2\frac{t_{\sigma}^{x}t_{\sigma}^{y}}{U_{xy}}\left(1 - 4\frac{U_{xy}^{2}}{U^{2}}\right),\tag{5.23}$$

$$J^{yy} = 2\frac{t_{\sigma}^{x}t_{\sigma}^{y}}{U_{xy}}\left(1 + 4\frac{U_{xy}^{2}}{U^{2}}\right),\tag{5.24}$$

$$J^{zz} = 4\frac{|t_{\sigma}^{x}|^{2}U_{yy}}{U^{2}} + 4\frac{|t_{\sigma}^{y}|^{2}U_{xx}}{U^{2}} - \frac{|t_{\sigma}^{x}|^{2}}{U_{xy}} - \frac{|t_{\sigma}^{y}|^{2}}{U_{xy}},$$
(5.25)

and

$$J^{z} = \sum_{\sigma} \left(2 \frac{|t_{\sigma}^{x}|^{2} U_{yy}}{U^{2}} - 2 \frac{|t_{\sigma}^{y}|^{2} U_{xx}}{U^{2}} \right) + \left(E_{x}^{\text{os}} - E_{y}^{\text{os}} \right).$$
 (5.26)

This is one of the main results of this thesis. It shows that the Mott insulator phase with a unit filling of bosonic atoms in the p band of a 2D optical lattice is effectively described by the XYZ Heisenberg model. In turn, this is one of the paradigm models in the study of quantum magnetism, making it possible to use known properties of the XYZ model to understand the physics in the p band. At the same time, as we argue here, it also makes the system of p-orbital bosons a useful tool in the context of quantum simulation [6].

The first property to notice in Eq. (5.22) is that contrary to the effective spin Hamiltonians obtained from Bose-Hubbard models in the ground-band of optical lattices⁴ [11], the effective spin model describing the first Mott lobe in the p band is fully anisotropic in its couplings. This is a consequence of the Z_2 symmetry of the orbital-changing processes, that break the U(1) symmetry typical of the (density-density) interactions of multi-species systems in the ground band. In the XYZ model, this symmetry corresponds to the invariance of the Hamiltonian (5.22) with respect to the transformation

⁴Due to the continuous symmetry in the interaction terms of the many-body Hamiltonian of this case, these systems typically yield Heisenberg models of the XXZ or XY types.

 $^{^5}$ As already stated in Sect. 2.4.1, spinor condensates have an interaction term describing processes similar to the orbital-changing interaction in the p band, but with a relative coupling constant that is small enough to be neglected. This follows from the fact that the scattering lengths of the different Zeeman levels are typically very similar.

$$\hat{S}^x \to -\hat{S}^x$$

$$\hat{S}^y \to -\hat{S}^y$$

$$\hat{S}^z \to \hat{S}^z.$$
(5.27)

Next, we notice that since the tunneling in the p band satisfies $t_{\sigma}^{x}t_{\sigma}^{y}<0$, the coupling constants for interaction between nearest neighbours in the x and y components of the spin, J^{xx} and J^{yy} , are negative, and therefore favor primarily anti-ferromagnetic order. This is an interesting result for a bosonic system, because exchange interactions preserve the sign of the wave-function in the bosonic case, making it more natural for the bosonic system to favor ferromagnetic order at neighbouring sites. This is not the case here, however, and only because of the particular tunneling in the p band.

In the 2D isotropic lattice, we notice in addition that $J^z=0$. In fact, since here $t_{\parallel}^x=t_{\parallel}^y$ and $t_{\perp}^x=t_{\perp}^y$, the vanishing external field is a direct consequence of the invariance under the parity transformation discussed in Eq. (2.51). However, whenever this symmetry is broken, the XYZ model has the additional external field in the spin z-component, as we discuss next in the realization of an effective 1D system.

Many-body quantum systems in one dimension are extremely attractive from both theoretical and experimental viewpoints. On the theoretical side, one of their striking features is the requirement of a description in terms of the collective rather than the individual behavior of their many constituent parts [12]. To give an example, let us consider the description of a system of spinless bosons with repulsive interactions in one dimension. The most general property one could guess, is that this system is characterized by a symmetric wave-function, as should be the case since bosonic particles are symmetric under exchange. Now let us consider the limit of infinitely repulsive interactions, called the *Tonks–Girardeau limit*. Here a very reasonable assumption is that the amplitude of the wave-function should decrease in the neighborhood of any of the bosonic particles, and vanish completely at the exact values where the probability of finding any of them is maximum, as shown in Fig. 5.1.

Now via reflection to the negative axis, this symmetric wave-function can be used to construct an alternative anti-symmetric wave-function that reproduces the nodes of the symmetric case. At the level of the wave-functions, the description provided by the symmetric and anti-symmetric wave-functions will be very different. In fact, collective anti-symmetric wave-functions describe systems of non-interacting fermions, not of bosons. But this anti-symmetric wave-function can be constructed, for example, in such a way that its absolute value reproduces the absolute value of the symmetric one. In this case, even though the wave-functions are describing different systems or even more, systems with particles of different statistics, the properties of the bosonic system at the level of densities, as e.g. density-density correlation functions, can be completely inferred from the properties of a system of non-interacting fermions. This process is usually referred to as the *fermionization of bosons* [13]. It illustrates here one of the many peculiarities of many-body systems in 1*D*.

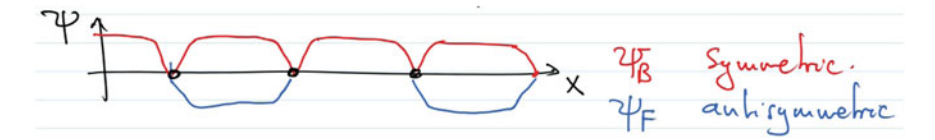


Fig. 5.1 1*D* system of infinitely repulsive bosonic particles. The position of the bosons are the *black dots* in the *x* axis and the *red* and *blue* wave-functions correspond, respectively, to the symmetric and anti-symmetric descriptions discussed above. This figure is taken from Ref. [13] with permission of the author (color figure online)

5.2.1 Properties of the Ground-State: The Phase Diagram of the XYZ Model

Very little is known about the XYZ Heisenberg model in 2D. In addition to not having known analytical solutions, numerical treatment of this problem becomes very hard due to the exponential growth of the Hilbert space that makes it intractable already for a system as small as a 6×6 lattice in 2D. Therefore, as we already stated, Eq. (5.22) puts forward the p-orbital system as an obvious candidate for simulating the XYZ model.

We will illustrate that this is indeed the case, by considering a lattice with very deep wells in the y direction, such that the dynamics is restricted to happen in the x axis. The idea is to obtain an effective 1D system out of the asymmetric 2D lattice, that is appropriately tuned to still keep the (quasi) degeneracy between the orbitals. In this setup, the Z_2 symmetry of Eq. (2.51) is broken and the system has the additional term describing the external field. In the presence of the field the XYZ model is non-integrable—and therefore the need for quantum simulation, but properties of the ground-state can still be extracted with a combination of different techniques. As we show here, this system has a rich phase diagram with different phases separated by different types of phase transitions. We will explore these in the context of p-band physics.

In 1D, the study of the XYZ model has a long history. It was first shown by Sutherland in 1970 [4, 14] that the transfer matrix of any eight-vertex model commutes with the Hamiltonian of the XYZ Heisenberg model. Baxter showed in 1971 and 1972 that the minimum eigenvalue of the XYZ model with no external field can be obtained for any values of the couplings, because this Hamiltonian is effectively a logarithmic derivative of an eight-vertex transfer matrix [4, 14]. Baxter studied the ground-state properties of the XYZ model by generalizing the Bethe ansatz [4] and in 1973 Baxter's results were generalized by other authors for computing the energy of excitations.

Before proceeding, let us first we re-write Eq. (5.22) in the standard notation

$$\hat{H}_{\text{Mott}_1} = \sum_{\langle i,j \rangle} J \left[(1+\gamma) \hat{S}_i^x \hat{S}_j^x + (1-\gamma) \hat{S}_i^y \hat{S}_j^y + \frac{\Delta}{J} \hat{S}_i^z \hat{S}_j^z \right] + \sum_i h \hat{S}_i^z, \quad (5.28)$$

and in 1D, where $J=-2t^xt^y/U_{xy}$, $\Delta=-J^{zz}$, $\gamma=-4U_{xy}^2/U^2$ and $h=J^z$ with $\sigma=x$ (see Eq. (5.26)). We re-write it once more with the use of the *Jordan–Wigner transformation*

$$\hat{S}_{i}^{-} = e^{i\pi \sum_{j=1}^{i-1} \hat{c}_{j}^{\dagger} \hat{c}_{j}} \hat{c}_{i}
\hat{S}_{i}^{+} = \hat{c}_{i}^{\dagger} e^{i\pi \sum_{j=1}^{i-1} \hat{c}_{j}^{\dagger} \hat{c}_{j}},$$
(5.29)

in terms of the fermionic operators \hat{c}_j satisfying $\{\hat{c}_i,\hat{c}_j\} = \{\hat{c}_i^\dagger,\hat{c}_j^\dagger\} = 0$ and $\{\hat{c}_i,\hat{c}_j^\dagger\} = \delta_{ij}$. This yields the fermionic Hamiltonian

$$\hat{H}_{\text{Kitaev}}/J = \sum_{n} \left[(\hat{c}_{n}^{\dagger} \hat{c}_{n+1} + \hat{c}_{n+1}^{\dagger} \hat{c}_{n}) + \gamma (\hat{c}_{n}^{\dagger} \hat{c}_{n+1}^{\dagger} + \hat{c}_{n+1} \hat{c}_{n}) + \frac{\Delta}{J} (\hat{c}_{n}^{\dagger} \hat{c}_{n} - \frac{1}{2}) (\hat{c}_{n+1}^{\dagger} c_{n+1}^{\dagger} - \frac{1}{2}) + \frac{h}{J} (\hat{c}_{n}^{\dagger} \hat{c}_{n} - \frac{1}{2}) \right],$$
(5.30)

that contains a pairing term proportional to the anisotropy parameter γ . The presence of a pairing term typically opens a gap in the energy spectrum, and accordingly, we expect the spectrum to be gapped whenever $\gamma \neq 0$. This should indeed be the case, because the anisotropy on the couplings is generated by the orbital-changing interactions, that reduce the otherwise U(1) continuous symmetry of the density-density interactions to a Z_2 discrete symmetry. In addition, we notice furthermore that the limit of $\Delta \to 0$ is a realization of the Kitaev chain [15].

Now in 1*D*, the ground-state of the *XYZ* Heisenberg model in an external field described by Eq. (5.28) is characterized by four different phases as one varies the system's parameters [16]. A schematic phase diagram is illustrated in Fig. 5.2. At zero field, the *XYZ* model is integrable and with known analytical expressions for the eigenvalues and eigenvectors [14]. At large and positive values of Δ/J the system has anti-ferromagnetic order in the *z* spin component. For small values of Δ/J , the system is in the so called *spin-flop* phase [16], that is characterized by Nèel order in the *x* or *y* spin component.⁶ For large and negative values of Δ/J and h=0, the *z* component of the spin is in a Z_2 -parity symmetry broken ferromagnetic state, and regardless of the sign of the couplings, the limit of very large external field is characterized by a highly magnetized state that is referred to as polarized phase. These three phases also characterize the phase diagram of the *XXZ* model in a longitudinal field.⁷ For non-zero anisotropy γ , however, the system has an additional phase between the anti-ferromagnetic and spin-flop phases that is called the *floating phase*. This is a gapless phase characterized by algebraic decay of correlations⁸ [2],

⁶It depends on the largest coupling. For the value of γ considered here the ordering occurs in the y component of the spin.

⁷Notice, however, that the spin-flop phase is called the XY phase in the phase diagram of the XXZ model. The difference between these two phases is the gapless versus gapped character of the excitations in the XXZ versus XYZ models, respectively.

⁸In terms of bosonization and renormalization group arguments [16, 17], the floating phase is characterized by irrelevant Umklapp terms and accordingly described by the Luttinger liquid theory. Upon entering the XY phase these terms are no longer irrelevant and the phase becomes gapped [16].

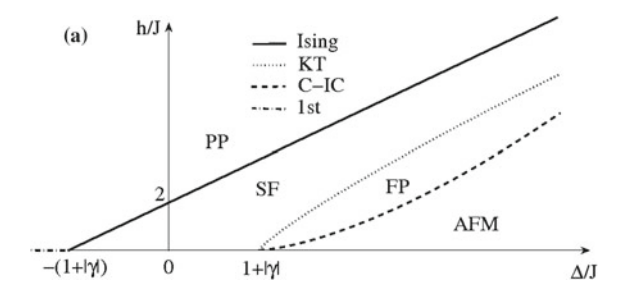


Fig. 5.2 Schematic phase diagram of the *XYZ* chain. AFM denotes the anti-ferromagnetic phase, FP the floating phase, SF the spin-flop phase and PP the polarized phase. The properties of these phases and different types of phase transitions are discussed in the text (Reprinted from Ref. [1])

which is rather unexpected from the viewpoint of the fermionic chain. In fact, since the pairing term in the Hamiltonian (5.30) is proportional to γ , we would expect the entire phase diagram to be gapped.

All these phases are separated by different types of phase transitions [16]. The transition from the anti-ferromagnetic to the floating phase is of the *commensurate-to-incommensurate* (C-IC) type, whereas the transition from the floating phase to the spin-flop phase is a *Berezinski–Kosterlitz–Thouless* (BKT) transition. For $\Delta < -(1+|\gamma|)$, at h=0, the transition between the two magnetized phases of positive and negative total magnetization is *first order*, and finally, between the spin-flop and the polarized phases there is an *Ising* transition.

In what follows we give a brief overview on the different phases and phase transitions discussed above. For illustrative purposes, magnetization properties are considered here in the context of an Ising-like Hamiltonian given by

$$H_{\text{Ising}} = -J \sum_{\langle i,j \rangle} \hat{S}_i \hat{S}_j + h \sum_i \hat{S}_i.$$

 Nèel order: Nèel order is the term generally used to describe a state with broken symmetry and for which

$$\langle \hat{\mathbf{S}}_i \rangle \neq 0$$

for all the spins [18]. Although this is most commonly used to refer to the bipartite lattice of the (Nèel) anti-ferromagnet, with alternating orientation of neighbouring spins [18], we notice the existence of more complex patterns that also correspond to a Nèel state [18].

• Anti-ferromagnetic phase (J < 0): as stated above, the anti-ferromagnetic phase is characterized by Nèel order with alternating neighboring spins. States of this type are characterized by staggered magnetization [18], and therefore with vanishing net magnetization:

$$M=\sum_{i}\langle \hat{S}_{i}\rangle=0.$$

 Floating phase (J < 0): this is a gapless phase without a local order parameter, and for which the correlations decay algebraically [19].

⁹The highly magnetized phase is also referred to as polarized phase.

- *Spin-flop phase* (*J* < 0): this corresponds to a gapped phase with Nèel order in the *x* and *y* components of the spin, with exponential decay of the correlations.
- Highly magnetized state or polarized phase (J < 0): for sufficiently large h, the phase
 diagram of spin models subjected to external fields will always display a highly magnetized state, where the spins align in the direction of the field. This corresponds to an
 "imposed" ordering, in the sense that it does not involve symmetry breaking and the spins
 are uncorrelated.
- Ferromagnetic phase (J > 0): all the spins align in the same direction, building a state of
 saturate magnetization. The ordering process involves symmetry breaking with an order
 parameter similar to that of the anti-ferromagnetic phase [18].

We now briefly discuss the properties of the different types of phase transitions that appear in the phase diagram of the infinite system, Fig. 5.2:

- Ising transition: the transition between the polarized and the spin flop phases belongs to the universality class of the 2D Ising model. It is classified as a continuous or second order phase transition, and therefore the discontinuities appear at the level of the order parameter (or second derivatives of the energy). In the Ising transition, the critical exponent related to the divergence of the correlation length goes as $\xi \propto$ (distance from the transition) $^{-1}$ as one approaches the critical point, and in addition, the dynamical critical exponent 10 (z) is also equal to one [21, 22].
- Berezinski-Kosterlitz-Thouless transition (BKT): BKT transitions also belong to the class
 of continuous phase transitions. They are rather special, however, because all the derivatives are continuous (they are sometimes referred to as infinite order phase transitions), and
 there is no local order parameter [23]. In fact, BKT transitions do not involve symmetry
 breaking and are not described by the Landau theory.
- Commensurate to incommensurate transition (C-IC): the C-IC transition happens due to the interplay of competing length scales in the system. In a periodic system, for example, the collective excitations can develop a periodic structure that has different period from the "natural period of the system". These structures could appear in the form of kinks, walls or solitons 11 [24].
- First order phase transition: in thermodynamic systems, first order phase transitions are defined as transitions that involve coexistence of phases, latent heat, and the discontinuities appear in the first derivative of the free energy [21]. In the same way, in quantum phase transitions, ¹² the discontinuities appear in the first derivative of the ground state energy as one of the Hamiltonian's parameters is varied.

Finite Size Effects

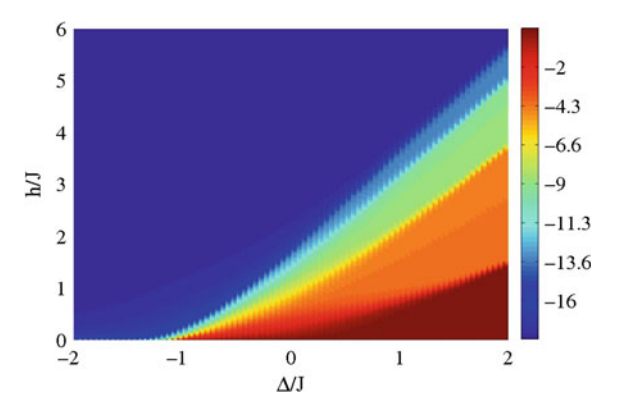
As we stated before, the rich phase diagram of the XYZ model in an external field makes the system of bosons in the p band an attractive tool for quantum

¹⁰The dynamical critical exponent is the exponent defined to characterize the behavior of the correlation time near the critical point. In the same way as it works for the correlation length, the correlation time also diverges in the vicinity of the phase transition. The divergence of the correlation time implies that the fluctuations become incredibly slow, a phenomenon that is known as the *critical slowing down* [20, 21].

¹¹A very good review on the subject is given in Ref. [19].

¹²Here there is no concept of temperature, i.e., quantum phase transitions happen at T=0 and due to competition between non-commuting terms in the Hamiltonian of the system [25].

Fig. 5.3 Finite size phase diagram obtained from exact diagonalization of a system with 18 spins and with the anisotropy parameter $\gamma=0.2$. It displays the total magnetization M (as defined in the text) which is characterized by an incomplete devil's staircase of SDW between the AFM and the PP phases (Reprinted from Ref. [1])



simulation. In fact, in a controllable environment this would open up for the possibility of probing properties of different phases in the vicinity of different types of phase transitions. However, the outcomes of any experiments of such systems should be analyzed with additional considerations to account the effects of finite size due to the harmonic confinement inevitably required in experiments with cold atoms. It is therefore important to reproduce the theoretical study in systems with finite size. We notice, first, that if the trap is smooth enough in the confined system, the couplings of the spin model are only renormalized to acquire a spatial dependence. If the size of the orbitals is very small compared to the length scale imposed by the trap, then this spatial dependence is not relevant for the physics and can be safely neglected.

We therefore restrict the study of finite size effects to the open chain¹³ with constant couplings, where we perform exact diagonalization for systems with up to 18 spins. We focus on the behavior of the total magnetization of the ground state

$$M = \sum_{i} \langle \hat{S}_{i}^{z} \rangle \tag{5.31}$$

for different values of h/J and Δ . γ is assumed to be fixed. The result for the case of 18 spins is presented in Fig. 5.3, that clearly shows the well defined values of total magnetization M expected for the anti-ferromagnetic and polarized phases. In between, however, we observe various plateaus that mark the different values of M due to modulation of the anti-ferromagnetic Nèel state with increasing values of h, building a *devil's staircase* structure of *spin-density waves* (SDW) [19, 26]. This also suggests that in terms of the total magnetization M, the Ising transition between the polarized and the spin flop phase is the one for which we expect a better quantitative estimate. While it is not clear whether the C-IC transition can be captured with this

¹³That is, with open boundary conditions.

order parameter,¹⁴ the BKT transition is most likely overshadowed due to the sharp transitions between the different spin density waves. In the thermodynamic limit this staircase becomes complete and one then recovers the phase diagram displayed in Fig. 5.2.¹⁵ These transitions between the different SDW are more pronounced for moderate system sizes and we estimate approximately 15 different SDW between the anti-ferromagnetic and polarized phases of a system with 50 spins.¹⁶

5.2.2 Experimental Probes, Measurements and Manipulations

All theory, dear friend, is gray, but the golden tree of life springs ever green.

—From Faust, Johann Wolfgang von Goethe.

The entire derivation of the effective spin model presented so far is based on the fact that the spins are encoded in spatial degrees of freedom rather than in internal atomic states. Accordingly, experimental manipulation/detection in this system requires the ability of controlling the spatial states of the atoms at single sites. As we argue here, a possible protocol for the experimental probes can be implemented with the use of trapped-ion techniques [29] combined with *single-site addressing* [30, 31].

Indeed, in the region of parameters relevant for the physics deep in the Mott insulator phase, the sites of the optical lattice can be accurately approximated by a harmonic potential with frequency $\omega_{\alpha} = \sqrt{2V_{\alpha}k_{\alpha}^2/m}$ (recall that k_{α} are the wave vectors of the optical lattice laser in the direction α) [32]. In this potential, different vibrational levels, that correspond to the different bands in the context of optical lattices, can then be coupled via stimulated Raman transitions performed in a two-level atom [33]. As we mentioned in Sect. 2.5 this technique has been successfully employed in Ref. [33] for promoting atoms from the s to p bands, in the Mott phase, of 1D, 2D and 3D lattices. However, since that study focused on the properties of coherence of the superfluid phase, further manipulation of the orbital degrees of freedom in the Mott phase have not been discussed. We therefore extend the method and propose an experimental scheme to account for this case. Before this, we revise the key concepts involved in the experimental procedure.

Consider thus a Raman coupling between the $|1\rangle = |F = 1\rangle$ and $|2\rangle = |F = 2\rangle$ atomic electronic states of ⁸⁷Rb. These are two-photon processes where the two levels are coupled with an intermediate virtual state, far detuned from all the other states of

¹⁴Notice, however, that this is not excluding the possibility of having different order parameters with more accurate predictions for the phases in between the polarized and the anti-ferromagnetic ones.

¹⁵In fact, it has been conjectured [27] that using similar heuristics for going up and down the steps of a complete devil's staircase, Chuck Norris counted to infinity—twice [28].

¹⁶We consider here that the chain with 50 spins is supposed to provide a very good experimental picture of the system that we would like to realize.

the system [33]. Because of this intermediate coupling, implementation of Raman transitions require the use of two different lasers, whose corresponding wave vectors are denoted here by k_{L_1} and k_{L_2} . The matrix element characterizing this transition is given by

$$\frac{\Omega_1 \Omega_2^*}{\delta} \langle 2|e^{i(k_{L_1} - k_{L_2}) \cdot \mathbf{x}}|1\rangle, \tag{5.32}$$

where Ω_i are the Rabi frequencies between the $|i\rangle$ states, i=1,2 with another far detuned auxiliary state of this system, say $|aux\rangle$, and δ is the detuning between $|aux\rangle$ and the virtual intermediate state.

After adiabatic elimination of the auxiliary state, the interaction between the atom in the harmonic potential with the lasers driving the Raman coupling is given by [32]

$$H = \sum_{\alpha} \omega_{\alpha} \hat{a}^{\dagger} a - \sum_{\alpha} \left[\frac{\Delta_{\alpha}}{2} \sigma_{z} + \frac{1}{2} \Omega \left(\sigma_{+} e^{i \eta_{\alpha} (\hat{a} + \hat{a}^{\dagger})} + H.c. \right) \right], \tag{5.33}$$

where the first term accounts for the center of mass motion of the atom in the harmonic potential, and the second and third terms describe the driven two-level system in the rotating-wave approximation [32]. In this notation $\Omega = \Omega_1 \Omega_2^* / \delta$ is the effective Rabi frequency, $\sigma_+ = (\sigma_-)^\dagger = |2\rangle\langle 1|$, $\sigma_z = |2\rangle\langle 2| - |1\rangle\langle 1|$, $\Delta_\alpha = \omega_\alpha - \omega_{12}$ are the detunings of the lasers with respect to the atomic transition, of frequency ω_{12} , and $\eta_\alpha = \Delta k_{L,\alpha} \sqrt{\hbar/2m\omega_\alpha}$ is the Lamb-Dicke parameter, with $\Delta k_{L,\alpha} = k_{L_1,\alpha} - k_{L_2,\alpha}$.

In the $Lamb-Dicke\ regime$, when $\eta_{\alpha}\ll 1$, the expansion of the exponential can be truncated to $e^{i\eta_{\alpha}(\hat{a}+\hat{a}^{\dagger})}\approx 1+\eta_{\alpha}(\hat{a}+\hat{a}^{\dagger})$ [32], and the corresponding Hamiltonian describes a two-level system coupled to the phonon excitations of the harmonic oscillator with bare Hamiltonian given by $H_0=\hat{a}^{\dagger}a-\frac{1}{2}\Delta_{\alpha}\sigma_z$. The eigenstates of this system can be denoted by $|1,n\rangle$ and $|2,n\rangle$, with n labeling the vibrational level. By carefully choosing the driver frequency, three possible transitions can be implemented [32]:

(i) The carrier transition, when $\Delta_{\alpha} = 0$,

$$H_{car} = \frac{\hbar}{2} \Omega \left[\sigma_+ + H.c. \right], \tag{5.34}$$

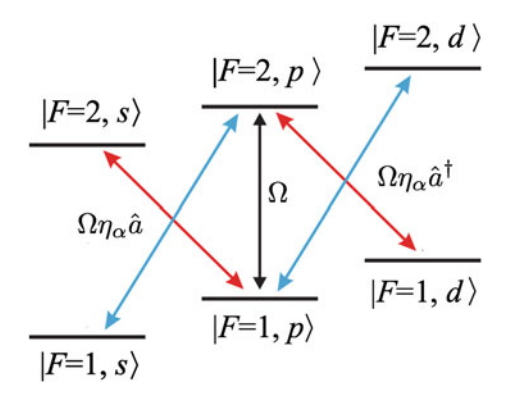
which couples the orbital states but has no effect in the vibrational state.

(ii) The red sideband transitions, when $\Delta_{\alpha} = -\omega_{\alpha}$,

$$H_{rsb} = \frac{\hbar}{2} \Omega \eta_{\alpha} \left[\hat{a} (\sigma_{-})^{\dagger} + \hat{a}^{\dagger} \sigma_{-} \right], \tag{5.35}$$

that decrease the vibrational state n by one quanta, when the atom swaps from $|1\rangle$ to $|2\rangle$.

Fig. 5.4 Schematic couplings between the different orbital states. While the carrier transition does not change the vibrational state of the atom, *red* and *blue* sideband transitions can be used to lower and to raise the vibrational states of the atom, which therefore couples different orbital states (color figure online)



(iii) The blue sideband transitions, when $\Delta_{\alpha} = \omega_{\alpha}$

$$H_{bsb} = \frac{\hbar}{2} \Omega \eta_{\alpha} \left[\hat{a}^{\dagger} (\sigma_{-})^{\dagger} + \hat{a} \sigma_{-} \right], \tag{5.36}$$

that increase the vibrational level n by one for the same atomic transition as above.

These transitions are schematically shown in Fig. 5.4.

In addition to selective transitions, it is also possible to selectively address the different orbital states [30]. p_x orbitals, for example, can be addressed by choosing driver lasers with no component in the y and z directions, i.e., $k_{L_1} - k_{L_2} = k_{L_x}$. Analogous relations hold for manipulations of p_y orbitals only.

Now in order to show that these techniques provide full control of the system, we discuss implementation of arbitrary rotations $\hat{R}_{\beta}(\phi) = e^{\hat{S}^{\beta}\phi}$, where $\beta = \{x, y, z\}$ and ϕ is an effective angle of rotation. The simplest case, of rotations around the z component of the spin, can be performed by noticing that $\hat{S}^z = \hat{S}^+\hat{S}^- - 1$. Therefore, it is enough to realize the operation $\hat{S}^+\hat{S}^-$, which phase shifts one of the orbitals. This is nothing but a Stark shift of one of the orbitals, ¹⁷ which can be implemented via driving the carrier transition off-resonantly for one of the two-orbitals.

The $R_x(\phi)$ operation can be implemented by simultaneously driving off-resonantly the red sidebands of the two orbitals. Due to the large detuning, the *s*-band will never become populated but the transition between the two orbitals can be made resonant. This operation involves the three states that we denote here as $\{|x,0,0\rangle,|0,y,0\rangle$ and $|0,0,s\rangle\}$, where the last entry of the ket refers to the state in the *s* band. The *p* orbitals are coupled to the *s* orbital in a *V*-configuration [34], that in the *rotating wave approximation* is described by [34, 35]

¹⁷Recall that the driving occurs in the largely detuned case.

$$\hat{H}_V = \begin{bmatrix} 0 & 0 & \Omega_1 \\ 0 & 0 & \Omega_2 \\ \Omega_1 & \Omega_2 & \delta \end{bmatrix}, \tag{5.37}$$

where Ω_1 and Ω_2 are taken to be real and spatially dependent. For $\delta \gg \Omega_1$, Ω_2 the Hamiltonian that generates a rotation with the *x* component of the spin, $\hat{R}_x(\phi)$ [34],

$$\hat{H}_x = \begin{bmatrix} 0 & \Omega \\ \Omega & 0 \end{bmatrix} = \Omega \hat{S}_x, \tag{5.38}$$

is then obtained after adiabatic elimination of the state $|0,0,s\rangle$. Note, however, that if the Raman transition between the two orbitals is not resonant, then this process will perform a combination of rotations with the x and z spin components. Finally, the rotations with the y component of the spin can be performed in two ways, either by adjusting the phases of the lasers, or by noticing that $\hat{R}_{y}(\phi) = \hat{R}_{z}(\pi/4)\hat{R}_{x}(\phi)\hat{R}_{z}(-\pi/4)$.

This method allows thus for any manipulation of single spins at a given site. To measure the state of the spin in a given direction, one then combines the rotations with single site resolved fluorescence (which measures \hat{S}_i^z) [36]. More precisely, since the drive laser can couple to the two orbitals individually, one of the orbitals will be transparent to the laser while the other one will show fluorescence. In other words, this is equivalent to measuring \hat{S}_i^z on a single site. The other components of the spin can also be measured in this way, but after the correct rotation to the spin state has been previously implemented. Furthermore, with the help of coincident detection [37], it is possible to extract correlators of the type $\langle \hat{S}_i^{\alpha} \hat{S}_j^{\beta} \rangle$, α , $\beta = \{x, y\}$ [38].

External Tuning of the Couplings

The spin mapping carried out in Sect. 5.2 provides a route for obtaining the Hamiltonian that effectively describes the physics of Mott-1 phase of p-orbital bosons. In that procedure, all the couplings in the spin model are shown to depend initially on the parameters of the bosonic system, and therefore also on the configuration of the optical potential.

In order to gain some intuition on the character of the couplings and to locate the system in the phase diagram of Fig. 5.2, we compute the couplings of the spin model with use of the analytical expressions of the parameters of the bosonic system in the harmonic approximation (see Appendix "p-band Hamiltonian parameters in the harmonic approximation"). Introducing σ_{α} to denote the widths of the orbital wave functions for the spatial directions $\alpha = \{x, y, z\}$, ¹⁸ we obtain

$$U_{xx} = U_{yy} = 3U_{xy} = \frac{u_0}{\sigma_x \sigma_y \sigma_z},$$
 (5.39)

 $^{^{18}}$ Notice that the two-orbital system is obtained from the ^{3}D lattice with the dynamics suppressed in z direction and without preserving the degeneracy of the third orbital.

where u_0 is the effective strength of the interactions, proportional to the s-wave scattering length. Now by noticing that $|t^x|^2 \gg |t^y|^2$, from Eq. (5.25),

$$\Delta \approx -|t^{x}|^{2} \left(4 \frac{U_{yy}}{U_{xx}U_{yy} - U_{xy}^{2}} - \frac{1}{U_{xy}} \right), \tag{5.40}$$

which corresponds to

$$\Delta = -|t^x|^2 \frac{3\sigma_x \sigma_y \sigma_z}{2u_0} < 0. \tag{5.41}$$

Since this estimate yields $\Delta < 0$, the exchange interactions in the z spin component favor primarily ferromagnetic order. Similar computation yields $\gamma = 1/2$, which according to Eqs. (5.23) and (5.24) yield interactions favoring anti-ferromagnetic ordering in the x and y spin components. Although this is quantitatively different from the result obtained from numerical computation with use of the lattice Wannier functions, the qualitative picture provided by the estimate with the couplings in the harmonic approximation is correct. Namely, numerical computation always yields $\Delta < 0$ and therefore puts the system in the ferromagnetic side of the phase diagram. For the p-band system, this means that the orbitals are "ferromagnetically" aligned in the direction of the node, while anti-aligned in the perpendicular direction.

However, the schematic phase diagram of Fig. 5.2 shows that a great deal of interesting physics is found in the region of anti-ferromagnetic type of interactions in the z component of the spin. Now is it possible to drive the p-orbital system into the anti-ferromagnetic part of the phase diagram?

Fortunately, the experimental techniques discussed in the previous section can be used to selectively reshape the orbital states in such a way to control the relative magnitude of the parameters of the many-body system. This can be experimentally implemented by driving the carrier transition of either of the two orbitals dispersively, with a spatially dependent field. ¹⁹ If the shape of the drive is chosen in such a way that the resulting Stark shift is weaker in the center of the sites, then this procedure will narrow the orbital in one of the directions and we say that the orbital is squeezed. Let us assume that the squeezing is implemented here in the y direction. Then the only requirement is that the spatial profile of the field driving the carrier transition changes in the length scale of the lattice spacing in this direction. The tunneling rates t^x and t^y will not be affected by the squeezing but both U_{yy} and U_{xy} and therefore also the coupling constants, will.

To be more specific, let us assume that the ratio σ of the harmonic length scales of the p_x and the p_y orbitals is tuned (in the y direction). A straightforward calculation using harmonic oscillator functions yields

¹⁹This is nothing but a potential that reshapes the lattice sites in different ways for the different orbitals, and that can be implemented as a change in the σ_y widths of the different Wannier functions $(w_x(\mathbf{r}))$ and $w_y(\mathbf{r})$ of the orbitals, while the widths σ_x are kept unaltered.

$$\alpha \equiv \frac{U_{xx}}{U_{xy}} = 2^{-3/2} 3 \frac{(1 + \sigma^2)^{3/2}}{\sigma}$$
 (5.42)

and

$$\beta \equiv U_{yy}/U_{yx} = 2^{-3/2}3(1+\sigma^2)^{3/2},$$
 (5.43)

from where we can write the dependence of the coupling constants on the width $\boldsymbol{\sigma}$ by

$$\Delta/J = 2t^{x}(t^{y})^{-1} \frac{\beta}{(\alpha\beta - 1)} = 2t^{y}(t^{x})^{-1} \frac{\alpha}{(\alpha\beta - 1)} - \frac{t^{x}(t^{y})^{-1} + t^{y}(t^{x})^{-1}}{2}$$
(5.44)

and

$$\gamma = -\frac{4}{(\alpha\beta - 1)}. (5.45)$$

This allows for experimentation with different types of XYZ chains. Indeed, while the interactions of \hat{S}^y always favor antiferromagnetic order, the interactions in \hat{S}^x and \hat{S}^z can happen with couplings that support both ferro and anti-ferromagnetic ordering as shown in Fig. 5.5. Therefore, the *p*-orbital system is a tunable quantum simulator for different types of XYZ Heisenberg models.

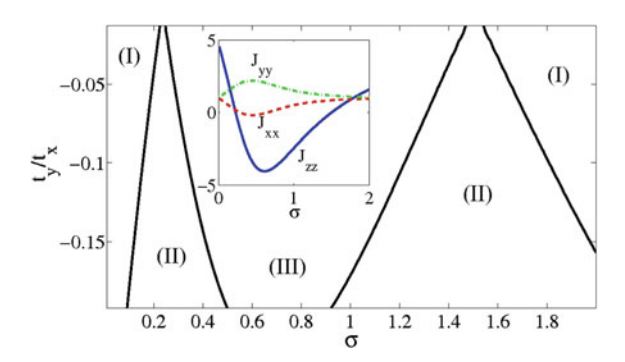


Fig. 5.5 Different types of models that are achieved by varying the relative tunneling strength and the relative orbital squeezing. The three different parameter regions are: (I) anti-ferromagnetic couplings in all the components of the spin with $\Delta > J(1+|\gamma|)$, (II) ferromagnetic or anti-ferromagnetic couplings in the z component of the spin and anti-ferromagnetic in the y component with $J(1+|\gamma|) > \Delta$, and (III) the same as in (II) but with $|\Delta| > J(1+|\gamma|)$. The inset shows one example of the spin parameters where $t^y/t^x = -0.1$, and $J^{xx} = (1+\gamma)$, $J^{yy} = (1-\gamma)$ and $J^{zz} = \Delta/J$ (Reprinted from Ref. [1]. We notice that $J_{\alpha\alpha} = J^{\alpha\alpha}$, and $t_{\alpha} = t^{\alpha}$ in the notation of this thesis)

5.2.3 Experimental Realization

As discussed in Sect. 2.5, the lifetimes in experimental realizations with bosonic atoms in the p band are surprisingly long. In fact, in the study of Ref. [33], the atoms could tunnel hundreds of times before decaying to the s band in a 1D realization with mean occupation of two atoms per site. Since the main decay mechanism stems from atom-atom collisions [33, 39], the lifetimes are expected to increase considerably when the lattice is prepared with a unit filling.²⁰

We can estimate the typical values for the tunneling times from the overlap integrals of neighboring Wannier functions (see Eq. (2.47)). Considering ⁸⁷Rb atoms, for example, and $\lambda_{lat}=843\,\mathrm{nm}$ to be the wavelength (in the *y*-direction) which sets the recoil energy E_R , we obtain $J/E_R\sim0.01$ and the characteristic tunneling time $\tau=\hbar/J\sim5\,\mathrm{ms}$ for the system with $V_x=30E_R$, $V_y=50E_R$ and $V_z=60E_R$. This corresponds to a few dozens of times smaller than the expected lifetimes [33], which should allow for experimental explorations of the systems proposed here. In addition, it is possible to use the external driving discussed above to increase the lifetimes even further.

As a last remark we notice that the temperatures required for observation of the spin correlations are of the order of $k_BT \lesssim J \sim t^2/U$ [11]. Although it might be experimentally challenging to reach such low temperatures in the laboratory at the moment, the rapid development in the field of cold atoms gives an optimistic prospect for explorations of this type of physics in the near future [40].

5.2.4 Effective Model Including Imperfections Due to s-Orbital Atoms

In addition to the low temperatures required for the implementation of effective spin models with systems of cold atoms, another experimental challenge for the system in the p band is related to experimental imperfections on the process of loading. The techniques used in Ref. [33], based on stimulated Raman transitions reported 80 % fidelity in the process of promoting the atoms from the Mott phase in the s to the p band. Therefore, it is important to understand how the presence of residual s-orbital atoms affects the physics discussed so far.

Let us start by considering

$$U_{sp_{\alpha}} = U_0 \int d\mathbf{r} |w_{s,j}(\mathbf{r})|^2 |w_{\alpha,j}(\mathbf{r})|^2, \qquad (5.46)$$

 $^{^{20}}$ In fact, Ref. [33] estimates an increase of up to a factor of 5 in the lifetimes for the situation with unit filling of the lattice sites.

which characterize the strength of repulsive interactions between an s- and a p_{α} -orbital atom at the site j. Since the p_{α} -orbital wave-functions are spatially broader than the s-orbital ones, $U_{sp_{\alpha}} > U_{\alpha\beta}$, and accordingly, the repulsive interaction between s-orbital and p-orbital atoms is larger than the repulsive interaction when both atoms are in the p band.

Now to the list of Sect. 5.1, two additional processes should be added in the effective model. The first one, which includes tunneling of s-orbital atoms, can be safely neglected due to the reduced rate of tunneling in the s band and the larger value of the coupling constant for repulsive interaction U_{sp} . The second process, which involves tunneling of p_{α} -orbital atoms, will contribute to the Hamiltonian with the following term

$$-\frac{|t_{\sigma}^{\alpha}|^2}{U_{sn}}\hat{a}_{\alpha,i}^{\dagger}\hat{a}_{s,j}^{\dagger}\hat{a}_{\alpha,i}\hat{a}_{s,j} = -\frac{|t_{\sigma}^{\alpha}|^2}{U_{sn}}\hat{n}_{\alpha,i}, \qquad (5.47)$$

where $\hat{a}_{s,j}$ ($\hat{a}_{s,j}^{\dagger}$) annihilates (creates) an *s*-orbital atom at the site *j* and where we used that $\hat{n}_{s,j} = 1$. The presence of residual *s*-orbital atoms is therefore associated with local fluctuations of the external fields, that is described by the additional term

$$\hat{H}_{i}^{\text{dis}} = \frac{1}{2U_{sp}} \left(|t_{\sigma}^{x}|^{2} - |t_{\sigma}^{y}|^{2} \right) \delta_{1,n_{i}^{s}} \, \hat{S}_{i}^{z} = h_{i}^{z} \hat{S}_{i}^{z}. \tag{5.48}$$

The result is the Hamiltonian of the XYZ model in a random external field,

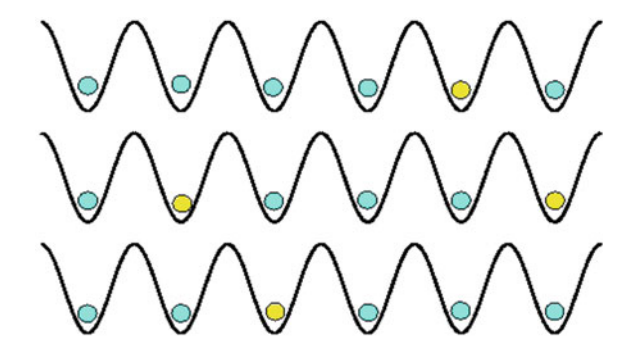
$$\hat{H}_{\text{Mott}_{1}}^{(\text{dis})} = -\sum_{\langle i,j \rangle_{\sigma}} \left(J^{zz} \hat{S}_{i}^{z} \hat{S}_{j}^{z} + J^{xx} \hat{S}_{i}^{x} \hat{S}_{j}^{x} + J^{yy} \hat{S}_{i}^{y} \hat{S}_{j}^{y} \right) - \sum_{i} J_{i}^{z} \hat{S}_{i}^{z}, \tag{5.49}$$

where

$$J_i^z \to J^z + h_i^z. \tag{5.50}$$

Since the loading of atoms to the p band is implemented globally, a coherent loading will prepare translationally invariant states with a fraction of the population in the s band. However, whenever the loading is not perfectly coherent, we may envision situations where decoherence process lock the s-band atoms at fixed sites. In such cases, the collapse of the state describing these residual atoms, induced by decoherence, will break the translational symmetry and the overall effect of the s-band atoms will be that of static disorder in the fields as in Eq. (5.49). In light of the Imry-Ma argument [41], which establishes a criteria for the stability of ordered phases in the presence of disorder, we expect the phase diagram of the 1D system (see Fig. 5.2) to be robust against a small number of s-orbital atoms. As the fraction of impurity atoms increases, and as such, the number of sites with a disordered external field, we expect the disorder to become relevant, and the qualitative picture to change. However, the study of the random-field XYZ chain is out of the scope of the present thesis and is left for the future (Fig. 5.6).

Fig. 5.6 Schematic plot of three random experimental realizations of the insulating state. The *yellow balls* represent an *s*-orbital atom, while the *blue* ones represent *p*-orbital atoms



Let us consider the effect of random-field disorder in the classical Ising model²¹ described by

$$H = -J \sum_{\langle i,j \rangle} S_i S_j - \sum_i h_i S_i,$$
 (5.51)

where $\langle h_i \rangle = 0$ ensures that global symmetries of the clean system remains untouched, and $\langle h_i h_i \rangle = W \delta_{ij}$.

In the limit where $W\gg J^2$, the ground state is a random paramagnet, where each S_i aligns with the local fields h_i . In the other limit, where $W\ll J^2$, the ground state is a state with most of the spins aligned with the neighbors. Now the question behind the Imry-Ma argument is: "is it still possible to have ferromagnetic order in the presence of a weak random field?". Here it is important to understand whether it is favorable for the system to form domains. According to Imry and Ma, the relevant energetic balance lies on the tradeoff between the energy loss due to the formation of domain walls with the energy gain due to the random field. Therefore in d dimensions, one needs to compute the energy cost for creating the domain wall with respect to its size, and the uniform state is stable if the random field energy E_{RF} is smaller than the domain wall energy E_{DW} ,

$$\sqrt{W}L^{d/2} < JL^{d-1}$$
, or $\sqrt{W} < JL^{d/2-1}$. (5.52)

Since for weak disorder $\sqrt{W} \ll J$, if d>2 the ordered state is stable and the ferromagnetic state is possible to be attained, whereas if $d\leq 2$ the ordered state is unstable and it is more favorable for the system to form domains if L is large enough. This also means that if $d\leq 2$, arbitrarily weak disorder can destroy ferromagnetic order in a classical model. ²²

The rigorous proof of this result, the Aizenman–Wehr theorem, states that the presence of a random field is capable of destroying long range order if the system has an order parameter with discrete symmetry for all $d \le 2$, while if the order parameter has continuous symmetry, 23 random fields destroy long-range order for all $d \le 4$.

²¹This discussion is based on Ref. [21].

²²Due to the classical to quantum correspondence via partition function in imaginary time, a quantum system in d dimensions is usually equivalent to a classical system in d+1 dimensions.

²³The energy of domain walls in systems with continuous symmetries scales as $E_{DW} \sim L^{d-2}$.

5.3 3D System and Simulation of Heisenberg Models Beyond Spin-1/2

The analysis of the two-orbital system in the p band revealed an interesting correspondence between this and the XYZ Heisenberg model, that furthermore, due to the particular dynamics in the p band, extends the realizations of spin systems with cold atoms in optical lattices to the Hamiltonian of the fully anisotropic Heisenberg model. Now how to describe the three-orbital system in terms of an effective pseudospin Hamiltonian and what are the properties of the corresponding model?

From the mean-field analysis of Sect. 3.1.2 we have seen that in 3D lattices, the three-orbital system has a plethora of interesting properties that are absent in the 2D model, as for example the possibility of frustrated configurations for the phase of the order parameter. But what happens in the Mott insulating phase?

In this section, we study the physics of the first Mott lobe of the three-orbital system in the p band of 3D optical lattices. We will show that this system is effectively described by a Hamiltonian with nearest neighbors interactions, where the degrees of freedom are the generators of the SU(3) group. We will extend the method used in the previous sections to account for the third orbital, and we discuss properties of both the bosonic and the fermionic many-body systems, starting next with the bosonic case.

5.3.1 The Bosonic Case

Let us recall the explicit expression of the local part of the Hamiltonian of the three-orbital system in the p band,

$$\begin{split} \hat{H}_{U}^{b} &= \sum_{i} \left[\frac{U_{xx}}{2} \hat{n}_{x,i} \left(\hat{n}_{x,i} - 1 \right) + \frac{U_{yy}}{2} \hat{n}_{y,i} \left(\hat{n}_{y,i} - 1 \right) + \frac{U_{zz}}{2} \hat{n}_{z,i} \left(\hat{n}_{z,i} - 1 \right) \right] \\ &+ \sum_{i} \left(2U_{xy} \hat{n}_{x,i} \hat{n}_{y,i} + 2U_{xz} \hat{n}_{x,i} \hat{n}_{z,i} + 2U_{yx} \hat{n}_{y,i} \hat{n}_{z,i} \right) \\ &+ \sum_{i} \left[\frac{U_{xy}}{2} \left(\hat{a}_{x,i}^{\dagger} \hat{a}_{x,i}^{\dagger} \hat{a}_{y,i} \hat{a}_{y,i} \right) + \frac{U_{xz}}{2} \left(\hat{a}_{x,i}^{\dagger} \hat{a}_{x,i}^{\dagger} \hat{a}_{z,i} \hat{a}_{z,i} \right) + \frac{U_{yz}}{2} \left(\hat{a}_{y,i}^{\dagger} \hat{a}_{y,i}^{\dagger} \hat{a}_{z,i} \hat{a}_{z,i} \right) + H.c. \right] \end{split}$$

$$(5.53)$$

and define the basis in the \mathcal{H}_P and \mathcal{H}_O subspaces by (see Sect. 5.1)

$$\mathcal{H}_{P} = \{ |x, x\rangle, |x, y\rangle, |x, z\rangle, |y, x\rangle, |y, y\rangle, |y, z\rangle, |z, x\rangle, |z, y\rangle, |z, z\rangle \}, \quad (5.54)$$

and

$$\mathcal{H}_{\mathcal{Q}} = \{ |0, 2x\rangle, |0, 2y\rangle, |0, 2z\rangle, |0, xy\rangle, |0, xz\rangle, |0, yz\rangle \}. \tag{5.55}$$

With the basis of \mathcal{H}_Q ordered according to (5.55), the projected Hamiltonian²⁴ \hat{H}_Q can be written in block diagonal form of 3 × 3 matrices as

$$\hat{H}_{Q} = \begin{pmatrix} \hat{H}_{Q_{1}} & 0\\ 0 & \hat{H}_{Q_{2}} \end{pmatrix}, \tag{5.56}$$

where the first block captures the action of \hat{H}_U in the states of the type $|0, 2\alpha\rangle$, while the second block accounts for the effects of \hat{H}_U in the $|0, \alpha\beta\rangle$ states for $\alpha, \beta = \{x, y, z\}$. The explicit expressions follow,

$$\hat{H}_{Q_1} = \begin{pmatrix} U_{xx} & U_{xy} & U_{xz} \\ U_{xy} & U_{yy} & U_{yz} \\ U_{xz} & U_{yz} & U_{zz} \end{pmatrix}$$
(5.57)

and

$$\hat{H}_{Q_2} = \begin{pmatrix} 2U_{xy} & 0 & 0\\ 0 & 2U_{xz} & 0\\ 0 & 0 & 2U_{yz} \end{pmatrix},\tag{5.58}$$

from where $\hat{K} = \hat{H}_Q^{-1}$ is easily computed. In the first block, the elements of $\hat{K}^{(1)} = \hat{H}_{Q_1}^{-1}$ can be written as

$$K_{\alpha\alpha}^{(1)} = \frac{1}{2\Lambda} \sum_{\beta\gamma} \left(\epsilon^{\alpha\beta\gamma} \right)^2 \left(U_{\beta\beta} U_{\gamma\gamma} - U_{\beta\gamma}^2 \right),$$

$$K_{\alpha\beta}^{(1)} = \frac{1}{\Lambda} \sum_{\gamma} \left(\epsilon^{\alpha\beta\gamma} \right)^2 \left(U_{\alpha\beta} U_{\beta\gamma} - U_{\alpha\beta} U_{\gamma\gamma} \right)$$
(5.59)

where $\epsilon^{\alpha\beta\gamma}$ is the Levi-Civita symbol and $\{\alpha,\beta,\gamma\}=(1,2,3)$ whenever $\{\alpha,\beta,\gamma\}=(x,y,z)$, and

$$\Lambda = \left(U_{xx} U_{yy} U_{zz} - U_{xz}^2 U_{yy} - U_{yz}^2 U_{xx} - U_{xy}^2 U_{zz} + 2 U_{xy} U_{xz} U_{yz} \right). \tag{5.60}$$

For simplicity, the elements of $K^{(2)} = \hat{H}_{Q_2}^{-1}$, in the second block, are denoted by

$$K_{\alpha\beta}^{(2)} = \frac{1}{2U_{\alpha\beta}},\tag{5.61}$$

and in the same way, $\{\alpha, \beta\} = (1, 2, 3)$, whenever $\{\alpha, \beta\} = (x, y, z)$.

According to the list of processes in Sect. 5.1 and the symmetries of the Hamiltonian of the bosonic case with three-orbitals, Eq. (2.42), the processes contributing to the effective Hamiltonian of the Mott-1 phase are (i), (iv), (v) and (vi). In the same way as for the two-orbital system, the transitions that break the conservation

²⁴Recall the derivation of Sect. 5.1 if necessary.

of number modulo 2 in each of the orbital states yield non-vanishing contributions, as should indeed be the case since such processes are absent in Eq. (5.53).

Now gathering the different contributions with the explicit expressions of the non-vanishing matrix elements for the different transitions, the effective Hamiltonian describing the Mott-1 phase of bosons in the p band of the three orbital system is given by

$$\hat{H}_{M_{1}}^{b} = -\sum_{\sigma} \sum_{\langle i,j \rangle_{\sigma}} \sum_{\alpha,\beta,\gamma} \left[\frac{|t_{\sigma}^{\alpha}|^{2}}{\Lambda} \left(\epsilon^{\alpha\beta\gamma} \right)^{2} \left(U_{\beta\beta} U_{\gamma\gamma} - U_{\beta\gamma}^{2} \right) \hat{n}_{\alpha,i} \hat{n}_{\alpha,j} + \frac{|t_{\sigma}^{\alpha}|^{2}}{U_{\alpha\beta}} \hat{n}_{\alpha,i} \hat{n}_{\alpha,j} \right. \\ \left. + 2 \frac{t_{\sigma}^{\alpha} t_{\sigma}^{\beta}}{\Lambda} \left(\epsilon^{\alpha\beta\gamma} \right)^{2} \left(U_{\alpha\beta} U_{\beta\gamma} - U_{\alpha\beta} U_{\gamma\gamma} \right) \hat{a}_{\beta,i}^{\dagger} \hat{a}_{\alpha,i} \hat{a}_{\beta,j}^{\dagger} \hat{a}_{\alpha,j} + \frac{t_{\sigma}^{\alpha} t_{\sigma}^{\beta}}{U_{\alpha\beta}} \hat{a}_{\beta,i}^{\dagger} \hat{a}_{\alpha,i} \hat{a}_{\alpha,j}^{\dagger} \hat{a}_{\beta,j} \right].$$

$$(5.62)$$

We now use the generators of the SU(3) group to encode the pseudospins of the three-orbital system. Although individually the orbital states have the structure of angular momentum, the generators of the SU(2) group fail to give a description of the effective dynamics of the many-body system with three orbitals in the p band. The reason is that the dynamical processes in the p band treat any combination of different orbital states at the same footing, and as a consequence, the ladder operators act as in the Lie algebra of the SU(3) group (see Fig. 5.7).

The SU(3) group has 8 generators, that are considered here in the representation defined by the Gell-Mann matrices [42]

$$\lambda_1 = \begin{pmatrix} 0 & 1 & 0 \\ 1 & 0 & 0 \\ 0 & 0 & 0 \end{pmatrix}, \quad \lambda_2 = \begin{pmatrix} 0 & -i & 0 \\ i & 0 & 0 \\ 0 & 0 & 0 \end{pmatrix}, \quad \lambda_4 = \begin{pmatrix} 0 & 0 & 1 \\ 0 & 0 & 0 \\ 1 & 0 & 0 \end{pmatrix}, \quad \lambda_5 = \begin{pmatrix} 0 & 0 & -i \\ 0 & 0 & 0 \\ i & 0 & 0 \end{pmatrix},$$

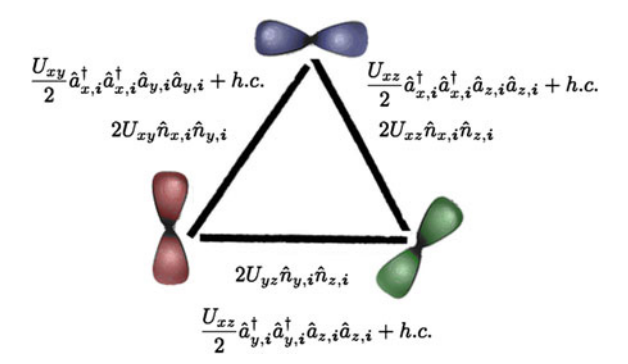


Fig. 5.7 Dynamical processes relating the different orbital states in the many-body bosonic system (as discussed in Eq. (2.54), the fermionic case contains only the density-density interactions part). Due to the symmetric coupling among the three orbital states, pairs of atoms in different orbitals scatter with equal amplitude for all the combinations of states, and a correct description requires the use of the generators of the SU(3) group. In fact, in the language of p orbitals, rather than the triangular scheme displayed above, the ladder operators of a three-state system with SU(2) symmetry act as $p_{\alpha} \rightleftharpoons p_{\beta} \rightleftharpoons p_{\gamma}$

$$\lambda_{6} = \begin{pmatrix} 0 & 0 & 0 \\ 0 & 0 & 1 \\ 0 & 1 & 0 \end{pmatrix}, \quad \lambda_{7} = \begin{pmatrix} 0 & 0 & 0 \\ 0 & 0 & -i \\ 0 & i & 0 \end{pmatrix}, \quad \lambda_{3} = \begin{pmatrix} 1 & 0 & 0 \\ 0 & -1 & 0 \\ 0 & 0 & 0 \end{pmatrix}, \quad \lambda_{8} = \frac{1}{\sqrt{3}} \begin{pmatrix} 1 & 0 & 0 \\ 0 & 1 & 0 \\ 0 & 0 & -2 \end{pmatrix}.$$
(5.63)

The Lie algebra of SU(3) is given by $[\lambda_i, \lambda_j] = 2if_{ijk}\lambda_k$, where i, j = 1, ..., 8 $f_{ijk} =$ $-f_{jik} = -f_{ikj}\dots$ are totally antisymmetric structure constants. The values for the different combinations of indices follow $f_{123} = 1$, $f_{147} = -f_{156} = f_{246} = f_{257} = f_{345} = -f_{367} = f_{367} = f_{367$ $\frac{1}{2}$ and $f_{458} = f_{678} = \frac{\sqrt{3}}{2}$. In addition, the two *Casimir operators* of the SU(3) group are

$$C_1(\lambda_i) = \frac{1}{4} \sum_i \lambda_i^2$$
 and

$$C_2(\lambda_i) = \frac{1}{8} \sum_{ijk} d_{ijk} \lambda_i \lambda_j \lambda_k,$$

where $d_{118} = d_{228} = d_{338} = -d_{888} = \frac{1}{\sqrt{3}}, d_{146} = d_{157} = d_{344} = d_{355} = -d_{366} =$ $-d_{377} = \frac{1}{2}$, and $d_{448} = d_{558} = d_{668} = d_{778} = -\frac{1}{2\sqrt{2}}$.

Now using the condition that $\hat{n}_{x,i} + \hat{n}_{y,i} + \hat{n}_{z,i} = 1$ in the Mott-1 phase, the diagonal elements λ_3 and λ_8 can be written as

$$\hat{n}_{x,i} = \frac{1}{3} + \frac{1}{2}\lambda_{3,i} + \frac{\sqrt{3}}{6}\lambda_{8,i},$$

$$\hat{n}_{y,i} = \frac{1}{3} - \frac{1}{2}\lambda_{3,i} + \frac{\sqrt{3}}{6}\lambda_{8,i},$$

$$\hat{n}_{z,i} = \frac{1}{3} - \frac{\sqrt{3}}{6}\lambda_{8,i}.$$
(5.64)

The SU(3) ladder operators are defined in terms of the non-diagonal Gell-Mann matrices. In terms of the orbital states,

$$\frac{\hat{T}_{i}^{\pm}}{2} = \hat{a}_{x,i}^{\dagger} \hat{a}_{y,i} = \lambda_{z,i}^{1} \pm i \lambda_{z,i}^{2},
\frac{\hat{V}_{i}^{\pm}}{2} = \hat{a}_{x,i}^{\dagger} \hat{a}_{z,i} = \lambda_{y,i}^{1} \pm i \lambda_{y,i}^{2},
\frac{\hat{U}_{i}^{\pm}}{2} = \hat{a}_{z,i}^{\dagger} \hat{a}_{y,i} = \lambda_{x,i}^{1} \pm i \lambda_{x,i}^{2},$$
(5.65)

where we simplified notation by relabelling the Gell-Mann matrices with the index of the symmetry axis of rotation of the corresponding SU(2) sub-algebra. In the usual setting $\lambda_z^1 = \lambda^1$, $\lambda_z^2 = \lambda_2$, $\lambda_y^1 = \lambda^4$, $\lambda_z^2 = \lambda_5$, $\lambda_x^1 = \lambda^6$ and $\lambda_x^2 = \lambda_7$. This allows the Hamiltonian (5.62) to be written in a more compact form as,

$$\hat{H}_{M_{1}}^{b} = -\sum_{\sigma} \sum_{\langle i,j \rangle_{\sigma}} \left[J_{3,\sigma}^{b} \lambda_{3,i} \lambda_{3,j} + J_{8,\sigma}^{b} \lambda_{8,i} \lambda_{8,j} + J_{38,\sigma}^{b} \left(\lambda_{3,i} \lambda_{8,j} + \lambda_{8,i} \lambda_{3,j} \right) + \sum_{\gamma} J_{\gamma,\sigma}^{1} \lambda_{\gamma,i}^{1} \lambda_{\gamma,j}^{1} + J_{\gamma,\sigma}^{2} \lambda_{\gamma,i}^{2} \lambda_{\gamma,j}^{2} \right] - \sum_{i} \left(h_{3}^{b} \lambda_{3,i} + h_{8}^{b} \lambda_{8,i} \right).$$
(5.66)

Since the explicit expressions of the coupling constants are not very informative at first sight, we leave them to Appendix "Coupling Constants of the SU(3) Pseudospin

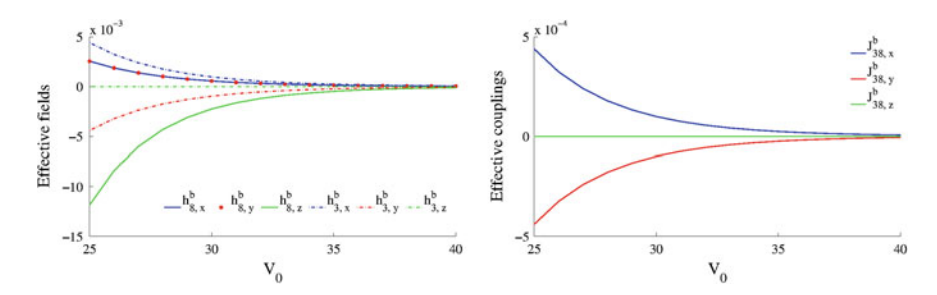


Fig. 5.8 Left panel Effective fields for the bosonic system. The indices labeling different directions are used to illustrate the contribution of external field terms in asymmetric lattices, i.e., where effective 1D and 2D systems are obtained by suppressing the tunneling in 1 or 2 directions. In particular, due to the symmetries of the dynamics in the cubic lattice, the term associated to h_3^b vanishes in this case. Right panel Effective couplings for the nearest neighbors interactions $(\lambda_{8,i}\lambda_{3,i}+\lambda_{3,i}\lambda_{8,i})$. In the same way as for the external fields shown in Fig. 5.8, the relative sign for the couplings of the dynamics in the x and y directions follow directly from the symmetries in the y band of isotropic cubic lattices (see details in the text). In addition, these processes vanish in the case of isotropic cubic lattices

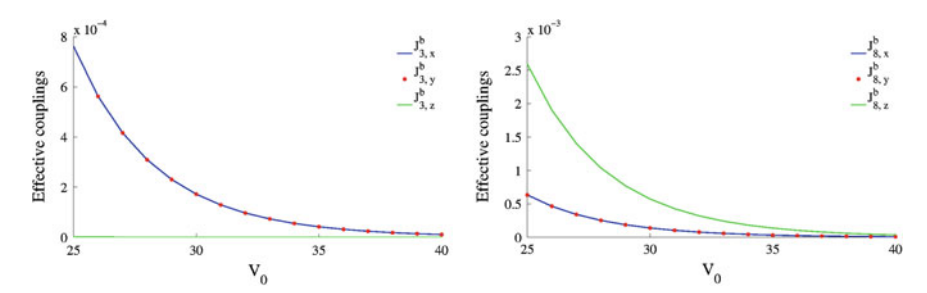


Fig. 5.9 *Left panel* Effective couplings of the bosonic many-body system for $\lambda_{3,i}\lambda_{3,j}$ interactions in the different directions. *Right panel* Effective couplings of the bosonic many-body system for $\lambda_{8,i}\lambda_{8,j}$ interactions in the different directions

Hamiltonians" and we proceed by analyzing the properties of the system in the isotropic lattice, where much of the physics can be understood from symmetry arguments. For reference, Figs. 5.8, 5.9 and 5.10 display the strength of the couplings of the spin model, computed with use of the lattice Wannier functions²⁵ for $V_{\sigma} = V_0$ and $\sigma = \{x, y, z\}$. All the energies are scaled with E_R .

The first notable difference, as compared to other systems of cold atoms used to mimic SU(3) Heisenberg models, ²⁶ is that due to the tunneling anisotropy in the p band, the values of the couplings depend on the dynamics direction. This system contains two external fields, associated to the diagonal λ_3 and λ_8 matrices. These are,

 $^{^{25}}$ The Wannier functions are obtained from diagonalization of the Mathieu equation of a free particle in a sinusoidal lattice in 3D as discussed in Sect. 2.2.

²⁶They are mainly based on implementations of the pseudospin degree of freedom with use of internal atomic states. See, e.g., Refs. [43, 44].

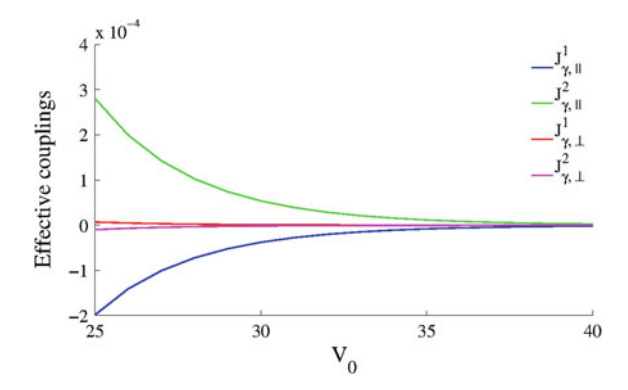


Fig. 5.10 Effective couplings for nearest neighbors interactions obtained from the ladder operators. Notice, in particular, that the couplings associated to the $\lambda_{\gamma,i}^1 \lambda_{\gamma,j}^1$ interactions are not the same as the couplings of $\lambda_{\gamma,i}^2 \lambda_{\gamma,j}^2$. This is a *XYZ*-like anisotropy, which is typical for the bosonic system in the *p* band [1]. In fact, this is a direct consequence from the combination of anisotropic tunneling with orbital-changing interaction terms

respectively, the isospin and hypercharge operators in the study of strong interactions in QCD, whose eigenvalues are used to label the states of the SU(3) multiplet [42]. In the context of p-band physics, the external fields are related to the onsite population imbalance of the different orbital states, and due to the parity symmetries discussed in Eq. (2.51), they yield vanishing contributions in the isotropic cubic lattice. However, whenever these symmetries are broken, as e.g. by engineering effective 2D or 1D lattices, the contributions of the external fields are restored.

The second one is seen from a quick inspection of Eq. (5.66), which reveals that in the same way as for the effective dynamics of the two-orbital system in the p band [1], nearest neighbors interactions derived from the ladder operators yield XYZ-like anisotropies in the couplings of λ_{γ}^1 and λ_{γ}^2 , $J_{\gamma,\sigma}^1$ and $J_{\gamma,\sigma}^2$. Due to the tunneling anisotropies and the different types of interactions in the many-body system, $J_{\gamma,\parallel}^{\{1,2\}} \neq J_{\gamma,\perp}^{\{1,2\}}$, but as long as we are considering the isotropic case $J_{\gamma,\parallel}^{\{1,2\}}$ and $J_{\gamma,\perp}^{\{1,2\}}$ are the same for all $\gamma = \{x,y,x\}$ (recall that γ labels the different SU(2) subalgebras). This should indeed be the case, since this anisotropy stems from the orbital-changing processes, that have identical couplings in the cubic lattice regardless of the states involved.

Now the leading couplings in this pseudospin Hamiltonian stem from contributions of density-density interactions in the many-body system, that are both between atoms in the same and in different orbital states. They also give rise to Dzyaloshinskii–Moriya exchange, that vanish in the cubic lattice due to the parity symmetry, but are again restored whenever this symmetry is broken. This provides an interesting framework for quantum simulation, because ferromagnetic SU(3) models with Dzyaloshinskii–Moriya interactions in 1D and 2D are expected to have ground states with spiral spin textures [45], and the appearance of such terms in effective 1D and 2D lattices is very natural for this system. Indeed, the spiral spin textures would

be manifest here as a rotation (or change in the relative angle of the onsite orbital orientations) of one of the orbital states at each lattice site. Moreover, we expect that in the same way as for the superfluid phase in 3D, discussed in Sect. 3.1.2, the Mott-1 phase of the three-orbital system in the p band has a degeneracy stemming from frustrated configurations of the orbitals in the lattice. A further step, however left for the future, is the study of this system with use of *flavor-wave theory*.²⁷ The aim is to identify the possibility of an *order-by-disorder* mechanism [46, 47], where quantum fluctuations help stabilizing the classical ground state between the various possibilities in this degenerate manifold.

5.3.2 The Fermionic Case

The derivation of the effective Hamiltonian describing the Mott-1 phase of fermions in the p band of 3D lattices is simplified due to the absence of interactions involving two atoms in the same orbital state. Indeed, in this case

$$\hat{H}_{U}^{f} = \sum_{i} \left(2U_{xy} \hat{n}_{x,i} \hat{n}_{y,i} + 2U_{xz} \hat{n}_{x,i} \hat{n}_{z,i} + 2U_{yx} \hat{n}_{y,i} \hat{n}_{z,i} \right), \tag{5.67}$$

and although the basis spanning the \mathcal{H}_P subspace is the same as the one defined for the bosonic case in (5.16), the basis in the \mathcal{H}_Q has only the $\hat{a}^{\dagger}_{\alpha,i}\hat{a}^{\dagger}_{\beta,i}|0\rangle$ states with $\alpha \neq \beta = \{x, y, z\}$.

Here, \hat{H}_Q is diagonal in the basis of intermediate states of the perturbative calculation, and has the same expression of Eq. (5.58) discussed together with the bosonic case. The only processes with non-vanishing matrix elements are described by items (v) and (vi) in the list of Sect. 5.1, and therefore, gathering the corresponding contributions with the explicit expressions of the $K_{\alpha\beta}^{(2)}$ defined in (5.61), the effective Hamiltonian describing the Mott phase with a unit filling of the fermionic system in the p band is given by

$$\hat{H}_{M_1}^f = -\sum_{\langle i,j \rangle} \sum_{\alpha,\beta \neq \alpha} \left[2|t_{\sigma}^{\alpha}|^2 \frac{1}{2U_{\alpha\beta}} \hat{n}_{\alpha,i} \hat{n}_{\beta,j} + 2t_{\sigma}^{\alpha} t_{\sigma}^{\beta} \frac{1}{2U_{\alpha\beta}} \hat{a}_{\beta,i}^{\dagger} \hat{a}_{\alpha,i} \hat{a}_{\alpha,j}^{\dagger} \hat{a}_{\beta,j} \right]. \quad (5.68)$$

Furthermore, this is given in terms of the Gell-Mann matrices (see Eqs. (5.64) and (5.65)) by (Fig.5.11)

²⁷The flavor-wave theory is a generalization of the spin-wave theory for systems with three components (see Refs. [46, 47]).

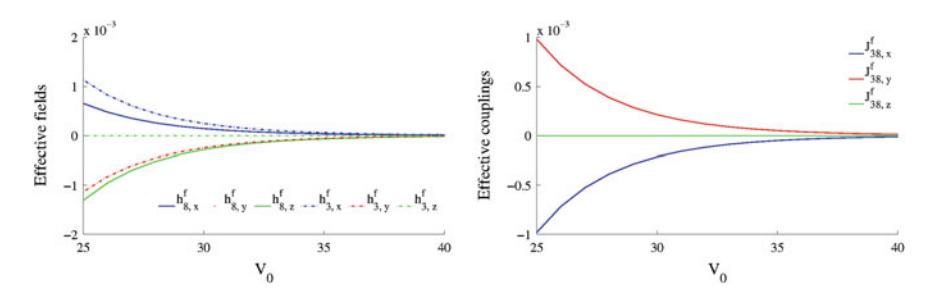


Fig. 5.11 Left panel Effective fields of the effective model with fermionic atoms in isotropic cubic lattices. The situation is again similar to what is discussed for the bosonic case in Fig. 5.8. This should be the case, since the external fields account for single particle contributions and therefore are independent from the statistics of the atoms. In the p-band system, in particular, the external fields encode the degree of imbalance in the occupation of the different orbital states. Right panel Coefficients of $(\lambda_{3,i}\lambda_{8,j} + \lambda_{8,i}\lambda_{,j})$ for the fermionic case. In the same way as discussed in the bosonic case, these terms yield no contribution to the energy in the isotropic cubic lattice

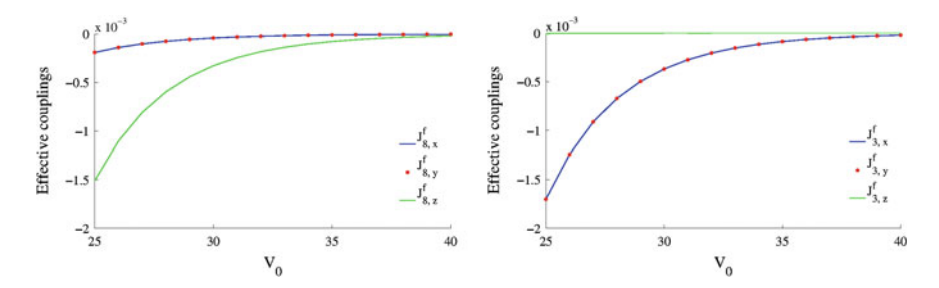
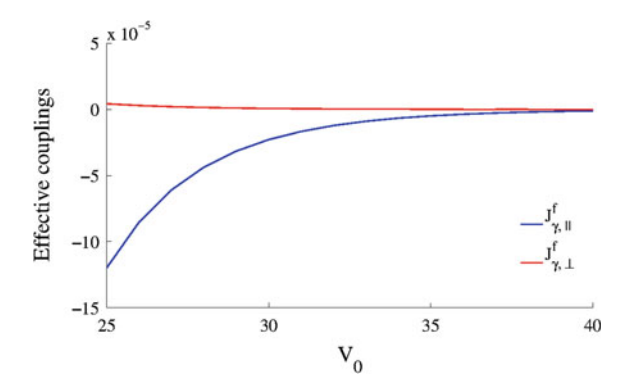


Fig. 5.12 Left panel J_8^f for the fermionic case. Notice here that the $\lambda_{8,i}\lambda_{8,j}$ term contributes very little for the dynamics in the x and y directions, while it is very significant for the dynamics in the z direction. Right panel Coefficients of $\lambda_{3,i}\lambda_{3,j}$ for interactions in the fermionic case in the different directions and as a function of the lattice depth

$$\hat{H}_{M_{1}}^{f} = -\sum_{\sigma} \sum_{\langle i,j \rangle_{\sigma}} \left[J_{3,\sigma}^{f} \lambda_{3,i} \lambda_{3,j} + J_{8,\sigma}^{f} \lambda_{8,i} \lambda_{8,j} + J_{38,\sigma}^{f} \left(\lambda_{3,i} \lambda_{8,j} + \lambda_{8,i} \lambda_{3,j} \right) + \sum_{\gamma} J_{\gamma,\sigma}^{f} \left(\lambda_{\gamma,i}^{1} \lambda_{\gamma,j}^{1} + \lambda_{\gamma,i}^{2} \lambda_{\gamma,j}^{2} \right) \right] - \sum_{i} \left(h_{3}^{f} \lambda_{3,i} + h_{8}^{f} \lambda_{8,i} \right).$$
(5.69)

The strength of the various couplings is shown in Figs. 5.12 and 5.13. In the same way as for the bosonic case, the leading terms stem from contributions due to the density-density interactions that are accordingly described by the diagonal Gell-Mann matrices. In the fermionic case, however, the density-density interactions happen only between atoms in different orbital states. For the same reason as already discussed in the study of the bosonic case, the vanishing of the external fields and of the Dzyaloshinskii–Moriya interactions in the isotropic cubic lattice is a conse-

Fig. 5.13 Coefficients of the interaction stemming from the ladder operators in the fermionic case. Notice, in particular, the *XXZ*-like type of couplings, which differ from the *XYZ*-like couplings obtained for the same terms in the bosonic case (see Fig. 5.10)



quence of the parity symmetry. These terms, are nevertheless restored whenever this symmetry is broken, as again, for example, in effective 1D or 2D realizations.

The fermionic case differs from the bosonic one in two main aspects: First, that instead of ferromagnetic, the couplings of the pseudospin model favor antiferromagnetic ordering. Second, that due to the absence of orbital changing interactions in Eq. (5.53), the exchange terms deriving from ladder operators have the same couplings for both the $\lambda^1_{\gamma,i}\lambda^1_{\gamma,j}$ and $\lambda^2_{\gamma,i}\lambda^2_{\gamma,j}$ processes. Therefore, the fermionic version of the SU(3) model has a structure of couplings that is similar to that of the XXZ Heisenberg model for spin 1/2 systems.

The study of anti-ferromagnetic SU(3) Heisenberg models has a long history [48], and owing to the complexity of the ground states, they constitute very attractive systems for quantum simulation. In 1D, the case with (fully) isotropic couplings admits a Bethe ansatz solution [46], the spectrum of excitations is known to be gapless [46] and correlations decay algebraically [46]. Much less is known for this system in higher dimensions [46, 47]. In fact, studies of both the triangular and the square lattices in 2D and the cubic lattice in 3D have been carried out numerically rather recently [46, 47], and complement an important previous analysis based on applications of flavor-wave theory [48]. These studies confirm the prediction of a highly degenerate manifold of ground states with both 2- and 3-sublattice ordering for the square and cubic lattices, whose degeneracy is lifted by a mechanism of order-by-disorder [46, 47]. More specifically, while the low energy states favor the 2-sublattice structure, the ground state at zero temperature is expected to have a 3sublattice ordering both in 2D and 3D. Therefore, lowering the temperature drives the system through a phase transition from a state with 2- to a state with 3-sublattice structure. In 2D, this is expected to be a thermal transition. The mechanism of this transition in 3D is not fully known. However, it is possible that the 3-sublattice state is formed from the 2-sublattice one due to quantum fluctuations, or else, directly from a paramagnetic state associated to a first-order phase transition [46].

The above are some examples of the physics that can be encountered in the SU(3) models described here. More precisely, by monitoring the system as the temperature

decreases, we expect different sublattice structures to be detected. However, the properties discussed above characterize the SU(3) model with fully isotropic couplings. Although this is not the same case as in Eq. (5.67), in analogy with SU(2) spin systems we expect the anisotropic case to have a rich phase diagram, both in the limit of very low energies and at zero temperature. Furthermore we also notice that effective 1D and 2D realizations can be engineered with external fields and Dzyaloshiskii–Moriya interactions, leading to rather unexplored models of magnetism. As well as for the bosonic case, the flavor-wave analysis of these cases, both in 2D and 3D, is also an interesting future direction.

Extension of the Manipulation/Detection Schemes for the SU(3) Case

Detection and manipulation of the systems discussed here are based on the same ideas presented in Sect. 5.2.2 for the spin-1/2 case. Since the pseudospins are encoded in the different orbital states, we are required to operate on the vibrational levels of the lattice. Here, however, those techniques must be extended to account for the third orbital, and arbitrary rotations are performed with the generators of the SU(3) group.

Let us start then by noticing that the carrier, the red and the blue sideband transitions are implemented in the same way as for the spin-1/2 case, but now with a laser with the wave vector having all three components. The p_x orbital can be selectively addressed by choosing driver lasers with no component in the y and z directions, i.e., $\mathbf{k}_{L_1} - \mathbf{k}_{L_2} = \mathbf{k}_{L_x}$, where \mathbf{k}_{L_i} with i = 1, 2 refer to the wave vectors of the two lasers used in the Raman transition.²⁹ Analogous relations hold for manipulations of only the p_y and/or the p_z orbitals.

Now rotations with the generators of the SU(3) group are given by $\hat{R}_{\beta}(\phi) = e^{-\lambda_{\beta}\phi/2}$, where $\beta=1,\ldots,8$ and ϕ is the effective angle. To implement such operations we make use of the three SU(2) subgroups. The simplest case, of rotations with λ_8 , can be achieved via Stark shift of the p_z orbital without any disturbance of p_x and p_y orbitals. $\hat{R}_3(\phi)$ rotations are also implemented via Stark shift, but now with a dispersive coupling between both p_x and p_y orbitals which already renders the shift with correct (opposite) sign. $\hat{R}_1(\phi)$, $\hat{R}_4(\phi)$ and $\hat{R}_6(\phi)$ rotations are implemented by driving red sideband transitions off-resonantly, for two orbitals. The first case will involve the p_x and p_y orbitals, while in the second and third, p_x and p_z , and p_y and p_z orbitals, respectively. The other three rotations, around λ_2 , λ_5 and λ_7 can be achieved by noticing that $\hat{R}_2(\phi) = \hat{R}_3(\pi/2)\hat{R}_1(\phi)\hat{R}_3(-\pi/2)$, $\hat{R}_5(\phi) = \hat{R}_3(\pi)\hat{R}_8(-\sqrt{3}\pi)R_4(\phi)\hat{R}_3(-\pi)\hat{R}_8(\sqrt{3}\pi)$, and $\hat{R}_7(\phi) = \hat{R}_3(\pi/2)\hat{R}_8(\sqrt{3}\pi/2)R_6(\phi)\hat{R}_3(-\pi/2)$ $\hat{R}_8(-\sqrt{3}\pi/2)$.

To resolve the SU(3) pseudospins, we borrow again the scheme discussed for SU(2) case. Namely, the p_x and p_y states are resolved via single-site fluorescence after measurement of λ_3 , and the p_z orbital after measurement of λ_8 . Likewise, $\langle \lambda_\alpha \lambda_\beta \rangle$ correlation functions can be obtained by using the same techniques, but now combined with coincident measurement of the fluorescent photons. Finally, since

²⁸We discuss detection schemes/measurements in the next subsection.

²⁹Recall the matrix elements $\Omega_1\Omega_2^*/\delta\langle 2|e^{i(k_{L_1}-k_{L_2})}|1\rangle$, where Ω_i are the Rabi frequencies and the notation is the same used in Sect. 5.2.3.

temperature considerations are exactly the same discussed for the spin-1/2 case, we refer to Sect. 5.2.3.

Imperfections Due to the Presence of Residual s Atoms

In the three-orbital case, the random field due to the presence of residual s-band atoms is given by (see Sect. 5.2.4)

$$H_{dis} = \left[\frac{\sqrt{3}}{6U_{sp}}\lambda_{8,i} \left(|t_{\sigma}^{x}|^{2} + |t_{\sigma}^{y}|^{2} - 2|t_{\sigma}^{z}|^{2} \right) + \frac{\lambda_{3,i}}{2U_{sp}} \left(|t_{\sigma}^{x}|^{2} - |t_{\sigma}^{y}|^{2} \right) \right] \delta_{1,n_{s_{i}}}$$
(5.70)

for both the bosonic and fermionic cases. Based on the Imry-Ma argument, we notice that even though the ground-state properties of the fermionic model might be affected by the random field in 1D and 2D, the discrete symmetry of the bosonic model helps stabilizing the phases of the clean system even in low dimensions. In higher dimensions, however, both cases are expected to be robust when the disorder is not too strong.

5.4 The *d*-Band System in 2*D* Lattices

The last system which will have the Mott phase investigated from the perspective of a pseudospin model is described by Eq. (2.55), of bosons in the d band. Recall that throughout this thesis we consider it in the 2D isotropic lattice.

This system is interesting for different reasons: First, due to the presence of density-assisted processes (see Eqs. (2.67) and (2.68)), it lacks the Z_2 -parity symmetry³⁰ characteristic of the system in the p band. Second, according to the Gutzwiller study of Sect. 3.2, this is a two-orbital system for a large region of experimentally relevant parameters. Therefore, let us consider the dynamics involving only the d_{α^2} orbitals³¹ and write

$$\hat{H}_{U}^{d} = \sum_{i} \left\{ \frac{U_{xx}}{2} \hat{n}_{x^{2},i} (\hat{n}_{x^{2},i} - 1) + \frac{U_{yy}}{2} \hat{n}_{y^{2},i} (\hat{n}_{y^{2},i} - 1) + 2U_{xy} \hat{n}_{x^{2},i} \hat{n}_{y^{2},i} \right.$$

$$\left. + \frac{U_{xy}}{2} \left[\left(\hat{d}_{x^{2},i}^{\dagger} \hat{d}_{x^{2},i}^{\dagger} \hat{d}_{y^{2},i} \hat{d}_{y^{2},i} + \hat{d}_{y^{2},i}^{\dagger} \hat{d}_{y^{2},i}^{\dagger} \hat{d}_{x^{2},i} \hat{d}_{x^{2},i} \right) \right]$$

$$+ U_{n_{x}xy} \left(\hat{d}_{x^{2},i}^{\dagger} \hat{n}_{x^{2},i} \hat{d}_{y^{2},i} + \hat{d}_{y^{2},i}^{\dagger} \hat{n}_{x^{2},i} \hat{d}_{x^{2},i} \right)$$

$$+ U_{n_{y}xy} \left(\hat{d}_{x^{2},i}^{\dagger} \hat{n}_{y^{2},i} \hat{d}_{y^{2},i} + \hat{d}_{y^{2},i}^{\dagger} \hat{n}_{y^{2},i} \hat{d}_{x^{2},i} \right)$$

$$+ U_{n_{y}xy} \left(\hat{d}_{x^{2},i}^{\dagger} \hat{n}_{y^{2},i} \hat{d}_{y^{2},i} + \hat{d}_{y^{2},i}^{\dagger} \hat{n}_{y^{2},i} \hat{d}_{x^{2},i} \right)$$

$$(5.71)$$

³⁰Related to conservation of particles modulo 2 in each of the orbital states.

³¹Recall that here $\alpha = \{x, y\}$ and that in the isotropic lattice $U_{xx} = U_{yy}$ and $U_{n_xxy} = U_{n_yxy}$ (see (2.69)).

Using the same basis of Eqs. (5.16) to span \mathcal{H}_P , and the basis in the \mathcal{H}_Q subspace in the order $\{|0, 2x\rangle, |0, xy\rangle, |0, 2y\rangle\}$, we obtain

$$\hat{H}_{Q}^{d} = \begin{pmatrix} U_{xx} & \sqrt{2}U_{n_{x}xy} & U_{xy} \\ \sqrt{2}U_{n_{x}xy} & 2U_{xy} & \sqrt{2}U_{n_{y}xy} \\ U_{xy} & \sqrt{2}U_{n_{y}xy} & U_{yy} \end{pmatrix}$$
(5.72)

and

$$\begin{split} \hat{K}_{d} &= \left(\hat{H}_{Q}^{d}\right)^{-1} \\ &= \Lambda \begin{pmatrix} 2\left(U_{xy}U_{yy} - U_{n_{x}xy}^{2}\right) & \sqrt{2}(U_{xy}U_{n_{y}xy} - U_{n_{x}xy}U_{yy}) & 2\left(U_{n_{x}xy}U_{n_{y}xy} - U_{xy}^{2}\right) \\ \sqrt{2}(U_{xy}U_{n_{y}xy} - U_{n_{x}xy}U_{yy}) & U_{xx}U_{yy} - U_{xy}^{2} & \sqrt{2}(U_{xy}U_{n_{x}xy} - U_{n_{y}xy}U_{xx}) \\ 2\left(U_{n_{x}xy}U_{n_{y}xy} - U_{xy}^{2}\right) & \sqrt{2}(U_{xy}U_{n_{x}xy} - U_{n_{y}xy}U_{xx}) & 2\left(U_{xy}U_{xx} - U_{n_{x}xy}^{2}\right) \end{pmatrix}, \end{split}$$
(5.73)

with

$$\Lambda = \left(2U_{xy}^3 + 4U_{n_xxy}U_{xy}U_{n_yxy} - 2U_{xx}U_{n_yxy}^2 - 2U_{n_xxy}U_{yy} + 2U_{xx}U_{xy}U_{yy}\right)^{-1}.$$
(5.74)

To determine the final form of the effective Hamiltonian, we notice that all the processes listed in Sect. 5.1 have non-vanishing matrix elements such that

$$\begin{split} \hat{H}_{n_{0}=1} &= -\Lambda \sum_{\alpha\beta} \sum_{\langle i,j \rangle_{\sigma}} \left\{ 8 \, |t_{\sigma}^{\alpha}|^{2} \left(U_{\alpha\beta} U_{\beta\beta} - U_{n_{\beta}\alpha\beta}^{2} \right) \hat{n}_{\alpha,i} \hat{n}_{\alpha,j} \right. \\ &+ 2 \left(|t_{\sigma}^{\alpha}|^{2} + |t_{\sigma}^{\beta}| \right) \left(U_{\alpha\alpha} U_{\beta\beta} - U_{\alpha\beta}^{2} \right) \left(\hat{n}_{\alpha,i} \hat{n}_{\beta,j} + \hat{n}_{\beta,i} \hat{n}_{\alpha,j} \right) \\ &+ 8 \, t_{\sigma}^{\alpha} t_{\sigma}^{\beta} \left(U_{n_{\alpha}\alpha\beta} U_{n_{\beta}\alpha\beta} - U_{\alpha\beta}^{2} \right) \left(\hat{d}_{\beta,i}^{\dagger} \hat{d}_{\alpha,i} \, \hat{d}_{\beta,j}^{\dagger} \hat{d}_{\alpha,j} + \hat{d}_{\alpha,i}^{\dagger} \hat{d}_{\beta,i} \, \hat{d}_{\alpha,j}^{\dagger} \hat{d}_{\beta,j} \right) \\ &+ 2 \, t_{\sigma}^{\alpha} t_{\sigma}^{\beta} \left(U_{\alpha\beta} U_{\beta\beta} - U_{n_{\beta}\alpha\beta}^{2} \right) \left(\hat{d}_{\beta,i}^{\dagger} \hat{d}_{\alpha,i} \, \hat{d}_{\alpha,j}^{\dagger} \hat{d}_{\beta,j} + \hat{d}_{\alpha,i}^{\dagger} \hat{d}_{\beta,i} \, \hat{d}_{\beta,j}^{\dagger} \hat{d}_{\alpha,j} \right) \\ &+ 2 \left(|t_{\sigma}^{\alpha}|^{2} + t_{\sigma}^{\alpha} t_{\sigma}^{\beta} \right) \left(U_{n_{\beta}\alpha\beta} U_{\alpha\beta} - U_{n_{\alpha}\alpha\beta} U_{\beta\beta} \right) \left[\hat{n}_{\alpha,i} \left(\hat{d}_{\beta,j}^{\dagger} \hat{d}_{\alpha,j} + \hat{d}_{\alpha,j}^{\dagger} \hat{d}_{\beta,j} \right) \right. \\ &+ \hat{n}_{\alpha,i} \left(\hat{d}_{\beta,j}^{\dagger} \hat{d}_{\alpha,j} + \hat{d}_{\alpha,j}^{\dagger} \hat{d}_{\beta,j} \right) \right] \right\}. \end{split}$$

By further employing the Schwinger angular momentum representation [3, 10]

$$\hat{S}_{i}^{z} = \frac{1}{2} \left(\hat{n}_{x^{2},i} - \hat{n}_{y^{2},i} \right)$$

$$\hat{S}_{i}^{+} = \hat{S}_{i}^{x} + i \hat{S}_{i}^{y} = \hat{d}_{x^{2},i}^{\dagger} \hat{d}_{y^{2},i}$$

$$\hat{S}_{i}^{-} = \hat{S}_{i}^{x} - i \hat{S}_{i}^{y} = \hat{d}_{y^{2},i}^{\dagger} \hat{d}_{x^{2},i}$$
(5.76)

together with the constraint of unit filling, i.e., $\hat{n}_i = \hat{n}_{x,i} + \hat{n}_{y,i} = 1$, Eq. (5.75) can be mapped into a spin-1/2 XYZ model with DM interactions [49, 50] and external fields

$$\hat{H}_{XYZ} = -\sum_{\langle i,j \rangle_{\sigma}} J \left[(1+\gamma) S_{i}^{x} S_{j}^{x} + (1-\gamma) S_{i}^{y} S_{j}^{y} \right]$$

$$-\sum_{\langle i,j \rangle_{\sigma}} \left[\Delta S_{i}^{z} S_{j}^{z} + \delta \left(S_{i}^{x} S_{j}^{z} + S_{i}^{z} S_{j}^{x} \right) \right] + \sum_{i} \left(\Gamma S_{i}^{x} + h S_{i}^{z} \right).$$

$$(5.77)$$

Here $J=-t_{\sigma}^{x}t_{\sigma}^{y}U^{2}/\Lambda$, with $U^{2}=4(U_{xx}U_{yy}-U_{xy}^{2})$ and Λ given by Eq. (5.74), the anisotropy parameter $\gamma=16\left(U_{n_{x}xy}U_{n_{y}xy}-U_{xy}^{2}\right)/U^{2}$,

$$\Delta = 8|t_{\sigma}^{x}|^{2} \left(U_{xy}U_{yy} - U_{n_{y}xy}^{2} \right) + 8|t_{\sigma}^{y}|^{2} \left(U_{xy}U_{xx} - U_{n_{x}xy}^{2} \right)$$

$$-2 \left(|t_{\sigma}^{x}|^{2} + |t_{\sigma}^{y}|^{2} \right) \left(U_{xx}U_{yy} - U_{xy}^{2} \right),$$

$$\delta = 4 \left(U_{n_{y}xy}U_{xy} - U_{n_{x}xy}U_{yy} \right) \left(|t_{\sigma}^{x}|^{2} + t_{\sigma}^{x}t_{\sigma}^{y} \right)$$

$$-4 \left(U_{n_{y}xy}U_{xy} - U_{n_{y}xy}U_{xx} \right) \left(|t_{\sigma}^{y}|^{2} + t_{\sigma}^{x}t_{\sigma}^{y} \right),$$

$$\Gamma = 2 \left(U_{n_{y}xy}U_{xy} - U_{n_{x}xy}U_{yy} \right) \left(|t_{\sigma}^{x}|^{2} + t_{\sigma}^{x}t_{\sigma}^{y} \right)$$

$$+2 \left(U_{n_{y}xy}U_{xy} - U_{n_{y}xy}U_{xx} \right) \left(|t_{\sigma}^{y}|^{2} + t_{\sigma}^{x}t_{\sigma}^{y} \right),$$

and

$$h = 8|t_{\sigma}^{x}|^{2} \left(U_{xy}U_{yy} - U_{n_{x}xy}^{2} \right) - 8|t_{\sigma}^{y}|^{2} \left(U_{xy}U_{xx} - U_{n_{x}xy}^{2} \right).$$

In the isotropic lattice, however, the external field h and the DM interactions vanish due to the parity symmetry of Eq. (2.51),³² and are accordingly restored whenever the symmetry is broken, i.e., when $t_{\parallel}^{y} \neq t_{\parallel}^{y}$ and $t_{\parallel}^{x} \neq t_{\parallel}^{y}$, such that $\delta \neq 0$.

We notice that in the same way as for the system of bosons in the p band, d-orbital bosons can provide an alternative realization of the XYZ model, albeit here in the presence of an external field even in the isotropic case. This is a consequence of the density-assisted processes breaking the Z_2 symmetry of the orbital-changing inter-

³²This symmetry is translated in the spin language by $\hat{S}_i^x \to \hat{S}_i^x$, $\hat{S}_i^y \to -\hat{S}_i^y$, and $\hat{S}_i^z \to -\hat{S}_i^z$.

actions such that only the total number of particles is now conserved. Indeed, the external field contains a \hat{S}^x -dependent term, and moreover, the presence of \hat{S}^x in the DM interactions derives also from density-assisted processes.³³ In the limit of vanishing density-assisted interactions, the effective spin Hamiltonian becomes identical to the corresponding one for the system in the p band discussed in Sect. 5.2, as should indeed be the case since the γ anisotropy is due to orbital changing processes. These two systems are different, however in the character of the interactions, since the $t_{\parallel}^{\alpha}t_{\perp}^{\beta}<0$ property of the tunneling in the p band naturally yields anti-ferromagnetic exchange for some of the spin components, while in the p band p ban

To the best of our knowledge, the phase diagram of this model is not fully known in 2D even for the simplest case of the isotropic lattice, where $\delta=0$. However, due to the parity symmetry of Eq. (2.51) we expect a rich phase diagram with the possibility of symmetry broken phases. For example, the limit of $\Gamma/J\gg\Delta/J$ ($|\gamma|<1$) should be characterized by a highly magnetized state in the x component of the spin, while in the opposite limit the system is in a ferromagnetic state (noting that $\Delta>0$) with broken symmetry in the z component. If the relative strength of Γ/J and Δ/J is much larger than the other couplings in the model, this system is a natural realization of the *transverse Ising model*. In fact, the techniques discussed in Sect. 5.2.2 could be used to engineer such a situation. When $J\sim\gamma$, Δ , the ground state could be in another symmetry broken ferromagnetic state in the xy plane or else, in a gapless floating phase as discussed for the 1D XYZ model in Sect. 5.2.1. Furthermore we notice that effective 1D realizations are also interesting, since the XYZ model with DM interactions has been recently reported to have a rich phase diagram, with both ferromagnetic and Luttinger liquid phases [51].

Finally we remark that if occupation of the \hat{d}_{xy} orbital becomes non-negligible, then the pseudospins must be described by the generators of the SU(3). In addition, the corresponding spin model will feature DM interactions in all the components.

Appendix: Coupling Constants of the SU(3) Pseudospin Hamiltonians

The expressions of the various coupling constants used in the text are given below for both the bosonic and fermionic many-body systems.

Bosonic Case

In the notation below we use σ to denote $\langle i, j \rangle_{\sigma}$. This defines the values of the tunneling amplitudes, which are different for various orbital states in the different directions.

 $^{^{33}}$ Notice here the difference with the SU(3) case, where the DM interactions still conserve the orbital-changing Z_2 symmetry and accordingly, depend only on the diagonal Gell-Mann matrices (see Eqs. (5.62) and (5.66)).

$$J_{8,\sigma}^{b} = \frac{K_{xx}^{(1)}}{3} |t_{\sigma}^{x}|^{2} + \frac{K_{yy}^{(1)}}{3} |t_{\sigma}^{y}|^{2} + \frac{4}{3} K_{zz}^{(1)} |t_{\sigma}^{z}|^{2} + \frac{K_{xy}^{(2)}}{6} \left(|t_{\sigma}^{x}|^{2} + |t_{\sigma}^{y}|^{2} \right) - \frac{2}{9} K_{xz}^{(2)} \left(|t_{\sigma}^{x}|^{2} + |t_{\sigma}^{z}|^{2} \right) - \frac{2}{9} K_{yz}^{(2)} \left(|t_{\sigma}^{y}|^{2} + |t_{\sigma}^{z}|^{2} \right)$$

$$- \frac{2}{9} K_{yz}^{(2)} \left(|t_{\sigma}^{y}|^{2} + |t_{\sigma}^{z}|^{2} \right)$$

$$(5.78)$$

$$J_{38,\sigma}^{b} = \frac{\sqrt{3}}{3} K_{xx}^{(1)} |t_{\sigma}^{x}|^{2} - \frac{\sqrt{3}}{3} K_{yy}^{(1)} |t_{\sigma}^{y}|^{2} - \sqrt{3} \frac{K_{xz}^{(2)}}{6} \left(|t_{\sigma}^{x}|^{2} + |t_{\sigma}^{z}|^{2} \right) + \sqrt{3} \frac{K_{yz}^{(2)}}{6} \left(|t_{\sigma}^{y}|^{2} + |t_{\sigma}^{z}|^{2} \right)$$

$$(5.79)$$

$$h_{8,\sigma}^{b} = 4\frac{\sqrt{3}}{9}K_{xx}^{(1)}|t_{\sigma}^{x}|^{2} + 4\frac{\sqrt{3}}{9}K_{yy}^{(1)}|t_{\sigma}^{y}|^{2} - 8\frac{\sqrt{3}}{9}K_{zz}^{(1)}|t_{\sigma}^{z}|^{2} - \frac{\sqrt{3}}{9}K_{xy}^{(2)}\left(|t_{\sigma}^{x}|^{2} + |t_{\sigma}^{y}|^{2}\right) - \frac{\sqrt{3}}{9}K_{yz}^{(2)}\left(|t_{\sigma}^{y}|^{2} + |t_{\sigma}^{z}|^{2}\right)$$

$$(5.80)$$

$$h_{3,\sigma}^{b} = \frac{4}{3}K_{xx}^{(1)}|t_{\sigma}^{x}|^{2} - \frac{4}{3}K_{yy}^{(1)}|t_{\sigma}^{y}|^{2} + \frac{K_{xz}^{(2)}}{3}\left(|t_{\sigma}^{x}|^{2} + |t_{\sigma}^{z}|^{2}\right) - \frac{K_{yz}^{(2)}}{3}\left(|t_{\sigma}^{y}|^{2} + |t_{\sigma}^{z}|^{2}\right)$$
(5.81)

$$J_{3,\sigma}^{b} = K_{xx}^{(1)} |t_{\sigma}^{x}|^{2} + K_{yy}^{(1)} |t_{\sigma}^{y}|^{2} - \frac{K_{xy}^{(2)}}{2} \left(|t_{\sigma}^{x}|^{2} + |t_{\sigma}^{y}|^{2} \right)$$
 (5.82)

$$J_{\gamma,\sigma}^{1} = K_{\alpha\beta}^{(1)} t_{\sigma}^{\alpha} t_{\sigma}^{\beta} + 2K_{\alpha\beta}^{(2)} t_{\sigma}^{\alpha} t_{\sigma}^{\beta}$$

$$(5.83)$$

$$J_{\gamma,\sigma}^2 = K_{\alpha\beta}^{(1)} t_{\sigma}^{\alpha} t_{\sigma}^{\beta} - 2K_{\alpha\beta}^{(2)} t_{\sigma}^{\alpha} t_{\sigma}^{\beta} \tag{5.84}$$

Fermionic Case

In the same way as for the bosonic case discussed above, σ is used below to define the value of the tunneling amplitudes.

$$J_{8,\sigma}^{f} = \frac{K_{xy}^{(2)}}{6} \left(|t_{\sigma}^{x}|^{2} + |t_{\sigma}^{y}|^{2} \right) - 2 \frac{K_{xz}^{(2)}}{9} \left(|t_{\sigma}^{x}|^{2} + |t_{\sigma}^{z}|^{2} \right) - 2 \frac{K_{yz}^{(2)}}{9} \left(|t_{\sigma}^{y}|^{2} + |t_{\sigma}^{z}|^{2} \right)$$
(5.85)

$$J_{3,\sigma}^{f} = -\frac{K_{xy}^{(2)}}{2} \left(|t_{\sigma}^{x}|^{2} + |t_{\sigma}^{y}|^{2} \right)$$
 (5.86)

$$J_{38,\sigma}^{f} = -\sqrt{3} \frac{K_{xz}^{(2)}}{6} \left(|t_{\sigma}^{x}|^{2} + |t_{\sigma}^{z}|^{2} \right) + \sqrt{3} \frac{K_{yz}^{(2)}}{6} \left(|t_{\sigma}^{y}|^{2} + |t_{\sigma}^{z}|^{2} \right)$$
 (5.87)

$$h_{8,\sigma}^{f} = 2\frac{\sqrt{3}}{9}K_{xy}^{(2)}\left(|t_{\sigma}^{x}|^{2} + |t_{\sigma}^{y}|^{2}\right) - \frac{\sqrt{3}}{9}K_{xz}^{(2)}\left(|t_{\sigma}^{x}|^{2} + |t_{\sigma}^{z}|^{2}\right) - \frac{\sqrt{3}}{9}K_{yz}^{(2)}\left(|t_{\sigma}^{y}|^{2} + |t_{\sigma}^{z}|^{2}\right)$$
(5.88)

$$h_{3,\sigma}^{f} = \frac{K_{xz}^{(2)}}{3} \left(|t_{\sigma}^{x}|^{2} + |t_{\sigma}^{z}|^{2} \right) - \frac{K_{yz}^{(2)}}{3} \left(|t_{\sigma}^{y}|^{2} + |t_{\sigma}^{z}|^{2} \right)$$
 (5.89)

$$J_{\gamma,\sigma}^f = t_\sigma^\alpha t_\sigma^\beta K_{\alpha\beta}^{(2)} \tag{5.90}$$

References

- Pinheiro F, Bruun GM, Martikainen J-P, Larson J (2013) XYZ quantum Heisenberg models with p-orbital bosons. arXiv:1304.3178
- Mikeska H-J, Kolezhuk AK (2004) One-dimensional magnetism. In: Quantum magnetism. Springer, pp 1–83
- 3. Auerbach A (1994) Interacting electrons and quantum magnetism. Springer, Berlin
- 4. Baxter RJ (2007) Exactly solved models in statistical mechanics. Dover Publications, Mineola
- 5. Lewenstein M, Liu WV (2011) Optical lattices: orbital dance. Nat Phys 7(2):101–103
- Ignacio Cirac J, Zoller P (2012) Goals and opportunities in quantum simulation. Nat Phys 8(4):264–266
- Pinheiro F (2014) p orbitals in 3D lattices; fermions, bosons and (exotic) models of magnetism. arXiv:1410.7828
- Pinheiro F, Martikainen J-P, Larson J (2015) Phases of d-orbital bosons in optical lattices. arXiv:1501.03514
- 9. Essler FHL, Frahm H, Göhmann F, Klümper A, Korepin VE (2005) The One-dimensional Hubbard model. Cambridge University Press, Cambridge
- 10. Sakurai JJ (1985) In: Tuan SF (ed) Modern quantum mechanics. Wesley Addison, p 1985
- 11. Duan L-M, Demler E, Lukin MD (2003) Controlling spin exchange interactions of ultracold atoms in optical lattices. Phys Rev Lett 91(9):090402
- 12. Giamarchi T (2004) Quantum physics in one dimension., International series of monographs on physics (Book 121)Oxford University Press, USA
- 13. Giamarchi T (2013) Boulder summer school lecture notes
- Takhtajan LA (1981) The quantum inverse problem method and the XYZ Heisenberg model. Phys D: Nonlinear Phenom 3(1):231–245
- 15. Yu Kitaev A (2001) Unpaired Majorana fermions in quantum wires. Phys Uspekhi 44(10S):131
- Sela E, Altland A, Rosch A (2011) Majorana fermions in strongly interacting helical liquids. Phys Rev B 84(8):085114
- 17. Miranda E (2003) Introduction to bosonization. Braz J Phys 33(1):3-35
- 18. Henley CL http://people.ccmr.cornell.edu/clh/p654/5.6.pdf
- Bak P (1982) Commensurate phases, incommensurate phases and the devil's staircase. Rep Prog Phys 45(6):587–629
- 20. Vojta T (2013) Phases and phase transitions in disordered quantum systems. arXiv:1301.7746
- 21. Vojta T (2013) Boulder summer school lecture notes
- 22. Refael G (2013) Boulder summer school lecture notes
- 23. Jensen HJ http://www.mit.edu/~levitov/8.334/notes/xynotes1.pdf
- Ferguson DJ http://guava.physics.uiuc.edu/~nigel/courses/569/Essays-Spring2006/files/ ferguson.pdf
- 25. Sachdev S (2007) Quantum phase transitions. Wiley Online Library
- Hauke P, Cucchietti FM, Müller-Hermes A, Bañuls M-C, Ignacio Cirac J, Lewenstein M (2010)
 Complete devil's staircase and crystal–superfluid transitions in a dipolar XXZ spin chain: a trapped ion quantum simulation. New J Phys, 12(11):113037
- 27. Pinheiro F (2013) From weakly to strongly correlated physics of bosons in the p band. Licentiate thesis, Stockholm University
- 28. Chuck Norris facts
- 29. Esteve D, Raimond J-M, Dalibard J (2004) Quantum entanglement and information processing: lecture notes of the Les Houches Summer School 2003. Elsevier
- 30. Bakr WS, Gillen JI, Peng A, Fölling S, Greiner M (2009) A quantum gas microscope for detecting single atoms in a Hubbard-regime optical lattice. Nature 462(7269):74–77
- Weitenberg C, Endres M, Sherson JF, Cheneau M, Schauß P, Fukuhara T, Bloch I, Kuhr S (2011) Single-spin addressing in an atomic Mott insulator. Nature 471(7338):319–324
- 32. Haroche S, Raimond J-M (2013) Exploring the quantum: atoms, cavities, and photons (Oxford Graduate Texts). Oxford University Press, USA

References 105

33. Müller T, Fölling S, Widera A, Bloch I (2007) State preparation and dynamics of ultracold atoms in higher lattice orbitals. Phys Rev Lett 99(20):200405

- 34. Shore BW (2011) Manipulating quantum structures using laser pulses. Cambridge University Press, Cambridge
- 35. Allen L, Eberly JH (2012) Optical resonance and two-level atoms. Courier Dover Publications
- 36. Haroche S, Raimond J-M, Meystre P (2007) Exploring the quantum: atoms, cavities, and photons. Phys Today 60(8):61
- 37. Duan L-M, Monroe C (2010) Colloquium: quantum networks with trapped ions. Rev Mod Phys 82(2):1209
- 38. Knap M, Kantian A, Giamarchi T, Bloch I, Lukin MD, Demler E (2013) Probing real-space and time resolved correlation functions with many-body Ramsey interferometry, arXiv:1307.0006
- 39. Isacsson A, Girvin SM (2005) Multiflavor bosonic Hubbard models in the first excited Bloch band of an optical lattice. Phys Rev A 72(5):053604
- 40. Lewenstein M (2013) Comment after a presentation of the author in the quantum technologies IV conference
- 41. Imry Y, Ma S (1975) Random-field instability of the ordered state of continuous symmetry. Phys Rev Lett 35(21):1399
- 42. Greiner W, Müller B (1994) Quantum mechanics. Symmetries, vol 2. Springer, Berlin
- 43. Cazalilla MA, Maria Rey A (2014) Ultracold Fermi gases with emergent SU(N) symmetry. arXiv:1403.2792
- 44. Bonnes L, Hazzard KRA, Manmana SR, Maria Rey A, Wessel S (2012) Adiabatic loading of one-dimensional SU(N) alkaline earth fermions in optical lattices. arXiv:1207.3900
- 45. Graß T, Chhajlany RW, Muschik CA, Lewenstein M (2014) Spiral spin textures of a bosonic Mott insulator with SU(3) spin-orbit coupling. Phys Rev B, 90(19):195127
- 46. Tóth TA, Läuchli AM, Mila F, Penc K (2010) Three-sublattice ordering of the SU(3) Heisenberg model of three-flavor fermions on the square and cubic lattices. Phys Rev Lett 105(26):265301
- 47. Bauer B, Corboz P, Läuchli AM, Messio L, Penc K, Troyer M, Mila F (2012) Three-sublattice order in the SU(3) Heisenberg model on the square and triangular lattice. Phys Rev B, 85(12):125116
- Papanicolaou N (1988) Unusual phases in quantum spin-1 systems. Nucl Phys B 305(3):367– 395
- 49. Dzialoshinskii IE (1957) Thermodynamic theory of weak ferromagnetism in antiferromagnetic substances. Sov Phys JETP-USSR 5(6):1259–1272
- Moriya T (1960) Anisotropic superexchange interaction and weak ferromagnetism. Phys Rev 120(1):91
- Peotta S, Mazza L, Vicari E, Polini M, Fazio R, Rossini D (2014) The XYZ chain with Dzyaloshinsky-Moriya interactions: from spin-orbit-coupled lattice bosons to interacting Kitaev chains. J Stat Mech Theory Exp 2014(9):P09005

Chapter 6 Effects of Disorder in Multi-species Systems

In the previous Chapter we came across an example where experimental imperfections may give rise to disorder. Effects of disorder can affect qualitative properties of the physics, and serve as an interesting area of research on its own [1–3]. In the context of cold atoms, for example, it is possible to fabricate systems where the properties of the disorder can be externally controlled [4–6]. Motivated by these observations, in this chapter we study not multi-orbital, but multi-species systems in the presence of disorder. The reason for this shift is simply because the type of couplings considered here are easy to realize experimentally with multi-species atoms.

Effects of disorder in condensed matter systems have been intensely investigated since its formal appearance in the literature¹ in 1958. By studying a system of noninteracting electrons tunneling in a 3D lattice (tight-binding model) in a random energy landscape, Phillip Anderson showed that the presence of impurities can affect transport properties of quantum mechanical systems in a dramatic way [1], due to the existence of localized states.

After Anderson's seminal work, much effort was directed in understanding the role of dimensionality in the phenomenon of *Anderson localization*. In 1D, for example, all the eigenstates of this problem were shown to be localized,² even for arbitrarily weak disorder [7]. From analysis based on scaling arguments, 2D systems are also generically considered to have localized eigenstates in the entire spectrum.³ This situation is different in 3D systems, where localized and extended eigenstates are separated by a *mobility edge* [9]. These studies played a central role for the theory of metal-insulator transitions [2, 10], and nowadays, much of the current research in

¹According to [2], studies of disordered systems in condensed matter were very scarce and lacked a systematic framework before Anderson's work [1].

²That is, to decay exponentially from a center in real space.

 $^{^3}$ Exceptions to the scaling argument in 2D include chiral systems [8], some of which will be discussed in this chapter.

[©] Springer International Publishing Switzerland 2016

this area is focused on the properties of systems with interactions, in the phenomenon called *many-body localization* [11].

In this Chapter we study effects of disorder in bosonic multi-species systems that are coupled via a disordered potential. This is the material of Ref. [12]. We will start by presenting the different models under investigation in Sect. 6.1 and we follow with the study of the symmetries in different cases in Sects. 6.2 and 6.3. These different cases belong the different chiral orthogonal, chiral unitary, Wigner-Dyson orthogonal and Wigner-Dyson unitary symmetry classes. We characterize the spectral properties in Sect. 6.4. In particular, we show that when compared to the chiral classes, the onset of localization in terms of the disorder strength is delayed in the Wigner-Dyson classes, and we explain this result in terms of an effective model obtained after integrating out the fastest modes in the system, in Sect. 6.5. Finally, in Sect. 6.6, we briefly discuss the experimental relevance of the systems studied here. Far from being a survey on the theory of disordered systems, our aim is to report a series of results obtained in the latest year, and to illustrate the very rich physics appearing in systems of coupled multi-species. However, despite the non-introductory character of these discussions, we present it in a self-contained fashion. For reviews on the theory of Anderson localization and of disordered quantum systems we refer to [2, 10].

6.1 Meet the Hamiltonians

"One Hamiltonian to understand them all.."

—Adapted from another famous book.

Let us consider the Hamiltonian describing a system of two non-interacting species that are tunneling in a 2D lattice and that are randomly coupled at each site

$$\hat{H} = -\sum_{\langle i,j \rangle_{\sigma}} \left(\hat{a}_{i}^{\dagger} \hat{a}_{j} + \hat{b}_{i}^{\dagger} \hat{b}_{j} \right) + g \sum_{i} \left(h_{i} \hat{b}_{i}^{\dagger} \hat{a}_{i} + h_{i}^{*} \hat{a}_{i}^{\dagger} \hat{b}_{i} \right) + \sum_{i} \left(\mu^{a} \hat{n}_{i}^{a} + \mu^{b} \hat{n}_{i}^{b} \right).$$

$$(6.1)$$

 $\langle \pmb{i}, \pmb{j} \rangle_{\sigma}$ denotes the nearest neighbors in the direction $\sigma = \{x, y\}$, \hat{a}_i (\hat{a}_i^{\dagger}) and \hat{b}_i (\hat{b}_i^{\dagger}) destroy (create) a particle of the type a and b, respectively, at the site $\pmb{i}, g > 0$ is a coupling constant and h_i is a complex valued random field with $\langle \Re (h_i) \rangle = \langle \Im (h_i) \rangle = 0$, $\langle |h_i|^2 \rangle = \xi$, and $\langle \cdots \rangle$ denotes the disorder averaging. Such multispecies systems are typically implemented with use of two different Zeeman levels of an atom [13], and the random coupling with the use of Raman pulses [14].

We are interested in the spectral properties of this system for the four different cases: (i) of $\mu^a = \mu^b = 0$ and real-valued h_i ; (ii) of $\mu^a = \mu^b = 0$ and complex-valued h_i ; (iii) of μ^a , $\mu^b \neq 0$ and real-valued h_i ; and (iv) of μ^a , $\mu^b \neq 0$ and complex-valued h_i .

6.2 Symmetries of the Real-Valued Random-Field Case

Let us start by considering the symmetries of Eq. (6.1) for the case of real-valued h_i . Without loss of generality, ⁴ let us assume that $\mu^a = -\mu^b = \mu$, and re-write (6.1) as

$$\hat{H}_{R} = -t \sum_{\langle i,j \rangle_{\sigma}} \left[\hat{a}_{i}^{\dagger} \ \hat{b}_{i}^{\dagger} \right] \mathbb{1} \left[\hat{a}_{j} \\ \hat{b}_{j} \right] + \sum_{i} \left[\hat{a}_{i}^{\dagger} \ \hat{b}_{i}^{\dagger} \right] \left(g \, h_{i} \sigma^{x} + \mu \sigma^{z} \right) \left[\hat{a}_{i} \\ \hat{b}_{i} \right], \quad (6.2)$$

where σ^{α} , $\alpha=\{x,y,z\}$ are the Pauli matrices. The above expression is clearly invariant under multiplication of a global phase $\hat{a}_i \to e^{i\phi}\hat{a}_i$ and $\hat{b}_i \to e^{i\phi}\hat{b}_i$, which is related to conservation of total number of particles in the system. In addition, \hat{H}_R is real and symmetric, and therefore it is invariant under time-reversal transformations. Therefore, in spite of the intrinsic spin structure of Eq. (6.2), the presence of σ^z does not play the role of a magnetic field in this pseudo-spin picture.

The situation of $\mu = 0$ is of particular interest. In this case, the Hamiltonian is also invariant under $\hat{a}_i \rightarrow \hat{b}_i$ transformations, and in addition, since it is possible to find a unitary transformation that anti-commutes with the Hamiltonian,

$$U^{\dagger} \hat{H}_{R}^{(\mu=0)} U = -\hat{H}_{R}^{(\mu=0)}, \tag{6.3}$$

with

$$U = \operatorname{diag}\left(\underbrace{1, -1, 1, -1 \dots}_{N} | \underbrace{-1, 1, -1, 1 \dots}_{N}\right), \tag{6.4}$$

and N the number of sites, the Hamiltonian has *chiral symmetry* [15]. This means that there exists a basis for which this Hamiltonian has a manifestly off-diagonal block form, ⁵ that for each eigenvalue ϵ that is a solution of the characteristic equation, $-\epsilon$ is also a solution, and as a consequence, the spectrum is symmetric around the zero energy. It also means that the states with ϵ and $-\epsilon$ energies are related by a chiral transformation [15, 16].

The study of this system lead to an interesting observation about the properties of certain banded matrices with random entries as we show here. Consider the M_1 and M_2 matrices defined below, where h_i and μ are real numbers.

$$\underbrace{(a_{11},b_{12},a_{13},b_{14},\ldots,a_{1(n-1)},b_{1n},\ b_{21},a_{22},b_{23},a_{24},\ldots b_{2(n-1)},a_{2n}}_{\text{Rlock 1}}\mid \underbrace{b_{11},a_{12},b_{13},a_{14},\ldots,b_{1(n-1)},a_{1n},\ a_{21},b_{22},b_{24},\ldots,a_{2(n-1)},b_{2n}}_{\text{Rlock 2}},$$

for example, where a_{ij} and b_{ij} are the amplitudes of the wave-functions of particles a and b at the site (i, j), would rewrite the Hamiltonian in the desired off-diagonal shape.

⁴Defining the chemical potential in this way is equivalent to adding a constant to the Hamiltonian.

⁵Here a reordination of the basis as

$$M_{1} = \begin{bmatrix} \mu & J & 0 & \dots & \dots & h_{1} & 0 & 0 & \dots & \dots \\ J & \mu & J & 0 & \dots & 0 & h_{2} & 0 & 0 & \dots \\ 0 & J & \mu & J & 0 & 0 & 0 & h_{3} & 0 & 0 \\ \vdots & & \ddots & & \vdots & & \ddots & \ddots \\ \hline h_{1} & 0 & 0 & \dots & \dots & -\mu & J & 0 & \dots & \dots \\ 0 & h_{2} & 0 & 0 & \dots & J & -\mu & J & 0 & \dots \\ \vdots & & \ddots & & \vdots & & \ddots & \ddots \end{bmatrix}$$

$$\vdots & \ddots & \vdots & \ddots & \vdots$$

$$(6.5)$$

and

$$M_{2} = \begin{bmatrix} h_{1} & J & 0 & \dots & & \mu & 0 & 0 & \dots & \dots \\ J & h_{2} & J & 0 & \dots & 0 & \mu & 0 & 0 & \dots \\ 0 & J & h_{3} & J & 0 & 0 & 0 & \mu & 0 & 0 \\ \vdots & & \ddots & & \vdots & & \ddots & \ddots \\ \hline \mu & 0 & 0 & \dots & \dots & -h_{1} & J & 0 & \dots & \dots \\ 0 & \mu & 0 & 0 & \dots & J & -h_{2} & J & 0 & \dots \\ 0 & 0 & \mu & 0 & 0 & 0 & J & -h_{3} & J & \dots \\ \vdots & & \ddots & & \vdots & & \ddots & \ddots \end{bmatrix}.$$

$$(6.6)$$

The claim is that M_1 and M_2 have exactly the same eigenvalues.

We can show that this statement is true by noticing that M_1 and M_2 are the Hamiltonians of two tight-binding problems that can be mapped into each other by a linear transformation. Explicitly, consider the following Hamiltonians:

$$\hat{H}_{1} = J \sum_{\langle i,j \rangle} (\hat{a}_{i}^{\dagger} \hat{a}_{j} + \hat{b}_{i}^{\dagger} \hat{b}_{j} + H.c.) + \sum_{i} h_{i} (\hat{a}_{i}^{\dagger} \hat{b}_{i} + \hat{b}_{i}^{\dagger} \hat{a}_{i}) + \mu \sum_{i} (\hat{a}_{i}^{\dagger} \hat{a}_{i} - \hat{b}_{i}^{\dagger} \hat{b}_{i}), \quad (6.7)$$

describing a two-species system of non-interacting atoms that are randomly coupled, and

$$\hat{H}_{2} = J \sum_{\langle i,j \rangle} (\hat{c}_{i}^{\dagger} \hat{c}_{j} + \hat{d}_{i}^{\dagger} \hat{d}_{j} + H.c.) + \mu \sum_{i} (\hat{c}_{i}^{\dagger} \hat{d}_{i} + \hat{d}_{i}^{\dagger} \hat{c}_{i}) + \sum_{i} h_{i} (\hat{c}_{i}^{\dagger} \hat{c}_{i} - \hat{d}_{i}^{\dagger} \hat{d}_{i}), \quad (6.8)$$

describing a coupled system of non-interacting two-species that are tunneling in a random energy landscape. Since the transformation $\hat{c}_i \to (\hat{a}_i + \hat{b}_i)/2$ and $\hat{d}_i \to (\hat{a}_i - \hat{b}_i)/2$ maps $\hat{H}_1 \to \hat{H}_2$, and M_1 and M_2 are the matrix forms for representing the corresponding Hamiltonians, these systems must have identical eigenvalues. This accounts for a *Hadamard transformation* of the Pauli matrices,

$$\begin{split} \hat{\sigma}_x &\rightarrow \hat{U}_H \hat{\sigma}_x \hat{U}_H^{-1} = \hat{\sigma}_z, \\ \hat{\sigma}_z &\rightarrow \hat{U}_H \hat{\sigma}_z \hat{U}_H^{-1} = \hat{\sigma}_x, \\ \hat{\sigma}_y &\rightarrow \hat{U}_H \hat{\sigma}_y \hat{U}_H^{-1} = -\hat{\sigma}_y, \end{split}$$

which is nothing but a π rotation in xz-plane. Since \hat{U}_H is independent of the site index, the Hadamard transformation does not depend on the disorder realization. Furthermore, this is a canonical transformation and accordingly, it preserves the bosonic commutation relations $[\hat{c}_i, \hat{c}_j^{\dagger}] = \delta_{ij}$, $[\hat{d}_i, \hat{d}_j^{\dagger}] = \delta_{ij}$ and $[\hat{c}_i, \hat{d}_j^{\dagger}] = 0$. In addition, we notice that this property

extends⁶ to tight-binding Hamiltonians in 2D and 3D, and also for the case of a random chemical potential where $\mu \to \mu_i$.⁷

It would be interesting, therefore, to find different systems in other areas of physics⁸ that are described by the same type of matrix as (6.5) or (6.6). Such analogies not only allow for the use of technology developed in the context of tight-binding models for exploring the physics of these other models, but it could also establish a valuable connection between the corresponding systems and the systems of cold atoms we discuss here.⁹

With the above observation, we have shown, in addition, that for $\mu=0$ this system of randomly coupled species can be mapped into two independent Anderson problems, one for each type of atom, that are tunneling in a random energy landscape with the same magnitude but with opposite signs. Therefore, this provides an alternative setup for experimental studies of Anderson localization. Furthermore, we also notice that although the chiral symmetry and the corresponding off-diagonal block representation of the Hamiltonian are usually associated to the presence of only nonvanishing bonds in off-diagonal elements of the Hamiltonian¹⁰ [15, 16], we explore the multi-species character in $\hat{H}_{R}^{(\mu=0)}$ to obtain a chiral model with onsite disorder.¹¹

6.3 Symmetries of the Complex-Valued Random Field Case

Following the discussion of the real-valued field case, Eq. (6.2) can be written as

$$\hat{H}_{C} = -t \sum_{\langle i,j \rangle_{\sigma}} \left[\hat{a}_{i}^{\dagger} \ \hat{b}_{i}^{\dagger} \right] \mathbb{1} \left[\hat{b}_{j}^{\dagger} \right] + \sum_{i} \left[\hat{a}_{i}^{\dagger} \ \hat{b}_{i}^{\dagger} \right] \left(|h_{i}| \cos \theta_{i} \sigma^{x} + |h_{i}| \sin \theta_{i} \sigma^{y} + \mu \sigma^{z} \right) \left[\hat{a}_{i}^{\dagger} \right],$$

$$(6.9)$$

where we used that $h_i = |h_i|e^{i\theta_i}$. In this case the Hamiltonian is a Hermitian matrix, and therefore time-reversal symmetry is absent even for the situation in which $\mu = 0$. In fact, this system is only invariant under multiplication of a global phase, which again reflects the conservation of total number of particles in the system.

When $\mu = 0$, however, $\hat{H}_C^{(\mu=0)}$ is a chiral Hamiltonian, and can be written in block off-diagonal form with the basis ordered in the same way as discussed for the real-valued field case (see footnote 3 of Sect. 6.2). The spectral properties discussed

⁶The main difference with the 2D and 3D cases is that the tunneling part will be described by block matrices, in the same way as we discussed in Sect. 4.1 for the ideal gas in the p band.

⁷We could also think of situations where μ_i and h_i are taken from different distributions and so on.

⁸As for example in statistical mechanics of complex systems.

⁹The author also finds it extremely interesting to think of a cold atom system as a realization of a generic matrix.

 $^{^{10}}$ As would be the case, for example in a tight-binding Hamiltonian with random nearest-neighbors hopping.

¹¹Notice that the presence of an onsite term in a usual tight-binding type of model necessarily destroys the chiral symmetry.

in that case are also valid here: the spectrum is symmetric around the zero energy and the eigenstates of positive and negative eigenvalues ϵ and $-\epsilon$ are connected via the chiral transformation [15, 16]. The difference, however, as compared to that case, is the lack of time-reversal symmetry.

Let us now proceed with the study of (6.9), and for the chiral case with $\mu = 0$ by considering the following transformation of the operators:

$$\hat{\alpha}_{i}^{\dagger} = e^{-i\theta_{i}}\hat{a}_{i}^{\dagger}
\hat{\beta}_{i} = e^{-i\theta_{i}}\hat{b}_{i},$$
(6.10)

in such a way that

$$\hat{H}_{rf} = -t \sum_{\langle i,j \rangle_{\sigma}} \left(e^{-i(\theta_{i} - \theta_{j})} \hat{\alpha}_{i}^{\dagger} \hat{\alpha}_{j} + e^{i(\theta_{i} - \theta_{j})} \hat{\beta}_{i}^{\dagger} \hat{\beta}_{j} + H.c. \right) + \sum_{i} |h_{i}| \left(\hat{\alpha}_{i}^{\dagger} \hat{\beta}_{i} + \hat{\beta}_{i}^{\dagger} \hat{\alpha}_{i} \right).$$

$$(6.11)$$

It describes the coupled system where the α and β species acquire a random phase as they tunnel around in the lattice, and are randomly converted into each other by a random real-valued field. Due to the chiral symmetry, this system is closely related to the so called $random flux \ model^{12}$ [15] and therefore provides a controlable environment for experimental realizations of such system.

6.4 Spectral Properties

Before presenting the results of numerical studies, let us discuss qualitative properties of the spectrum by considering limiting situations. We start with the limit of vanishingly small disorder, $\xi \to 0$. Here, when the chemical potential is also zero, the matrix of Eq. (6.1) becomes essentially block diagonal, and the system approximately corresponds to two independent copies of a tight-binding model. Accordingly, all the energy levels are degenerate because all the eigenvalues appear once in each block. When $\mu \neq 0$, the two tight-binding copies become coupled at each site, and thereby the degeneracy is lifted.

By increasing the strength of the disorder ξ , and in particular, by increasing the coupling between the two species via varying g, the energies of the excitations are lowered, leading to avoided crossings of the energy levels. This is shown in Figs. 6.1 and 6.2. We have checked that these avoided crossings are smoothened out after averaging over different realizations.

 $^{^{12}}$ Although the random flux model does not have an onsite term, the chiral symmetry of Eq. (6.11) allows it to be re-written as $\tilde{H}_{rf} = \sum_{\langle i,j \rangle} e^{i\varphi_i} \hat{a}^{\dagger}_i \hat{a}_j + H.c.$, where e^{φ_i} is a random phase. We also note that the term "flux" derives from the fact that for charged particles hopping on a lattice, a random magnetic field, *i.e.*, flux, becomes manifested on the phases.

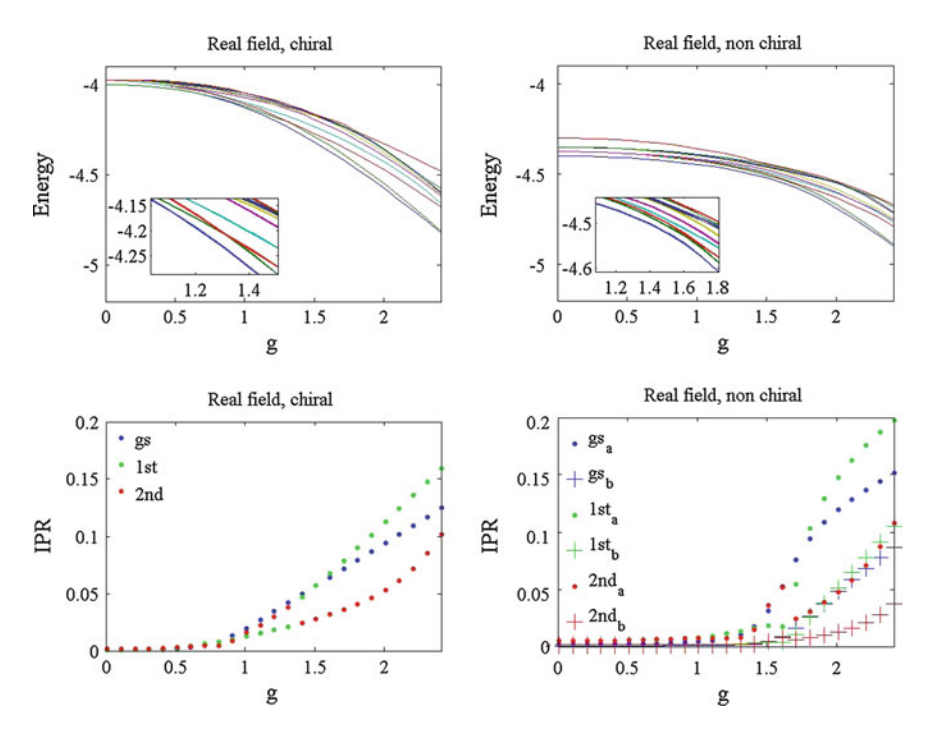


Fig. 6.1 Ten first energy levels (of a single realization) of the real-valued random field cases on a 40×40 lattice and the IPR for the three first states for the system with t=1 and $\xi=0.4$. In the non-chiral case $\mu=0.4$. Since in the wave-functions for the a and b particles are identical in the chiral case (see text), we do not distinguish the IPRs of the a and b eigenstates in the left panel. In the right panel the a and b labels refer to the IPR of the corresponding type of state. Notice here that the regions of discontinuity in the IPR are associated to the avoided crossings in the energy spectrum

6.4.1 Properties of the Ground State and Low Lying Excitations

Localization in the eigenstates is characterized with the inverse participation ratio (IPR) given by

$$IPR = \frac{\sum_{i} |\phi_{i}|^{4}}{\sum_{i} |\phi_{i}|^{2}}, \tag{6.12}$$

where $\phi_i = \langle x_i | \Psi \rangle$ are the coefficients of the eigenstates of the Hamiltonian in the space representation. In the limit of IPR \rightarrow 0, the states are extended over the entire lattice, ¹³ and larger values of the IPR signal the occurrence of localization. ¹⁴ As shown in Figs. 6.1 and 6.2, the regions of avoided crossings in single realizations of

¹³For finite lattices the IPR $\rightarrow 1/N$, where N is the number of sites.

¹⁴The extreme where IPR \rightarrow 1 would correspond to having a particle localized in one site.

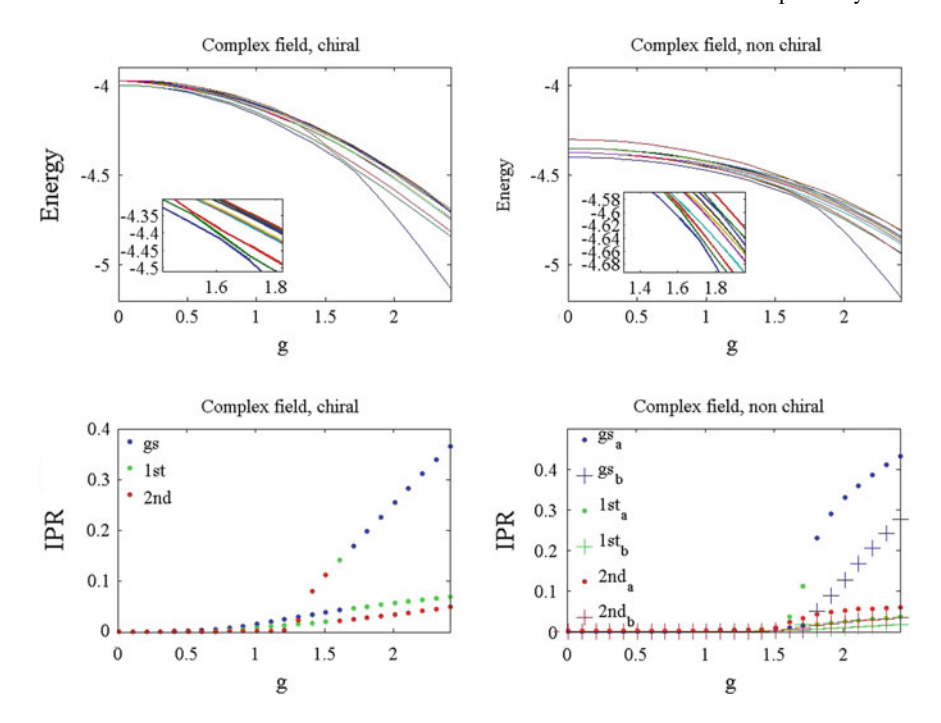


Fig. 6.2 Ten first energy levels (of a single realization) of the complex-valued random field cases on a 40×40 lattice and the IPR for the three first states for the system with t=1 and $\xi=0.4$. In the non-chiral case we use again $\mu=0.4$. In the same way as in Fig. 6.1, the a and b labels denote the IPR of the a and b particles in the *left panel*. The regions of discontinuity in the IPR are also associated here to the avoided crossings in the energy spectrum

the disorder are also associated to jumps in the IPR. This can be understood from the fact that typically, localized states that are close in energy, are localized in different regions of space [17].

All the cases studied here displayed localized eigenstates for strong enough disorder, but as shown in Figs. 6.1 and 6.2, the states of the non-chiral classes are more robust against the disorder and become localized for larger values of g. This will be characterized further in the next section, were we study these systems in terms of an effective model that accounts only for the dominant particles with the smaller value of μ . Localization in the excited states is also characterized with use of the IPR. Except for the states in the middle of the spectrum of the chiral Hamiltonians, which are known to be extended [8], all the different cases studied here show localized eigenstates for g/t > 1.

Let us now consider the region of parameters for which the coupling with the disorder is not strong enough to completely localize the states. In the presence of disorder, what are the properties of the phase of the eigenstates of these systems? Is

¹⁵By dominant we mean that the amplitude of the wave-functions of the particles with lowest chemical potential are the largest ones.

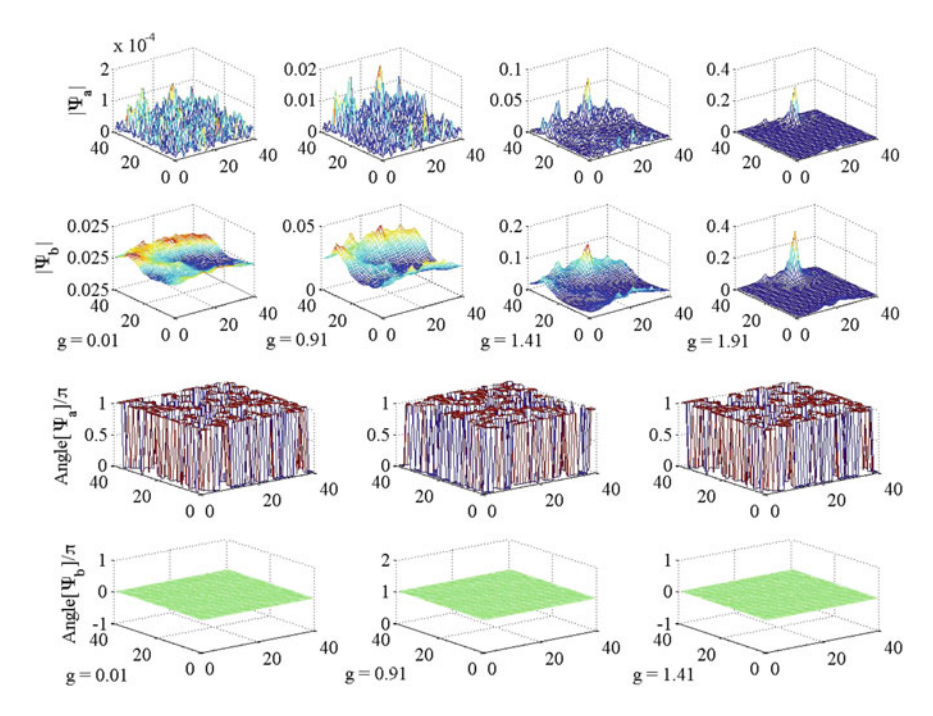


Fig. 6.3 Ground state amplitude and phase for different values of the coupling with the disorder g for the non-chiral Hamiltonian with a real-valued random field whose spectral properties are shown in the *left panel* of Fig. 6.1. Notice that despite the disorder, the wave-functions of the dominant b mode does not change sign in the lattice. It thus becomes clear that the system chooses to minimize the kinetic energy of the dominant particles via fixing the phase, while the less populated species carries a large kinetic energy

there any possibility of long-range phase coherence in the wave-functions of the a and b particles, ¹⁶ or else, is it possible for the relative phase of the a and b particles, due to the coupling with the disorder, to exhibit any type of phase locking?

Figure 6.3, displays the ground-state wave-functions of the a and b particles for a single realization of the non-chiral case with real-valued random field and with $\mu^a/t = -\mu^b/t = 0.4$. The different values of g/t for which we show the phases of Ψ_a and Ψ_b correspond to the values of g where the states are still extended, ¹⁷ and it is clear that Ψ_b has phase coherence along the lattice. Interestingly, this is not what happens for Ψ_a , whose sign oscillates between the different sites. It is also very interesting that the density of the dominant b particles is very smooth and extended, while the non-dominant a particles have a density with a large number of different peaks. This is not what happens in the chiral case, for which $|\Psi_a| = |\Psi_b|$. Here both wave-functions have phase coherence over the lattice, and therefore also relative phase coherence. We attribute this property to the fact that as opposed to the

¹⁶In the sense of phase coherence of the order parameter.

¹⁷In the sense of a large localization length.

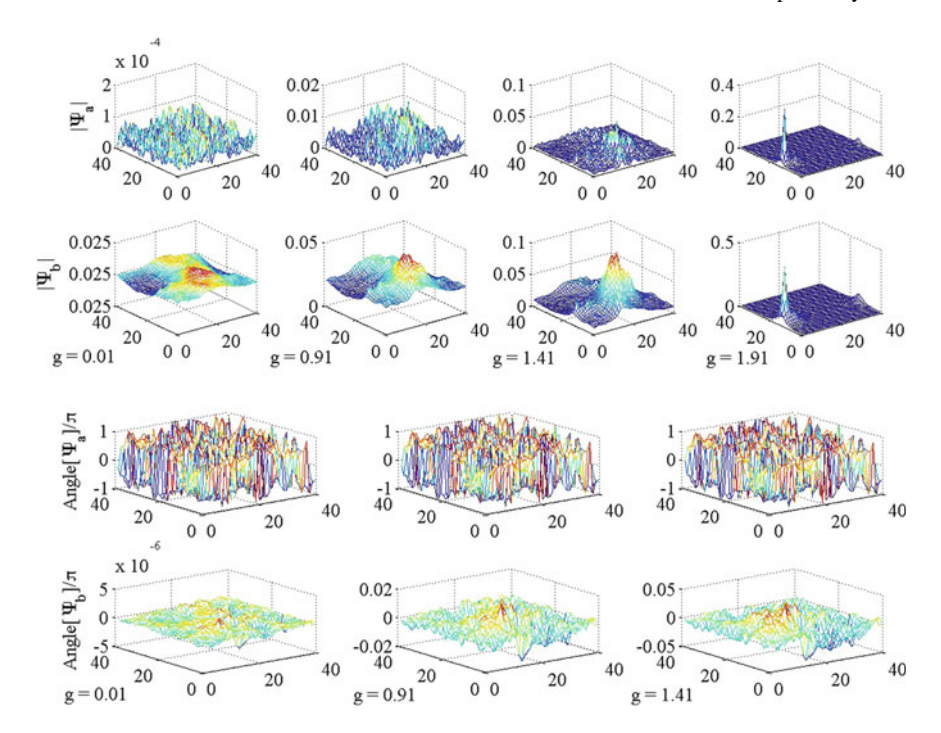


Fig. 6.4 Ground state amplitude and phase for different values of the coupling with the disorder g for the non-chiral Hamiltonian with a complex-valued random field. This is for the same system whose spectrum is shown in Fig. 6.2 and therefore t=1 and $\xi=0.4$

real-valued random field case, where the phase of the random field couples to the relative phase of the a and b wave-functions with discrete values, i.e., with a zero or π phase at each site, the relative phase of the a and b wave-functions couple to all the possible values between $[0,\pi]$ of the random phase in the complex-valued random field case.

The ground-state wave-function of the non-chiral case with complex-valued random field with $\mu^a/t = -\mu^b/t = 0.4$ is shown in Fig. 6.4. The properties of the density are similar to what was discussed above for the real-valued random field case, but with the difference that no phase coherence is present in the wave-function of the dominating b particles. In the same way, the chiral case with complex-valued field is also characterized by $|\Psi_a| = |\Psi_b|$. Contrary to the chiral real-valued field case, however, this case does not present any phase coherence in any of the wave-functions of the a and b particles, and accordingly, no relative phase is established.

The excited states of these systems also display a very interesting profile. In the non-chiral cases, the densities of the dominant and non-dominant particles follow the same trend already discussed for the ground-state: the dominant particles have extended and smooth wave-functions, while the amplitudes of the non-dominant ones are highly oscillating in the lattice. The phase behavior is also similar to that already

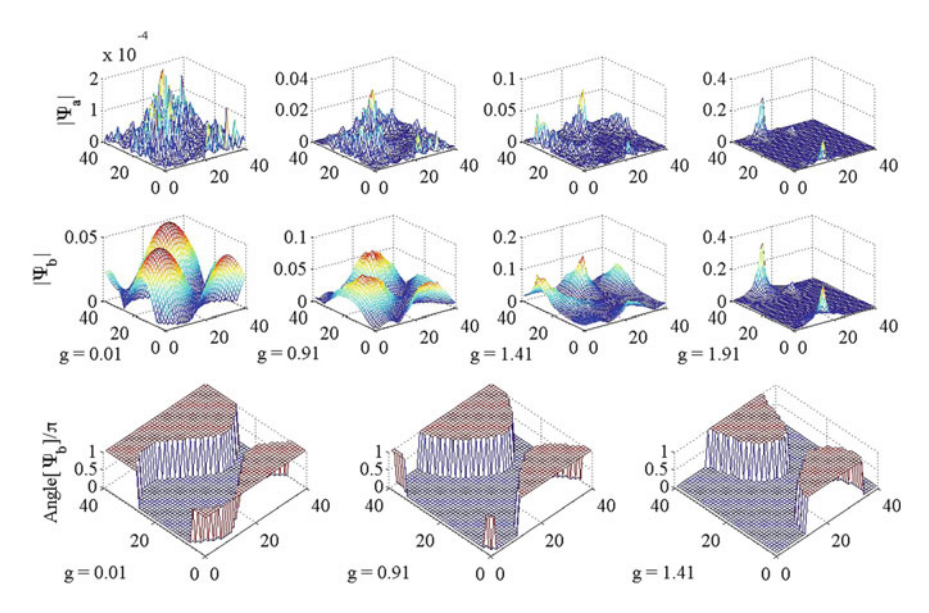


Fig. 6.5 Amplitudes and phases for different values of the coupling with the disorder g for the first excited state of the non-chiral Hamiltonian with a real-valued random field. The phase of the wave-function describing particles of the a type behaves in a very similar way to what is shown in Fig. 6.3 and therefore is not shown here. In contrast, notice the appearance of domain walls in the phase of the wave-function of particles of the b type

seen in the ground-state, and thus these plots are not repeated here. Now the main property of the excitations of these systems is that the phase of the dominant wavefunction Ψ_b is characterized by the appearance of domain walls in the real-valued random field case (see Figs. 6.5 and 6.6), while in the complex-valued random field case, the phase of Ψ_b features pairs of vortices/anti-vortices¹⁸ (see Figs. 6.7 and 6.8). These properties are the same in the chiral cases, with the difference that the densities of a and b particles are exactly the same. For real-valued random field, Ψ_a and Ψ_b exhibit phase coherence along the lattice, and therefore also relative phase coherence. Whether this relative phase coherence is a consequence of the *no-node theorem* [18] or a manifestation of the phenomenon known by the name of *random-field induced order* (see below) is still a matter of investigation. In the complex-valued random field case, Ψ_a and Ψ_b don't exhibit any type of phase coherence.

The phenomenon of random-field induced order [14, 19] refers to the ability that certain systems have of establishing order only in the presence of disorder. The reasoning is as follows: suppose we are studying a clean system in 1D or 2D, with a continuous symmetry, and that satisfies the assumptions of the Hohenberg–Mermin–Wagner theorem [20, 21]. Accordingly, this system is prohibited of having long-range order with an order parameter of the

 $^{^{18}}$ The number of vortices/anti-vortices is larger for higher excited states, but there does not seem to be a general rule which relates the number of vortex/anti-vortex pairs with the corresponding nth excitation number.

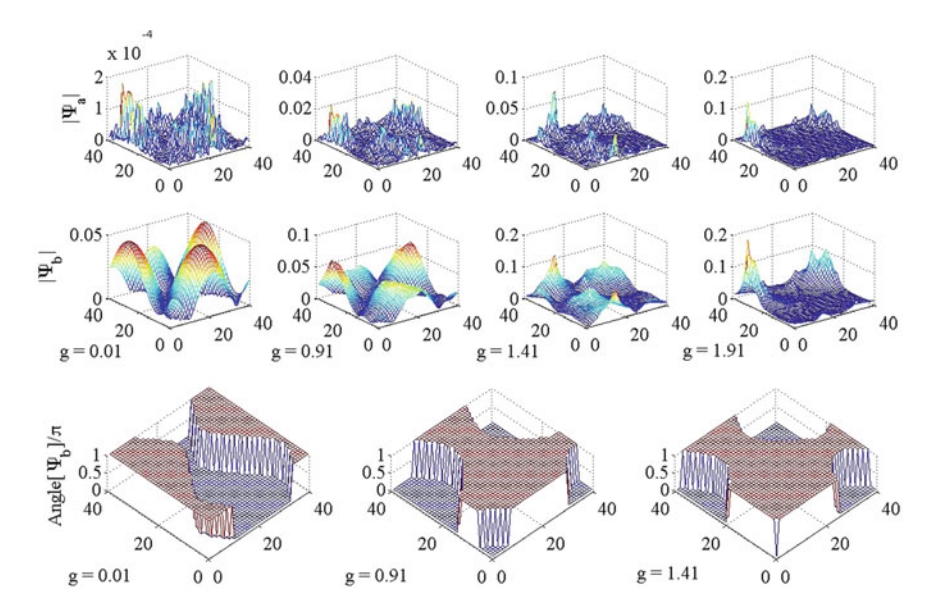


Fig. 6.6 In the same way as for Fig. 6.5, we show the amplitudes and phases for the second excited state of the non-chiral Hamiltonian with a real-valued random field. We again draw attention to the presence of domain walls in the phase of the wave-function of the *b* particles

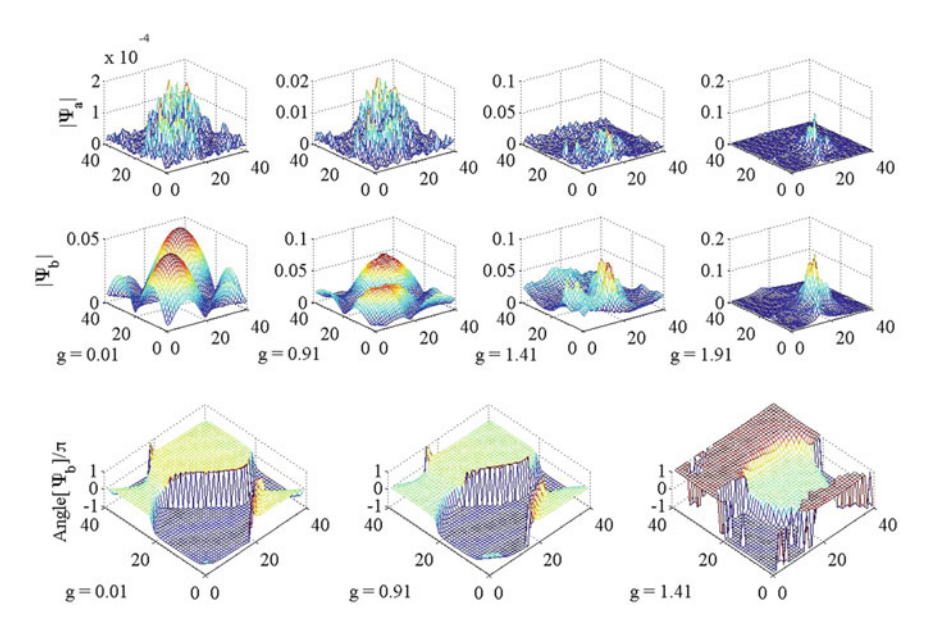


Fig. 6.7 Amplitudes and phases for different values of the coupling with the disorder g for the first excited state of the non-chiral Hamiltonian with a complex-valued random field. Since the phase of the wave-function describing the a particles is very similar to what is shown in Fig. 6.4, we present only the phase of the wave-function of particles of the b type. In particular, notice the appearance on vortices/anti-vortices pairs, as discussed in the text

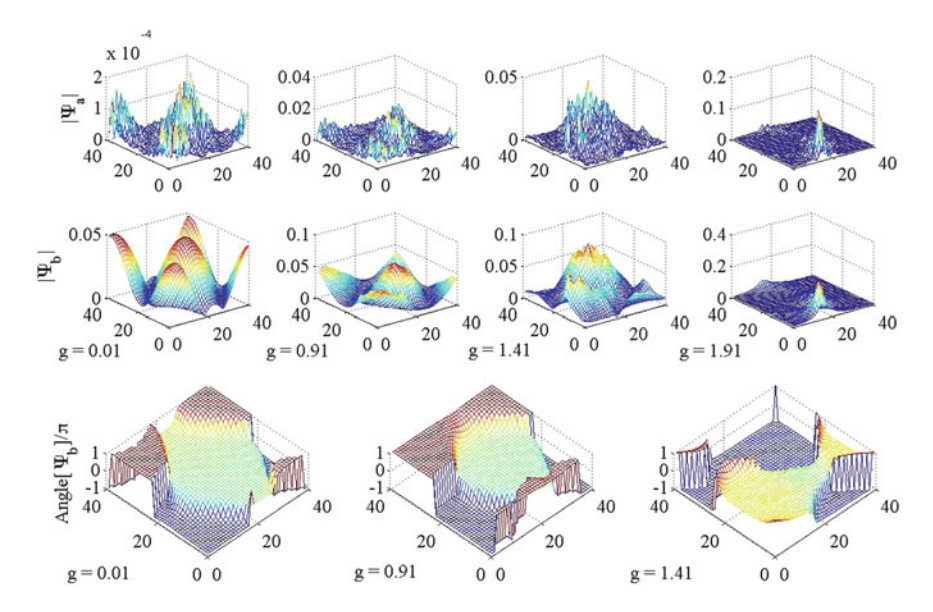


Fig. 6.8 Amplitudes and phases for different values of the coupling with the disorder g for the second excited state of the non-chiral Hamiltonian with a complex-valued random field. In the same way as for Fig. 6.7, we show only the phase of the b particles, which feature vortices/anti-vortices pairs

magnetization type [20, 21]. Now let us assume that it is possible to add a random field to this system in such a way to break the continuous symmetry. Because the system now has discrete rather than continous symmetry, it does not fulfil the assumptions of the Mermin-Wagner theorem and therefore there is nothing prohibiting global ordering in the strict sense [14, 22]. Although counterintuitive, this mechanism seems to be related to the possibility of order in graphene quantum Hall ferromagnets [23]. In interacting Bose–Einstein condensates that are randomly coupled via Raman pulses, for example, random-field induced order appears in the form of a fixed phase, of $\pi/2$, in the order parameters of the two condensates [14]. In addition, a rigorous mathematical proof has been recently given for the occurrence of random-field induced order in the classical XY model [19] and it is argued that this phenomenon should also occur in the quantum case [22].

6.5 Effective Model for the Non-chiral Systems

The numerical study of Sect. 6.4 revealed that by breaking the degeneracy of the onsite wave-functions with the additional species-dependent chemical potential and for not too strong values of ξ , the wave-functions of one of the species become essentially insensitive to the presence of disorder. This behavior can be understood from the construction of a simple effective model, obtained from tracing out the species with the fastest oscillating modes. In order to obtain this effective model, let us consider the coherent state representation of the partition function for the system

of Eq. (6.1). We consider here the functional integral in the frequency representation such that

$$Z = \int \mathcal{D}[\psi_a^*, \psi_a, \psi_b^*, \psi_b] e^{-S[\psi_a^*, \psi_a, \psi_b^*, \psi_b]}, \tag{6.13}$$

where ψ_{α} , $\alpha = a$, b are coherent states, $\mathcal{D}[\psi_a^*, \psi_a, \psi_b^*, \psi_b] = \Pi_n d[\psi_{a,n}^*, \psi_{a,n}, \psi_{b,n}^*, \psi_{b,n}]$ defines the measure with n the label of the nth mode and the Matsubara frequencies at temperature T are given by $\omega_n = 2n\pi T$. In this framework the action takes the form

$$S[\psi_{a}^{*}, \psi_{a}, \psi_{b}^{*}, \psi_{b}] = \sum_{n} \sum_{\langle i, j \rangle_{\sigma}} \psi_{an,i}^{*} \underbrace{\left[(-i\omega_{n} - \mu^{a})\delta_{ij} - 1 \right]}_{A_{ij}} \psi_{an,j} + \sum_{n} \sum_{\langle i, j \rangle_{\sigma}} \psi_{bn,i}^{*} \underbrace{\left[(-i\omega_{n} - \mu^{b})\delta_{ij} - 1 \right]}_{B_{ij}} \psi_{bn,j} + \sum_{n} \sum_{i} \left(\psi_{an,i}^{*} h_{i} \psi_{bn,i} + \psi_{bn,i}^{*} h_{i}^{*} \psi_{an,i} \right).$$

$$(6.14)$$

Now let us assume the species-dependent chemical potential to satisfy $\mu^a > \mu^b$, such that the fastest modes are associated to the dynamics of ψ_a . The effective action describing the dynamics of the species b can then be obtained after a partial trace over the degrees of freedom of the a species as

$$Z_{b} = \int d\psi_{b,n}^{*} d\psi_{b,n} e^{\sum_{n} \Psi_{bn}^{*} B \Psi_{bn}} \int d\psi_{a,n}^{*} d\psi_{a,n} e^{\left[\sum_{n} \Psi_{an}^{*} A \Psi_{an} + \Psi_{an}^{*} C \Psi_{bn} + \Psi_{bn}^{*} C^{*} \Psi_{an}\right]}$$

$$= \det \left[\mathbf{A} \right]^{-1} \int d\psi_{b,n}^{*} d\psi_{b,n} \exp \left[\sum_{n} \Psi_{bn}^{*} \underbrace{\left(\mathbf{B} - \mathbf{C}^{*} \mathbf{A}^{-1} \mathbf{C} \right)}_{H_{eff}^{b}} \Psi_{bn} \right], \tag{6.15}$$

where we use the matrix notation with $\Psi_{\alpha n} = (\psi_{\alpha n,1},\dots,\psi_{\alpha n,N})^T$, with N the number of sites, and H^b_{eff} is the effective Hamiltonian describing the b species. This expression makes it clear that the characteristic energy of the degrees of freedom that were integrated out enters the disorder, in such a way that the coupling with the disorder has different magnitudes in the effective modes describing the a and b particles. The elements of the a and b matrices are given above, and b is the matrix with the (random field) couplings between the a and b species. These are also the matrices obtained after expressing Eq. (6.1) in a block form

$$H = \left(\frac{A \mid C}{C^* \mid B}\right),\tag{6.16}$$

although we notice that in this form the A and B blocks in Eq. (6.1) do not contain the frequency dependence embedded in (6.15). In particular, it is interesting to notice the structure of H_{eff}^b , which is determined by the Green function of a tight-binding

model. 19 Indeed, the presence of a particles induces an effective long-range hopping for the dominating b particles, such that this long-range hopping counteracts localization. Since it does not have an exponential fall off, the states are not extended in the strict sense, but display a larger localization length, as seen in the results of the numerical study of Figs. 6.1 and 6.2.

6.6 Experimental Realizations of Disordered Systems

As discussed in this chapter, the different possibilities for the choice of the Raman coupling and chemical potential in Eq. (6.1) make the system of randomly coupled Bose–Einstein condensates an alternative candidate for the study of quantum systems in the presence of disorder.²⁰ At zero chemical potential, for example, the real-valued random field case can be mapped into the Anderson model, whereas the case with a complex-valued random field is related to the random flux model. The fact that (6.1) is a quadratic Hamiltonian allows the use of the classification scheme of disordered systems. In this scheme, the real-valued random field cases belong to orthogonal classes, whereas the Hamiltonians with complex-valued random field belong to unitary classes. The symmetries of each case subdivide the orthogonal and unitary classes even further [24, 25], as we show in Table 6.1.

The orthogonal class contains the matrices that are real and symmetric, which yield the models discussed in Sect. 6.2, with time-reversal symmetry [17, 25]. At zero chemical potential, the system has the additional chiral symmetry and belongs to the chiral orthogonal class. When $\mu \neq 0$, the Hamiltonian belongs to the orthogonal Wigner–Dyson one [17, 25]. The cases with a complex-valued random field belong to the unitary classes [17, 25]. At zero chemical potential the system is in the chiral unitary class, whereas it is in the Wigner–Dyson unitary one otherwise [17, 25].

As a final remark, we notice that these different cases can also be connected to the classification scheme of topological insulators [25]. This is particularly useful for characterizing Anderson localization as well as universal properties of these systems. The different possibilities are also listed in Table 6.1. In addition, these different classes allow for the existence of a topological insulator in different dimensions [25]. This means that a term of topological origin can be added to the *non-linear-* σ -model description of the system at the (d-1)-dimensional boundary which prevents Anderson localization [25]. From the cases discussed above, the BDI class admits a Z_2 in 0D and a Z term in 1D, the AIII class admits a Z term in 3D, the AI class admits a Z term in 0D, and last but not least, the A class admits a Z term in 2D [25].

¹⁹That is, the A^{-1} part.

²⁰Anderson localization has been studied in systems of cold atoms with the disorder created by laser speckels (see [5] and references therein).

Case	h_i	μ	Class	Classification scheme
(i)	Real-valued	Zero	Chiral orthogonal	BDI
(ii)	Complex-valued	Zero	Chiral unitary	AIII
(iii)	Real-valued	Non-zero	Wigner-Dyson orthogonal	AI
(iv)	Complex-valued	Non-zero	Wigner–Dyson unitary	A

Table 6.1 Classification of Eq. (6.1) for different choices of h_i and μ (see text for details)

Accordingly, these systems of randomly coupled Bose–Einstein condensates could also be relevant for experiments in this direction.

Beware! Too much disorder might localize your thoughts.

--(Not so) Common knowledge.

References

- 1. Anderson PW (1958) Absence of diffusion in certain random lattices. Phys Rev 109(5):1492
- Ziman JM (1979) Models of disorder: the theoretical physics of homogeneously disordered systems. CUP Archive
- 3. Abrahams E (2010) 50 years of anderson localization. World Scientific, Singapore
- Roati G, D'Errico C, Fallani L, Fattori M, Fort C, Zaccanti M, Modugno G, Modugno M, Inguscio M (2008) Anderson localization of a non-interacting Bose–Einstein condensate. Nature 453(7197):895–898
- Aspect A, Inguscio M (2009) Anderson localization of ultracold atoms. Phys Today 62(8):30– 35
- Modugno G (2010) Anderson localization in Bose–Einstein condensates. Rep Prog Phys 73(10):102401
- Nevill F (1961) Mott and WD twose. The theory of impurity conduction. Adv Phys 10(38):107– 163
- 8. König EJ, Ostrovsky PM, Protopopov IV, Mirlin AD (2012) Metal-insulator transition in 2d random fermion systems of chiral symmetry classes. arXiv:1201.6288
- 9. Abrahams E, Anderson PW, Licciardello DC, Ramakrishnan TV (1979) Scaling theory of localization: absence of quantum diffusion in two dimensions. Phys Rev Lett 42(10):673–676
- 10. Evers F, Mirlin AD (2008) Anderson transitions. Rev Mod Phys 80(4):1355
- 11. Huse D, Nandkishore R (2015) Many-body localization and thermalization in quantum statistical mechanics. Annu Rev Condens Matter Phys 6(1):15–38
- Pinheiro F, Larson J (2015) Disordered cold atoms in different symmetry classes. Phys Rev A 92(2):023612
- 13. Soltan-Panahi P, Struck J, Hauke P, Bick A, Plenkers W, Meineke G, Becker C, Windpassinger P, Lewenstein M, Sengstock K (2011) Multi-component quantum gases in spin-dependent hexagonal lattices. Nat Phys 7(5):434–440
- Niederberger A, Schulte T, Wehr J, Lewenstein M, Sanchez-Palencia L, Sacha K (2008)
 Disorder-induced order in two-component Bose–Einstein condensates. Phys Rev Lett 100(3):030403
- Altland A, Simons BD (1999) Field theory of the random flux model. Nucl Phys B 562(3):445– 476

References 123

 Bocquet M, Chalker JT (2003) Network models for localization problems belonging to the chiral symmetry classes. Phys Rev B 67(5):054204

- 17. Haake F (2010) Quantum Signatures of Chaos, vol 54. Springer, Berlin
- Feynman RP (1972) Statistical mechanics, a set of lectures., Frontiers in physicsPerseus Books, New York
- Crawford N (2013) Random field induced order in low dimension. EPL (Europhys Lett) 102(3):36003
- 20. Mermin ND, Wagner H (1966) Absence of ferromagnetism or antiferromagnetism in one- or two-dimensional isotropic Heisenberg models. Phys Rev Lett 17(22):1133
- 21. Hohenberg PC (1967) Existence of long-range order in one and two dimensions. Phys Rev 158(2):383
- 22. Niederberger A, Rams MM, Dziarmaga J, Cucchietti FM, Wehr J, Lewenstein M (2010) Disorder-induced order in quantum XY chains. Phys Rev A 82(1):013630
- 23. Abanin AD, Lee PA, Levitov LS (2007) Randomness-induced XY ordering in a graphene quantum hall ferromagnet. Phys Rev Lett 98(15):156801
- Altland A, Zirnbauer MR (1997) Nonstandard symmetry classes in mesoscopic normalsuperconducting hybrid structures. Phys Rev B 55(2):1142
- Ryu S, Schnyder AP, Furusaki A, Ludwig AWW (2010) Topological insulators and superconductors: tenfold way and dimensional hierarchy. New J Phys 12(6):065010

Chapter 7 Conclusions

In this thesis we presented different aspects of the physics of multi-species systems in optical lattices. Although the focus was mainly on orbital physics, we also discussed the properties of a simple two-species system in the presence of disorder.

We reserved final remarks to the Conclusions section, and in particular we will focus here on possible interesting directions for future research:

- Among the systems presented in Chap. 3, it would be interesting to study the *d*-band case further, from a perspective that goes beyond the tight-binding and single-band approximations. In the *p* band, for example, it has been argued that an additional nearest-neighbors interaction, if strong enough, could give rise to *supersolid phases* [1]. Since the Wannier functions in the *d* band are even broader than the ones in the *p* band, a study about the possibility of finding such phases in the *d* band system could be of relevance for experiments. Different lattice geometries provide another interesting continuation, specially since upcoming experiments on the *d* band consider non-separable lattices [2];
- Several interesting directions have the starting point on the systems discussed in Chap.5:

For the p band system in 1D, for example, one interesting problem is the study of the XYZ chain in an external random field with DMRG techniques. This is of experimental relevance, since implementation of such a setup can take advantage of the presence of residual s band atoms;

A throughout characterization of both the bosonic and fermionic SU(3) models via flavor-wave analysis would be of interest. In fact, together with the methods presented in Sect. 5.3.2, this would allow for experimental investigation of frustrated phases and of phenomena emerging from the mechanism of order-by-disorder; Still regarding the studies of orbital physics in the Mott phase of excited bands, another interesting direction corresponds to the spin mapping of the Hamiltonian describing the fermionic system in the d band. Since in this case it is possible to have the coupling between the different d_{x^2} and d_{y^2} orbitals via the d_{xy} one, the

126 7 Conclusions

corresponding spin system would loose the continuous symmetry, as opposed to the case of fermionic atoms in the p band. In addition, the situation of a multi-orbital system with an internal spin degree of freedom could also lead to the appearance of novel properties.

• The results presented in the last chapter are still part of ongoing research. However, the main question to be addressed in the future is related to the possibility of using that system to investigate, experimentally, the phenomenon of random-field-induced order. In particular, it would be important to understand how this phenomenon is related to the localization of the excitations in the systems where it occurs, or with the localization of spin waves.



References

- Scarola VW, Demler E, Das Sarma S (2006) Searching for a supersolid in cold-atom optical lattices. Phys Rev A 73(5):051601
- 2. Zhou X (2015) Private communication